

DISSERTATION

THE DEVELOPMENT OF HYALURONAN ENHANCED EXPANDED
POLYTETRAFLUOROETHYLENE AND LINEAR LOW DENSITY POLYETHYLENE FOR
BLOOD CONTACTING APPLICATIONS

Submitted by

Hieu T. Bui

School of Biomedical Engineering

In partial fulfillment of the requirements

For the Degree of Doctor of Philosophy

Colorado State University

Fort Collins, Colorado

Spring 2019

Doctoral Committee:

Advisor: Susan James

Melissa Reynolds

Ketul Popat

Christine Olver

Copyright by Hieu T. Bui 2019

All Rights Reserved

ABSTRACT

THE DEVELOPMENT OF HYALURONAN ENHANCED EXPANDED POLYTETRAFLUOROETHYLENE AND LINEAR LOW DENSITY POLYETHYLENE FOR BLOOD CONTACTING APPLICATIONS

Cardiovascular disease is the number one cause of death in high income, industrialized countries. Designing cardiovascular implants from synthetic polymers is a cost-effective solution to the growing demand for medical treatments such as heart valve replacements and cardiovascular bypass procedures. Synthetic polymers are often known for their tunability, durability, and low production cost. Unfortunately, these materials are also prone to induce thrombosis. Therefore, improving the blood compatibility of these polymers is still a major challenge in the biomedical field. This dissertation discusses the alteration of two synthetic polymers, linear low density polyethylene (LLDPE) and expanded polytetrafluoroethylene (ePTFE), using hyaluronan (HA) to improve their blood compatibility. HA, a naturally occurring polysaccharide in the human body, is known for its wound healing and anticoagulant properties. In this work, two unique methods were developed for HA enhancement of ePTFE (HA-ePTFE) and LLDPE (HA-LLDPE). This was a process driven research that aimed at designing HA-ePTFE and HA-LLDPE by analyzing the effect of different treatment parameters on the properties of the resultant materials.

In the case of ePTFE, it was demonstrated that HA can be incorporated into vascular ePTFE grafts by exploiting the micro pores of the polymer and adjusting the spraying treatment. In the HA-LLDPE fabrication process, its parameters were varied to assess their effects on the interpenetrating polymer network (IPN) formation. Surface characterization such as water contact angle goniometry, infrared spectroscopy, and toluidine blue O (TBO) staining prove that HA

treatment successfully changed the surface chemistry and increased the hydrophilicity of ePTFE and LLDPE. Thermal analysis and gas chromatography-mass spectrometry were used to quantify the effects of different treatment conditions on material properties. Tensile properties such as elastic modulus, tensile strength, yield stress and ultimate strain are unchanged by HA enhancement for both polymers. The biological results reveal that HA-ePTFE and HA-LLDPE are not cytotoxic and result in less blood clotting and platelet activation than ePTFE and LLDPE.

ACKNOWLEDGMENTS

I would like to thank my advisor, Dr. Susan James, for all that she has done to help me throughout my time in graduate school. Her advice, knowledge, and support have been the key reasons for my many accomplishments. I would also like to thank my committee members, Dr. Ketul Popat, Dr. Melissa Reynolds, and Dr. Christine Olver for taking time out of their busy schedules to be on my committee. A special thanks to Dr. David Prawel for many of his invaluable advice that have helped me develop both personally and professionally. I would also like to thank the faculty and staff at Colorado State University for training and equipment use, Dr. Patrick McCurdy, Dr. Arun Kota, and Dr. Matt Kipper. Thank you to Melesa Gonzales, Nicole Dixon, and the staff at the CSU Health Center for their assistance in drawing blood.

Thank you to John Cavicchia, for helping the lab establish the “factory” and laying the groundwork for me, and Richard Koch, for always being so patient and providing thoughtful feedback, and Dr. Rachael Simon-Walker, for offering advice and information on conducting the blood studies. I would also like to thank the many hardworking and talented undergraduate researchers in Brelab: Kylee Harris and Emily Li, for always being there for me whenever I needed help, Charlotte Mitchell, for managing Brelab and keeping many of the important chemistry work running, and Aidan Friederich, Noah Mills, and Josh Kannenberg, for performing the myriad engineering tasks that I could never have done.

Finally, I would like to thank my family and friends for always being there when I needed them the most. Their support and encouragement have kept me through some of the toughest times in my graduate school experience.

TABLE OF CONTENTS

ABSTRACT.....	ii
ACKNOWLEDGEMENTS.....	iv
Chapter 1: Introduction.....	1
1.1 Motivation for Research.....	1
1.2 Blood and Materials Interaction.....	2
1.2.1 The Coagulation Cascade	2
1.2.2 The Cell Based Model of Coagulation.....	3
1.2.3 Platelets	5
1.2.4 Material Surface Properties.....	6
1.2.5 Current Solutions and Their Shortcomings.....	8
1.3 Expanded Polytetrafluoroethylene	10
1.4 Linear Low-Density Polyethylene	12
1.5 Hyaluronan	15
1.5.1 Structure and Components.....	15
1.5.2 The Role of Hyaluronan in the Endothelial Glycocalyx Layer	16
1.5.3 Hyaluronan in Biomedical Research for Cardiovascular Applications	18
1.6 Objectives and Specific Aims	21
References.....	23
Chapter 2: Fabrication and Characterization of HA-ePTFE.....	35
2.1 Introduction & Preliminary Work	35
2.1.1 Preliminary Wicking Study.....	35
2.1.2 Preliminary HA-ePTFE Fabrication	37
2.2 Materials & Methods.....	44
2.2.1 Fabrication & Surface Characterization of HA-ePTFE	44
2.2.2 Mechanical Stability of HA on ePTFE	47
2.2.3 Circumferential Tensile Testing	50
2.2.4 Statistical Analysis.....	51
2.3 Results & Discussion	52
2.3.1 Fabrication and Surface Characterization of HA-ePTFE	52
2.3.2 Mechanical Stability Results.....	57
2.3.3 Circumferential Tensile Results.....	58
2.4 Limitations & Future Work.....	60
References.....	63
Chapter 3: Fabrication and Characterization of HA-LLDPE	65
3.1 Introduction & Preliminary Work	65
3.1.1 Preliminary HA-LLDPE Fabrication.....	66
3.1.2 Preliminary Results.....	70
3.2 Materials and Methods	72
3.2.1 SHACTA Concentration Study.....	73
3.2.2 Vapor Swelling Test	73
3.2.3 The Effect of Crosslinking Vapor Content on HA-LLDPE IPN	74
3.2.4 IPN Verification of HA-LLDPE.....	75
3.2.5 Tensile Testing.....	76

3.2.6	Statistical Analysis.....	76
3.3	Results & Discussion	77
3.3.1	SHACTA Concentration Study.....	77
3.3.2	Vapor Swelling Test	79
3.3.3	The Effect of Crosslinking Vapor Content on HA-LLDPE IPN	80
3.3.4	IPN verification of HA-LLDPE.....	88
3.3.5	Tensile Testing.....	89
3.4	Limitations and Future Work.....	90
	References.....	94
Chapter 4:	Thrombogenic Potential of HA-ePTFE and HA-LLDPE.....	97
4.1	Introduction	97
4.2	Materials and Methods	98
4.2.1	Cytocompatibility Assay.....	98
4.2.2	Whole Blood Clotting Assay	100
4.2.3	Platelet Activation Assay.....	102
4.2.4	Statistical Analysis.....	105
4.3	Results & Discussion	105
4.3.1	Cytocompatibility Assay.....	105
4.3.2	Whole Blood Clotting.....	108
4.3.3	Platelet Activation Assay.....	112
4.4	Limitations and Future Work.....	119
	References.....	121
Appendix	123
A.1	HA-CTA Complexation	124
A.2	HA-CTA Silylation	130
A.3	Acetone Distillation.....	137
A.4	Xylene Distillation	141
A.5	HA-ePTFE Enhancement.....	145
A.6	HA-LLDPE Enhancement.....	152
A.7	Water Contact Angle Goniometry: Captive Bubble Technique.....	159
A.8	Toluidine Blue O Staining Assay.....	163
A.9	Toluidine Blue Elution	165
A.10	TBO Elution Calculations	169
A.11	Pierce LDH Cytotoxicity Assay Protocol.....	172
A.12	Whole Blood Clotting/Free Hemoglobin Protocol.....	175
A.13	Platelet Activation	178
A.14	SEM Fixing.....	180
A.15	Calcein Staining	182

Chapter 1: Introduction

1.1 Motivation for Research

Synthetic polymers have been used as cardiovascular implants since 1952 when Vorhees developed the first vascular graft and Hufnagel designed the first ball and cage heart valve [1,2]. These early medical devices showed promising mechanical results. However, limited knowledge of their interaction with the body in the physiological environment led to a reiterative process in the field of testing different synthetic polymeric materials for cardiovascular devices [2,3]. The development of cardiovascular materials and, more specifically, polymers that can be used in cardiovascular devices is expanding. Polymers are large molecular weight, organic molecules consisting of repeating units, or mers, that are covalently bonded to each other. Synthetic polymers, without a doubt, have revolutionized the biomedical field [4].

Two polymers of great interest in the cardiovascular field are expanded polytetrafluorethylene (ePTFE) and linear low-density polyethylene (LLDPE) due to their high strength, ductility, and durability. Despite the many advantages of ePTFE and LLDPE, one of the main shortcomings of medical devices made from these two polymers is their inability to prevent adverse effects upon implantation and exposure to blood, such as thrombosis, the unwanted blood clotting that interferes with the function of the medical device (e.g., obstructs blood flow). The need for thrombotic resistant medical devices is further driven by the fact that heart disease is the number one killer in the industrialized world. By 2050, it is predicted that the number of patients worldwide who will require heart valve replacement is estimated to grow to over 850,000 annually [5]. Other cardiovascular complications such as atherosclerosis, myocardial infarction, and peripheral vascular disease also continue to be major causes of death in the United States being responsible for 31.9% of total mortality in 2010 [6]. Therefore, enhancement of polymers, such as LLDPE and

ePTFE, to make medical implants less thrombogenic is highly desirable. A potential solution is enhancing these synthetic polymers with hyaluronan (HA). HA has long been used in the biomedical field [7]. Modification of HA has been shown to promote hemocompatibility for synthetic polymers [8]. The following literature review provides background information regarding blood-material interactions, ePTFE, LLDPE, and HA.

1.2 Blood and Materials Interaction

1.2.1 The Coagulation Cascade

Figure 1.1 shows the coagulation cascade with the extrinsic and intrinsic pathways. The latter is also known as the contact activation pathway. Coagulations are usually triggered through the intrinsic pathway when blood interacts with foreign materials. The intrinsic pathway begins with activation of factor XII leading to activation of factor XI, IX, and then X. The extrinsic pathway occurs when tissue factor (TF) released from damaged cells activates factor VII, which then activates factor X. Although the extrinsic pathway is triggered upon vascular injury, both intrinsic and extrinsic pathways eventually lead to the activation of factor X where both pathways intersect. This is known as the common pathway. Factor X is activated when factor VIII, phospholipids, and calcium ions (Ca^{2+}) are present. After being activated, factor X cleaves prothrombin (factor II) transforming it to thrombin (factor IIa), which in turn converts fibrinogen (factor I) into fibrin. Once the initial fibrin strand is formed, factor XIII is activated by thrombin to crosslink fibrin polymers. The insoluble fibrin network then binds to activated platelets, white blood cells, and red blood cells to form red thrombus, ultimately leading to thrombosis [9–11].

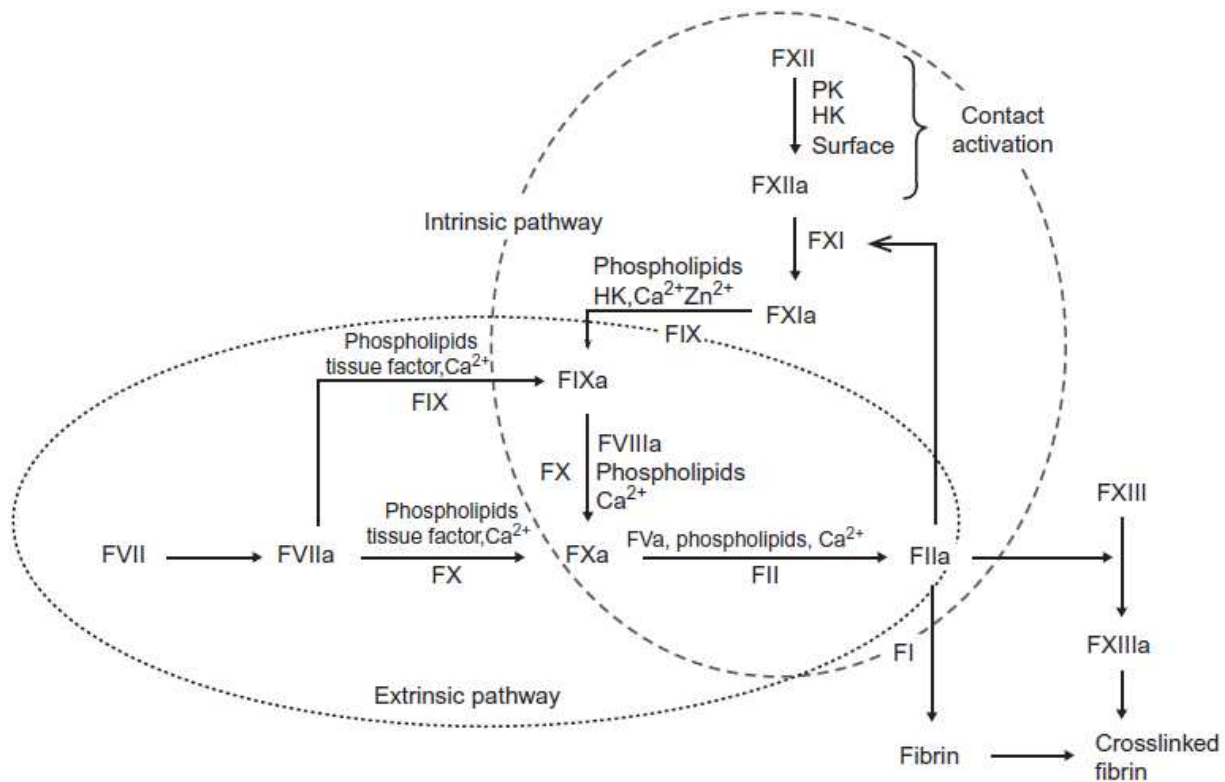


Figure 1.1: The intrinsic and extrinsic pathways in the coagulation cascade [11]. Reproduced with permission © 2018 Elsevier Ltd.

1.2.2 The Cell Based Model of Coagulation

Another model that has been proposed for triggering blood coagulation is the cell-based model, where cells play much more active roles than in the coagulation cascade. The cell-based model is the more updated system comparing to the coagulation cascade model, and it can be divided into the following phases: initiation, amplification, and propagation. During initiation, blood is exposed to tissue factor on cells not normally in contact with blood such as stromal fibroblast. The tissue factor can then bind to factor VII, creating a surface-bound tissue factor- factor VII activating complex (TF-FVIIa). The TF-FVIIa complex activates FIX and FX, and these two factors form a prothombinase complex that cleaves prothrombin (factor II) into thrombin (factor IIa). Thrombin catalyzes the conversion of fibrinogen to fibrin, but more importantly, it amplifies the coagulation

cascade. During amplification, thrombin activates platelets to create a thrombogenic surface on the cells. On the activated surface of platelets, the coagulation factors V and XI are activated by thrombin, and factor VIII is released by its carrier, von Willebrand factor. Factor XI activates factor IX, and the activated platelets bind to factors Va, VIIIa, and IXa. In the propagation phase, the factor VIIIa/IXa complex on platelets activates factor X, which in turn binds to platelets and form a complex with factor V (Xa/Va complex). Prothrombin is then activated by the Xa/Va complex, resulting in the proliferation thrombin. The “thrombin burst” leads to formation of fibrin strands crosslinked by activated factor XIII that creates a stable meshwork of fibrin with platelets [12–14]. Figure 1.2 shows the cell-based coagulation model. It shows the interconnection of the intrinsic and extrinsic pathways from the coagulation cascade model. The initiation phase, where the tissue factor is activated, is corresponded to the extrinsic pathway. Because of the activation of factors V, VIII, IX, and XI, the amplification phase is akin to the intrinsic pathway. As its name implies, the cell-based coagulation model is mediated by cells, and more specifically, platelets. Indeed, the activation of many coagulation factors occur on the surface of platelets, emphasizing the importance of the cell to the coagulation of blood.

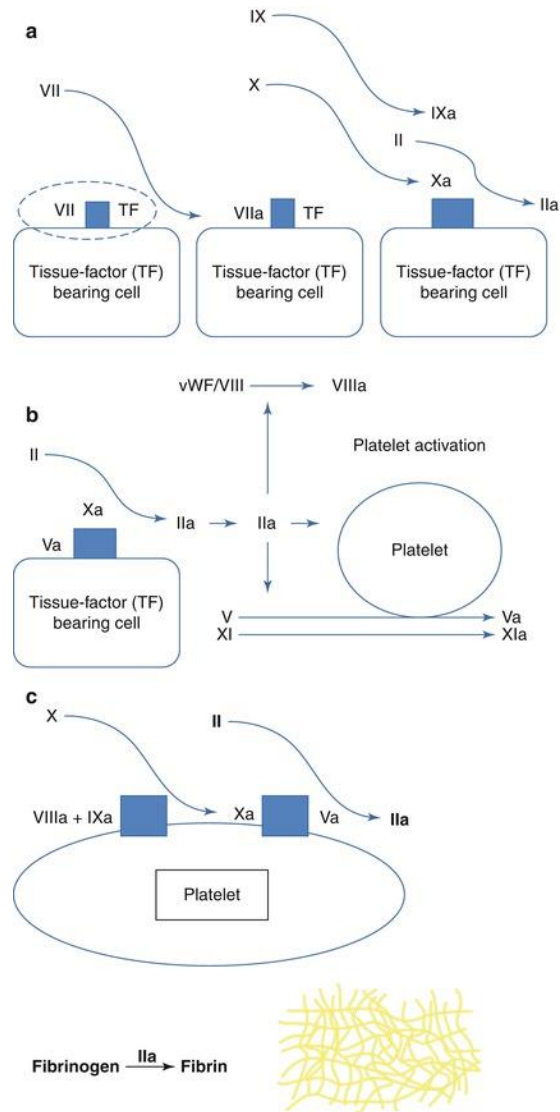


Figure 1.2: Schematic of the cell-based coagulation model. The initiation, amplification, and propagation phase are represented by a, b, and c, respectively. Reprinted with permission [12] © 2015, Springer-Verlag Berlin Heidelberg.

1.2.3 Platelets

As described in the cell-based model of coagulation, platelet play a critical role in blood coagulation [13]. Moreover, platelets are also important to primary hemostasis, where they become activated at vascular injury sites where they tether to damaged endothelium or exposed subendothelial layers [15]. They also interact with tissue factors from blood vessel damage to

trigger the extrinsic pathway [16]. Activated platelets secrete factors V, XI, XIII, prothrombin, phospholipids, and Ca^{2+} to further promote coagulation [17]. When factor VIIa is present, factor V can activate factor IX and act as a cofactor with factor X in the intrinsic pathway [18]. Activated platelets evidently create a positive feedback for blood clotting as they play a key role in hemostasis [10,11,18].

Platelets could bind to thrombogenic surfaces and get activated upon contact [19]. Their involvement begins with their adhesion to adsorbed proteins such as fibrinogen and the von Willebrand factor [20]. After contact, the adherent platelets change their shape from round to discoid and then to pseudopodal extension and full spreading. In the final stage, platelets release platelet factor 4, adenosine diphosphate, and serotonin to attract more platelets. The platelet surface glycoproteins Ib, and IIbIIIa can also bind to fibrinogen and to von willebrand factor. The recruitment of more platelets, along with the binding of coagulation proteins, leads to their aggregation and further coagulation [20].

1.2.4 Material Surface Properties

Wettability is known to affect the hemocompatibility of medical devices. A hydrophilic surface can tightly bind to water creating a water film that could act as a barrier between material and blood to prevent prothrombotic protein adsorption [21]. Figure 1.3 shows the adhesion force of factor XII and fibrinogen on plasma treated low density polyethylene (LDPE) with varying surface tension (τ). The data reveals that these proteins have a high binding affinity to an LDPE surface with water adhesion tension of less than 36 dyn/cm (τ), and the binding affinity decreases significantly with higher water adhesion tension. Surface tension can be related to water contacting at an angle in the equation $\tau = \gamma \cos(\theta_{adv})$ where γ is the water surface tension (72.8 dyn/cm) and

θ_{adv} is the advancing water contact angle. Based on this equation, a surface with an θ_{adv} of 65° has a low binding affinity for fibrinogen and factor XII [21,22].

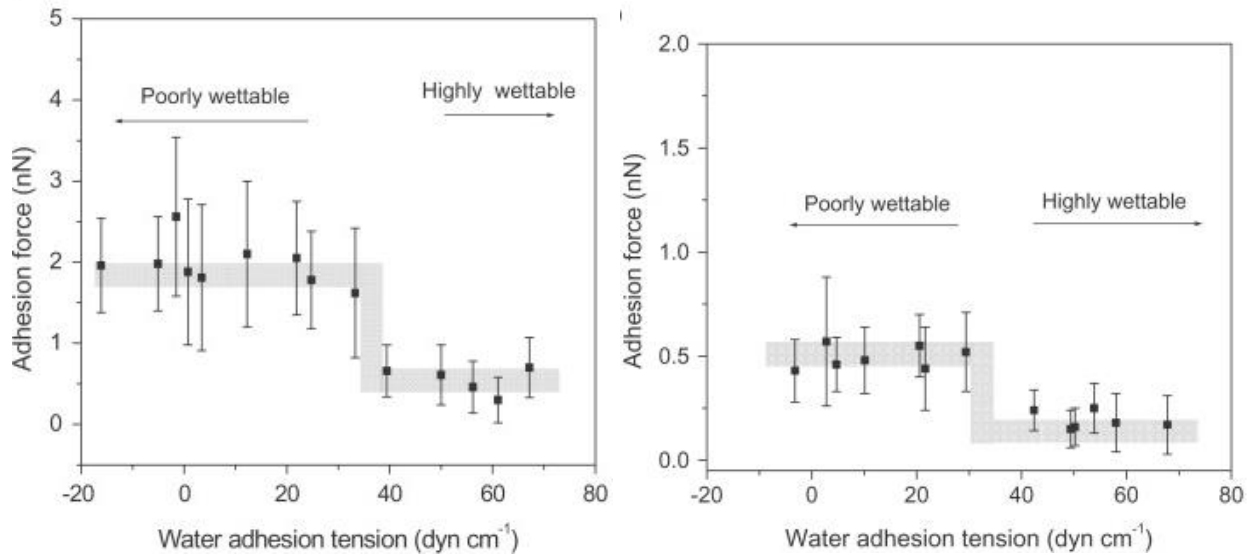


Figure 1.3: Reused with permission [22] © Elsevier Ltd. Adhesion force of fibrinogen (left) and human factor XII (right) on plasma treated LDPE surfaces with difference water adhesion tension. The decrease in adhesion force of the proteins are correspond to water adhesion tension (τ) of 36 dyn/cm, which corresponds to a 65° advancing water contact angle.

Surface functional groups of a material may also influence its blood compatibility. It is interesting to note that surface functional groups also correlate to wettability. -OH, -CONH₂, and -COOH are found on hydrophilic surfaces; whereas, -CH, -CF, -CN-, -OCH₃ are on hydrophobic ones [23]. Fibrinogen absorption and platelet adhesion have been shown to increase on -CH₃ containing surfaces, while this was observed significantly less on substrates with -COOH [24]. -OH, and -COOH groups are often utilized to enhance synthetic polymers for blood contact applications, because they are ubiquitous in naturally derived molecules that exist in physiological environments. These molecules include heparin, chondroitin sulfate, and hyaluronan, whose backbones often contain -OH and -COOH found at the extracellular space located between blood

and the endothelium [25,26]. Many commonly used synthetic polymers for biomedical applications tend to be hydrophobic and contain functional groups such as hydrocarbons and fluorocarbons [27]. Examples are polyethylene, polyesters, and PTFE. Therefore, surface enhancement to introduce -OH and -COOH on synthetic polymers have been implemented [28,29]. Surface topography and roughness are also important parameters that may affect the interaction of blood on foreign surfaces [20]. Surface roughness has been shown to correlate to platelet adhesion [30]. Studies have demonstrated that increasing surface roughness at the micron level increases platelet adhesion [31,32]. But an increasing roughness has also been demonstrated to promote adhesion of endothelial cells known to promote revascularization [33].

1.2.5 Current Solutions and Their Shortcomings

Carbon coating is a method developed in the 1960s that displayed how to improve the thromboresistance of synthetic medical devices. The high electronegativity of the carbon layer appeared to be inert and, in theory, can prevent adsorption of thrombogenic proteins. However, stability problems through carbide formation when iron is present were observed, and the hydrophobic carbon surface caused platelet adhesion [23]. Nevertheless, carbon coating is still being used for applications such as vascular grafts by Bard® under the trade name Carboflow [34]. Forming passivating protein layer on synthetic polymer is another technique still being implemented. Surface coating with albumin as a passivation strategy has shown to decrease platelet activation [61–63]. Albumin readily adsorbs to hydrophobic surfaces and it does not interact with platelets, leukocytes, or proteins of the coagulation cascades [64]. However, the immobilized albumin can be denatured upon entering the physiological environment and bind to

platelets. This can induce platelet activation [28]. The immobilized albumin can also be displaced by other proteins under a dynamic environment with high flow rate [23].

Heparin is a glycosaminoglycan (GAG) commonly coated on medical devices to reduce clotting upon blood contact [31,35]. Heparin is a known thrombin inhibitor and an anticoagulant. However, research has also shown that heparin can induce thrombocytopenia (HIT), a disorder characterized by more than 50% reduction in platelets [36,37]. During HIT, heparin may bind to platelet factor 4 (PF₄) released by activated platelets. This attracts PF₄/heparin-specific antibodies. Upon binding of these antibodies to the PF₄/heparin complexes, more platelets become activated to release more PF₄ creating a positive feedback that amplifies the clotting cascade. Not surprisingly, heparin has had mixed results in medical device applications [38].

To date, anticoagulant therapy (ACT) and antiplatelet therapy (APT) are still routinely used as part of medical device implantation. Table 1-1 shows examples of ACT and APT. Administering these drugs requires understanding of possible complications. Overdosage can lead to bleeding or thrombotic complications such as HIT. In addition, each ACT and APT does not fully suppress adverse coagulations [39]. As seen in Table 1-1, each treatment blocks the coagulation pathways differently at specific points, while the action of the other pathways may continue unhindered. A striking example is the activation of platelets when citrate anticoagulants are administered over a period of hours [19,39,40].

Table 1-1: List of bioactive components used in surface modification of biomedical devices. Used with permission [23] © 2018 Elsevier Ltd.

Bioactive component	Properties and action
Coagulation inhibitors	
Heparin	Negatively charged sulfated polysaccharide Catalyzes the inhibitory activity of antithrombin III against thrombin and FXa
Hirudin	Polypeptide from <i>Hirudo medicinalis</i> Direct thrombin inhibitor
Argatroban	Direct thrombin inhibitor
Benzamidine	Direct inhibitor of thrombin and other coagulation factors
Thrombomodulin	Membrane protein of endothelial cells Changes substrate specificity of thrombin for activation of anticoagulant protein C
Platelet inhibitors	
Dipyridamole	Vasodilator Platelet inhibitor that blocks ADP receptor
Prostacyclin	Platelet aggregation inhibitor with specific receptor
Apyrase	Decreases platelet activation and adhesion through ADP degradation
Abciximab, Tirofiban	Platelet inhibitor, GPIIb/IIIa receptor blocker
Other inhibitors	
Paclitaxel	Antiproliferative agents
Rapamycin (Sirolimus)	
Diazoniumdiolate (Nitric oxide release)	Cellular signaling molecule Inhibitor of smooth muscle cells and platelet activation
Plasmin/PA	Fibrinolytic blood enzyme Binds Lys-residues exposed during fibrin degradation
DNA	Plasmids and viruses used as vectors Targets: antithrombotic and antiproliferative genes, genes for reendothelialization

1.3 Expanded Polytetrafluoroethylene

ePTFE, or expanded Teflon®, has long been used for biomedical applications [41,42]. One of the earliest devices made from ePTFE was a heart valve [43], but this application was discontinued because the ePTFE leaflets were prone to stiffening due to calcification [44]. Nevertheless, ePTFE is popular due to its low cost, tunability, inertness, and ease of handling [27,41]. ePTFE is highly inert due to its strong C-F bonds along the C-C backbone of the polymer (Figure 1.4), which also makes it resistant to biodegradation [45,46]. Compared to other synthetic polymers, ePTFE has

one of the least thrombogenic surfaces. It is currently the leading material for vascular graft applications [27,47]. Table 1-2 contains examples of commercially available medical devices made of ePTFE that involve blood-material interaction.

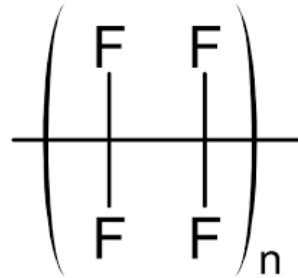


Figure 1.4: Chemical structure of PTFE.

Table 1-2: Medical applications of ePTFE that involves blood-material interactions.

Applications	References
Vascular grafts	[48]
Tissue patch for bony chest wall reconstruction	[49]
Suture materials	[50]
Septal occluders	[51]
Pericardial patches	[50]
Right ventricular outflow tract reconstruction	[52,53]
Artificial cord for mitral valve repair, also called Harpoon Mitral Valve Repair System (H-MVRS)	[54]
Hernia membrane	[55]

Although it is popular in the biomedical field, vascular grafts made from ePTFE are known to promote protein adsorption and platelet activation, which causes graft failure from thrombosis [56]. Large diameter (>8mm) synthetic vascular grafts can overcome thrombosis with a high blood flow rate, but surgical revision is still common with a five-year primary patency rate as low as

56% [47,57]. For small diameter (<6mm) synthetic vascular grafts, occlusion is more prevalent [41,57,58]. The five-year patency rate for small vascular grafts can be lower than 30% [47]. Furthermore, ePTFE is a poor surface for endothelial cell adhesion, which deprives the biomaterials of a naturally anti-thrombogenic endothelial lining [56]. Extensive work has focused on enhancing ePTFE to improve its hemocompatibility [41]. Table 1-3 shows commercially available medical products of modified ePTFE grafts that improve hemocompatibility. Researchers have tried to improve patency rate of ePTFE grafts through surface modification [59,60]. Examples included a poly (1,8-octanediol citrate) (POC) degradable elastomer that was coated on the inner lumen of ePTFE graft showing an increase in patency rate from a one-week in vivo study of iliac artery bypass model in pigs [61]. Similar results were found when heparin was coated on the POC-ePTFE layer [59].

Table 1-3: Surfaced modified ePTFE grafts currently on the market.

Commercial name	Technology	References
Jotec® Flowline Bipore	Heparin coating	[62]
Gore® Propaten	Heparin coating	[62,63]
Maquet Cardiovascular® Fusion Bioline	Albumin and heparin coating	[64]
Bard® Carboflow	Carbon coating	[34]

1.4 Linear Low-Density Polyethylene

Polyolefins such as polypropylene (PP) and polyethylene (PE) are widely utilized in the biomedical fields [55,65,66]. They are inert and do not degrade in vivo [27]. Nonetheless, polyolefins are rarely being used in the cardiovascular field. The main drawback of these materials is their methyl (-CH₃) functional groups and the hydrocarbons create a hydrophobic surface, which promotes the adhesion of fibrinogen, immunoglobulin G, and platelets. This leads to poor

hemocompatibility and increasing inflammatory responses because the bound proteins also attract inflammatory cells [67,68].

Although polyethylene is not known for its hemocompatibility, existing research is aiming at using linear low density polyethylene (LLDPE) to produce flexible heart valve leaflets for transcatheter and surgical heart valve design [8,69]. The left image of Figure 1.5 shows the chemical structure of LLDPE, typical of polyethylene, where the C-C backbone is covered by alkanes created by the hydrogen-carbon bonds. What distinguishes LLDPE from other forms of polyethylene such as high-density polyethylene (HDPE) and low-density polyethylene (LDPE) is the prevalence of spherulitic microstructures within the polymeric network of LLDPE (right image of Figure 1.5). Like most thermoplastics, LLDPE consists of crystalline and amorphous regions. The crystalline portion forms lamellar structure, but the linearity of LLDPE allows for the lamellae to orient into many spherulitic microstructures. This feature leads to more isotropic tensile properties for LLDPE in both machine and transverse directions with respect to the orientation of the film during material manufacturing [70].

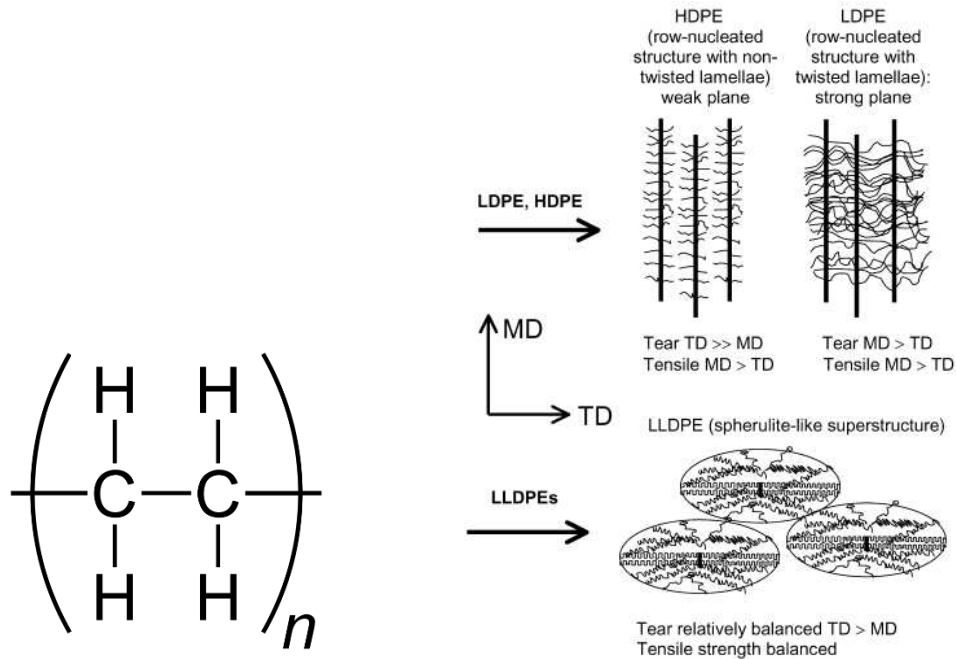


Figure 1.5: Chemical structure polyethylene (left) and microstructure of LLDPE (right) comparing to HDPE and LDPE. MD and TD stand for machine and transverse direction, respectively. These directions indicate the orientation of the polyethylene film during blow extrusion. Right image was reproduced with permission [70] © Elsevier Ltd.

Thanks to the flexibility and durability of LLDPE, flexible heart valve leaflets made from the polymer were shown to be hemodynamic. Hyaluronan (HA) enhancement of the LLDPE leaflets further reduced its thrombogenic potential [8,71]. HA was incorporated into LLDPE creating an interpenetrating polymer network (IPN) of HA and the base polymer. More specifically, a sequential IPN is designed based on known properties of LLDPE and modification of high molecular weight hyaluronan. In this system, LLDPE is the “host” polymer for the synthesis of the sequential IPN, and HA is the “guest” polymer introduced into the LLDPE by the swelling of the polyethylene [72,73]. HA is fixed in position by crosslinking it to itself after it is interpenetrated into the amorphous regions of the thermoplastic LLDPE. Despite the lack of chemical bond between the “host” and the “guest,” the durability of an IPN comes from the physical entanglement of two polymeric networks [73].



Figure 1.6: HA treated surgical (left) and transcatheter (right) heart valves containing flexible leaflets made from LLDPE [74].

1.5 Hyaluronan

1.5.1 Structure and Components

Hyaluronan (HA) is a naturally derived, anionic polysaccharide with no branching; it is the only known nonsulfated glycosaminoglycan (GAG) [75]. Under physiological conditions, the average molecular weight (MW) of HA ranges from 10 kDa up to 13,000 kDa [76]. Its conformation is highly dynamic depending on counter ions, pH, temperature, and humidity [77]. The hydrodynamic morphology also depends on the molecular weight. In physiological saline solutions, HA with molecular weight below 37.5 kDa is nearly rod like; whereas, higher MW HA molecules are weakly coiled. MWs higher than 100 kDa give rise to spherical like HA chains, which exist as crowded random coil molecules constantly rearrange and create a large hydrodynamic radius [78]. Computational modeling shows that intramolecular hydrogen bonds exist across the glycosidic linkages, and these bonds stabilize the chain conformation in low energy regions [77,79]. Its molecular length and structure are also influenced by the β -(1-4) and β -(1-3) linkages making it very mobile [80].

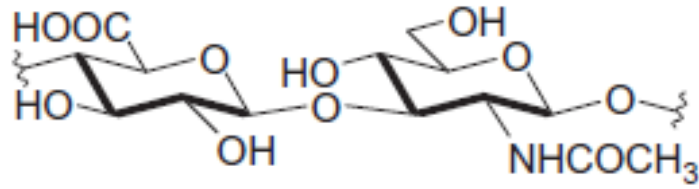


Figure 1.7: Chemical structure of hyaluronan

HA can be found in many places in the human body. Human knee joint synovial fluid contains approximately 2 to 3 mg/ml of HA. The HA concentration in human serum is usually less than 40 ng/ml, with the MW ranging between 100 and 500 kDa. Normal human urine contains HA at a concentration of about 100–300 ng/ml [78]. In mammals, HA synthesis occurs at the cellular membrane and is extruded into extracellular space [75,78]. HA is created through hyaluronan synthase 1, 2, and 3. HA is present in extracellular matrix both in a soluble form and in a covalently bond to a variety of proteins such as proteoglycans (brevican, neurocan, and versican) and SHAP (serum-derived hyaluronan-associated protein) [81,82]. HA is an integral part of the glycocalyx layer located between the endothelium layer and the blood flow in blood vessels [25,83].

1.5.2 The Role of Hyaluronan in the Endothelial Glycocalyx Layer

Hyaluronic acid (HA) is an integral part of the endothelial glycocalyx (EG) layer located between the endothelium layer and the blood flow in blood vessels [83]. HA is involved in EG structural integrity and function [7]. HA also helps regulate proliferation and alignment of endothelial cells under flow [84], reduces blood shear on the surface of the EG [85], and induces vasodilation by controlling nitric oxide production [86,87]. In addition, HA has demonstrated anti-inflammatory properties by acting as a barrier preventing leukocyte adhesion and activation on the EG [88].

The molecular weight of HA affects its biological functions [89]. High molecular weight (HMW) HA (>300 kDa) exists in healthy blood vessels, but excess HMW HA may inhibit adhesion of endothelial cell proliferation and migration [90]. An abundance of HMW HA may attract hyaluronidases to cleave the HA into LMW HA that can induce inflammation, thrombus formation, and promote the growth of pathological smooth muscle cells [90]. On the other hand, HMW-HA has been shown to reduce blood clotting and inflammation on synthetic surfaces of biomaterials [91,92]. Overall, there exists many diverse, sometimes dual, roles of HA [7].

Although LMW HA can induce inflammation, it has been demonstrated to promote angiogenesis by controlling the vascular endothelial cell factor expression leading to growth and proliferation of endothelial cells [93,94]. Moreover, LMW HA activates HA-binding proteins that promote actin cytoskeleton reorganization for endothelial cell-cell contacts [94]. It is not surprising that inhibition of hyaluronan synthesis leads to the disappearance of the EG layer and a rise in plaque areas. This is typical of cardiovascular complications such as atherosclerosis [95,96]. Due to its therapeutic properties, LMW-HA has been used in regenerative medicine to promote wound healing, tissue engineering, and various cardiovascular applications (Table 1-4).

Despite its importance in the blood vessels, hyaluronan can accumulate during vascular complications such as diabetic glomerulosclerosis, hyperlipidemia, and atherosclerosis. A striking example is the role of HA during fibrin formation. In such cases fibrin products bind to HA to maintain a local concentration of HA [97]. Nevertheless, the buildup of HA from vascular pathologies is indicative of dysregulation of HA where there is an unbalanced hyaluronidase to hyaluronan synthase ratio. In addition, a unique protein modification occurs on HA forming a pathological heavy chain-hyaluronan (HC-HA) complex that is not observed in healthy tissue [98].

1.5.3 Hyaluronan in Biomedical Research for Cardiovascular Applications

Although a GAG like heparin, the antithrombotic mechanism of HA, is different from that of heparin [99]. As described in Section 1.5.2, HA is a multi-functional polysaccharide with many roles in the cardiovascular system. Furthermore, studies have shown HA has bacteriostatic properties that make it an attractive biomaterial [100]. Much research has been devoted to developing HA for cardiovascular applications. For example, chitosan-hyaluronan/silk fibroin patches in the treatment of myocardial infarction promoted angiogenesis and the stimulation of vascular endothelial growth factors [101]. Table 1-4 shows more examples of recent work involving HA.

Table 1-4: Recent usage of hyaluronan in biomedical research for blood-material interactions.

Material	Linkage	HA MW	Applications	Results	Reference
HA/Dopamine coated stainless steel	carbodiimide - based linking chemistry of HA (COOH) and dopamine (NH)	4 kDa to 7 MDa	Multifunctional, hemocompatible surfaces with desirable vascular cell-material interaction	Decreasing surface roughness, platelet activation and adhesion, Increasing human umbilical vascular endothelial cell adhesion in the presence of dopamine with optimum at 100 kDa	[102,103]
methacrylated HA and methacrylated gelatin scaffold reinforced by	UV crosslinking of HA and gelatin, that were mixed blended with	7.52×10^5 kDa	Tissue engineering heart valves	improved 3D distribution and spreading of mitral valvular	[104]

electrospun poly(glycerol sebacate) poly(caprolactone) microfiber	PS-PCL forming one scaffold			interstitial cells.	
Shear thinning HA hydrogels	Guest-host complexation of modified HA to form a hydrogel	74 kDa	tissue-engineered injectables for minimizing post ischemic remodeling	reducing adverse myocardial remodeling and preservation of myocardial biomechanics when HA gel mixed with endothelial progenitor cells were injected into ischemic rat myocardium	[105,106]
HA-PEG RGDS hydrogels	Photo crosslinking of HA and RGDS conjugated PEG	35 kDa	Tissue engineered heart valve scaffolds	promotes the quiescent, healthy phenotype of vascular interstitial cells in 3D culture	[107]
HA-polyurethane copolymer scaffold	carbodiimide - based linking chemistry of HA (COOH) and segmented polyurethane (NH ₂)	4.7 kDa 9.7 kDa 64 kDa 104 kDa	Small diameter vascular grafts	In both static and dynamic tests, HA-PU resists protein adsorption, platelet adhesion, and bacterial adhesion, while supporting endothelial cell culture (optimum at 4.7 kDa) Hydrophilic	[99,100,108]

HA-SH coated PU films	Coating of PU films with polydopamine/ HA, where HA-SH complexed with octadecyl acrylate (C18) through “click reaction” of thiol groups (SH) and the alkene of C18	330 kDa	Antimicrobial and blood compatible biomaterial coating through selective binding of albumin (passivant protein). C18 works as binding agent.	Albumin passivated HA/dopamine PU surface reduces platelet activation, fibrinogen adsorption, and bacterial adhesion.	[109]
HA-PMEO ₂ MA coating on Teflon substrate	Amidation of HA (COOH) and PMEO ₂ MA (NH ₂)	1.6 MDa	Passivating surfaces of hydrophobic biomaterials.	Hydrophilic Reduction in fibrinogen and immunoglobulin adsorption.	[91]
Gellan gum-HA spongy-like hydrogel	Semi-interpenetrating polymer network of HMW HA and gellan gum. HA entangled in crosslinked gellan gum	1.5 MDa	Angiogenesis	Neovascularization in ischemic hind limb mice model	[92]

1.6 Objectives and Specific Aims

The many properties of HA and its long use in the biomedical field demonstrate that HA could improve hemocompatibility through lowering thrombogenicity. Much work has been put forth to enhance blood contacting synthetic polymers with hyaluronan for cardiovascular applications (Table 1-4). ePTFE is one of the least thrombogenic polymers with excellent mechanical performance, yet patency rates for small diameter vascular grafts is low [58]. LLDPE has shown to have good mechanical properties for flexible heart valve leaflet application, but they are prone to cause thrombosis. Therefore, this research aspires to create HA enhanced ePTFE and LLDPE biomaterials that are blood compatible while retaining their mechanical properties. Due to the vastly different material properties of ePTFE and LLDPE, their HA enhancement methods will be different. For ePTFE, the penetration of HA into the base polymer can be done by wicking the polysaccharide into the porous ePTFE. In the case of LLDPE, the polyolefin can be swollen to diffuse HA into the synthetic polymer. The objective of this dissertation is to explore two new methods of enhancing LLDPE and ePTFE with HA that can be used as biomaterials for cardiovascular applications. This is a process driven research that aims at analyzing the fabrication methods by adjusting various process parameters, characterizing the developing biomaterials, and performing preliminary in vitro assay to assess their thrombogenic potential. The proposed research expands on previous work described elsewhere [110–112]. The specific aims are listed below with each being addressed in each subsequent chapter of this dissertation.

1. Fabricate and characterize HA enhanced ePTFE by adjusting the spray coating parameters used on the ePTFE grafts and determining how fabrication process affects the materials properties.

2. Fabricate and characterize HA enhanced LLDPE through understanding the swelling properties of LLDPE, exploring a novel vapor crosslinking method, and determining how the fabrication process affects the material properties.
3. Evaluate the in vitro biological assessment of HA enhanced ePTFE and LLDPE with a focus on thrombogenicity.

References

- [1] A.B. Voorhees Jr, A.H.B. Alfred Jaretzki III, The use of tubes constructed from vinyon “N” cloth in bridging arterial defects: a preliminary report, *Annals of Surgery*. 135 (1952) 332.
- [2] V.L. Gott, D.E. Alejo, D.E. Cameron, Mechanical heart valves: 50 years of evolution, *The Annals of Thoracic Surgery*. 76 (2003) S2230–S2239.
- [3] P. Zilla, D. Bezuidenhout, P. Human, Prosthetic vascular grafts: wrong models, wrong questions and no healing, *Biomaterials*. 28 (2007) 5009–5027.
- [4] B.D. Ratner, S.J. Bryant, Biomaterials: where we have been and where we are going, *Annu. Rev. Biomed. Eng.* 6 (2004) 41–75.
- [5] M.H. Yacoub, J.J.M. Takkenberg, Will heart valve tissue engineering change the world?, *Nat Clin Pract Cardiovasc Med*. 2 (2005) 60–61.
- [6] A.S. Go, D. Mozaffarian, V.L. Roger, E.J. Benjamin, J.D. Berry, M.J. Blaha, S. Dai, E.S. Ford, C.S. Fox, S. Franco, Executive summary: heart disease and stroke statistics–2014 update: a report from the American Heart Association., *Circulation*. 129 (2014) 399.
- [7] K.T. Dicker, L.A. Gurski, S. Pradhan-Bhatt, R.L. Witt, M.C. Farach-Carson, X. Jia, Hyaluronan: A simple polysaccharide with diverse biological functions, *Acta Biomaterialia*. 10 (2014) 1558–1570. doi:10.1016/j.actbio.2013.12.019.
- [8] D.A. Prawel, H. Dean, M. Forleo, N. Lewis, J. Gangwish, K.C. Popat, L.P. Dasi, S.P. James, Hemocompatibility and hemodynamics of novel hyaluronan–polyethylene materials for flexible heart valve leaflets, *Cardiovascular Engineering and Technology*. 5 (2014) 70–81.
- [9] J. Sira, L. Eyre, Physiology of haemostasis, *Anaesthesia & Intensive Care Medicine*. 17 (2016) 79–82. doi:10.1016/j.mpaic.2015.11.004.
- [10] S.K. Austin, Haemostasis, *Medicine*. 45 (2017) 204–208. doi:10.1016/j.mpmed.2017.01.013.
- [11] Y. Yan, L.-C. Xu, E.A. Vogler, C.A. Siedlecki, Contact activation by the intrinsic pathway of blood plasma coagulation, in: *Hemocompatibility of Biomaterials for Clinical Applications*, Elsevier, 2018: pp. 3–28. doi:10.1016/B978-0-08-100497-5.00001-X.

- [12] C. Sucker, R.B. Zotz, The Cell-Based Coagulation Model, in: C.E. Marcucci, P. Schoettker (Eds.), *Perioperative Hemostasis: Coagulation for Anesthesiologists*, Springer Berlin Heidelberg, Berlin, Heidelberg, 2015: pp. 3–11. doi:10.1007/978-3-642-55004-1_1.
- [13] M. Hoffman, R. Pawlinski, Hemostasis: Old System, New Players, New Directions, *Thrombosis Research*. 133 (2014) S1–S2. doi:10.1016/j.thromres.2014.03.001.
- [14] M. McMichael, New Models of Hemostasis, *Topics in Companion Animal Medicine*. 27 (2012) 40–45. doi:10.1053/j.tcam.2012.07.005.
- [15] K.J. Clemetson, Platelets and Primary Haemostasis, *Thrombosis Research*. 129 (2012) 220–224. doi:10.1016/j.thromres.2011.11.036.
- [16] M.T. Kalathottukaren, J.N. Kizhakkedathu, Mechanisms of blood coagulation in response to biomaterials: Extrinsic factors, in: *Hemocompatibility of Biomaterials for Clinical Applications*, Elsevier, 2018: pp. 29–49. doi:10.1016/B978-0-08-100497-5.00003-3.
- [17] E.M. Golebiewska, A.W. Poole, Platelet secretion: From haemostasis to wound healing and beyond, *Blood Reviews*. 29 (2015) 153–162. doi:10.1016/j.blre.2014.10.003.
- [18] L. Jobling, L. Eyre, Haemostasis, blood platelets and coagulation, *Anaesthesia & Intensive Care Medicine*. 14 (2013) 51–53. doi:10.1016/j.mpaic.2012.12.001.
- [19] I. Reviakine, F. Jung, S. Braune, J.L. Brash, R. Latour, M. Gorbet, W. van Oeveren, Stirred, shaken, or stagnant: What goes on at the blood–biomaterial interface, *Blood Reviews*. 31 (2017) 11–21. doi:10.1016/j.blre.2016.07.003.
- [20] X. Liu, L. Yuan, D. Li, Z. Tang, Y. Wang, G. Chen, H. Chen, J.L. Brash, Blood compatible materials: state of the art, *J. Mater. Chem. B*. 2 (2014) 5718–5738. doi:10.1039/C4TB00881B.
- [21] L.-C. Xu, J.W. Bauer, C.A. Siedlecki, Proteins, platelets, and blood coagulation at biomaterial interfaces, *Colloids and Surfaces B: Biointerfaces*. 124 (2014) 49–68.
- [22] L.-C. Xu, C.A. Siedlecki, Effects of surface wettability and contact time on protein adhesion to biomaterial surfaces, *Biomaterials*. 28 (2007) 3273–3283. doi:10.1016/j.biomaterials.2007.03.032.

- [23] M. Fischer, M.F. Maitz, C. Werner, Coatings for biomaterials to improve hemocompatibility, in: *Hemocompatibility of Biomaterials for Clinical Applications*, Elsevier, 2018: pp. 163–190. doi:10.1016/B978-0-08-100497-5.00007-0.
- [24] C. Sperling, M. Fischer, M.F. Maitz, C. Werner, Blood coagulation on biomaterials requires the combination of distinct activation processes, *Biomaterials*. 30 (2009) 4447–4456. doi:10.1016/j.biomaterials.2009.05.044.
- [25] L.N. Broekhuizen, H.L. Mooij, J.J. Kastelein, E.S. Stroes, H. Vink, M. Nieuwdorp, Endothelial glycocalyx as potential diagnostic and therapeutic target in cardiovascular disease:, *Current Opinion in Lipidology*. 20 (2009) 57–62. doi:10.1097/MOL.0b013e328321b587.
- [26] M. Rinaudo, Main properties and current applications of some polysaccharides as biomaterials, *Polymer International*. 57 (2008) 397–430. doi:10.1002/pi.2378.
- [27] M.F. Maitz, Applications of synthetic polymers in clinical medicine, *Biosurface and Biotribology*. 1 (2015) 161–176. doi:10.1016/j.bsbt.2015.08.002.
- [28] B. Sivaraman, R.A. Latour, The Adherence of platelets to adsorbed albumin by receptor-mediated recognition of binding sites exposed by adsorption-induced unfolding, *Biomaterials*. 31 (2010) 1036–1044. doi:10.1016/j.biomaterials.2009.10.017.
- [29] M. Modic, I. Junkar, K. Stana-Kleinschek, R. Kostanjšek, M. Mozetič, Morphology Transformations of Platelets on Plasma Activated Surfaces, *Plasma Processes and Polymers*. 11 (2014) 596–605. doi:10.1002/ppap.201400001.
- [30] P. Parhi, A. Golas, E.A. Vogler, Role of proteins and water in the initial attachment of mammalian cells to biomedical surfaces: a review, *Journal of Adhesion Science and Technology*. 24 (2010) 853–888.
- [31] S. Lamichhane, J.A. Anderson, T. Remund, H. Sun, M.K. Larson, P. Kelly, G. Mani, Responses of endothelial cells, smooth muscle cells, and platelets dependent on the surface topography of polytetrafluoroethylene, *Journal of Biomedical Materials Research Part A*. 104 (2016) 2291–2304.
- [32] S. Braune, A. Hönow, C. Mrowietz, J. Cui, K. Kratz, J. Hellwig, C. Üzüüm, R.V. Klitzing, A. Lendlein, F. Jung, Hemocompatibility of soft hydrophobic poly (n-butyl acrylate) networks with elastic moduli adapted to the elasticity of human arteries, *Clinical Hemorheology and Microcirculation*. 49 (2011) 375–390.

- [33] K. Zhang, J. Chen, W. Qin, J. Li, F. Guan, N. Huang, Constructing bio-layer of heparin and type IV collagen on titanium surface for improving its endothelialization and blood compatibility, *J Mater Sci: Mater Med.* 27 (2016) 81. doi:10.1007/s10856-016-5693-6.
- [34] J.M. McHaney, C.E. Banas, Carbon containing vascular graft and method of making same, US5827327A, 1998. <https://patents.google.com/patent/US5827327A/en?q=carbon&q=coat&assignee=bard&oq=assignee:bard+carbon+coat> (accessed March 10, 2019).
- [35] R.A. Hoshi, R. Van Lith, M.C. Jen, J.B. Allen, K.A. Lapidos, G. Ameer, The blood and vascular cell compatibility of heparin-modified ePTFE vascular grafts, *Biomaterials.* 34 (2013) 30–41.
- [36] J.G. Kelton, T.E. Warkentin, Heparin-induced thrombocytopenia: a historical perspective, *Blood.* 112 (2008) 2607 LP – 2616.
- [37] C. Gao, B. Boylan, J. Fang, D.A. Wilcox, D.K. Newman, P.J. Newman, Heparin promotes platelet responsiveness by potentiating α IIb β 3-mediated outside-in signaling, *Blood.* 117 (2011) 4946 LP – 4952.
- [38] S. Sukavaneshvar, Device thrombosis and pre-clinical blood flow models for assessing antithrombogenic efficacy of drug-device combinations, *Advanced Drug Delivery Reviews.* 112 (2017) 24–34. doi:<https://doi.org/10.1016/j.addr.2016.07.009>.
- [39] Schneider David J., Tracy Paula B., Mann Kenneth G., Sobel Burton E., Differential Effects of Anticoagulants on the Activation of Platelets Ex Vivo, *Circulation.* 96 (1997) 2877–2883. doi:10.1161/01.CIR.96.9.2877.
- [40] S. Braune, M. Walter, F. Schulze, A. Lendlein, F. Jung, Changes in platelet morphology and function during 24 hours of storage, *Clinical Hemorheology & Microcirculation.* 58 (2014) 159–170. doi:10.3233/CH-141876.
- [41] A.I. Cassady, N.M. Hidzir, L. Grøndahl, Enhancing expanded poly(tetrafluoroethylene) (ePTFE) for biomaterials applications, *Journal of Applied Polymer Science.* 131 (2014) n/a-n/a. doi:10.1002/app.40533.
- [42] P. Roy-Chaudhury, M. El-Khatib, B. Campos-Naciff, D. Wadehra, K. Ramani, M. Leesar, M. Mistry, Y. Wang, J. Chan, T. Lee, Back to the future: how biology and technology could change the role of PTFE grafts in vascular access management, in: *Seminars in Dialysis*, Wiley Online Library, 2012: pp. 495–504.

- [43] W.H. Muller, W.D. Warren, J.F. Dammann, J.R. Beckwith, J.E. Wood, Surgical Relief of Aortic Insufficiency by Direct Operation on the Aortic Valve, *Circulation*. 21 (1960) 587–597. doi:10.1161/01.CIR.21.4.587.
- [44] F. Nistal, V. Garciamartinez, E. Arbe, D. Fernandez, E. Artinano, F. Mazorra, I. Gallo, In vivo Experimental Assessment of Polytetrafluoroethylene Trileaflet Heart-Valve Prosthesis, *J. Thorac. Cardiovasc. Surg.* 99 (1990) 1074–1081.
- [45] G.J. Puts, P. Crouse, B.M. Ameduri, Polytetrafluoroethylene: Synthesis and Characterization of the Original Extreme Polymer, *Chemical Reviews*. 119 (2019) 1763–1805. doi:10.1021/acs.chemrev.8b00458.
- [46] M.A. Hiob, S. She, L.D. Muiznieks, A.S. Weiss, Biomaterials and Modifications in the Development of Small-Diameter Vascular Grafts, *ACS Biomaterials Science & Engineering*. 3 (2017) 712–723. doi:10.1021/acsbiomaterials.6b00220.
- [47] H. Takagi, S. Goto, M. Matsui, H. Manabe, T. Umemoto, A contemporary meta-analysis of Dacron versus polytetrafluoroethylene grafts for femoropopliteal bypass grafting, *Journal of Vascular Surgery*. 52 (2010) 232–236. doi:10.1016/j.jvs.2010.02.010.
- [48] M. Tozzi, M. Franchin, G. Ietto, G. Soldini, G. Carcano, P. Castelli, G. Piffaretti, Initial Experience with the Gore® Acuseal Graft for Prosthetic Vascular Access, *J Vasc Access*. 15 (2014) 385–390. doi:10.5301/jva.5000276.
- [49] H. Huang, K. Kitano, K. Nagayama, J. Nitadori, M. Anraku, T. Murakawa, J. Nakajima, Results of Bony Chest Wall Reconstruction with Expanded Polytetrafluoroethylene Soft Tissue Patch, *Annals of Thoracic and Cardiovascular Surgery*. 21 (2015) 119–124. doi:10.5761/atcs.0a.14-00195.
- [50] P. Bristow, J. Sargent, V. Luis Fuentes, D. Brockman, Surgical treatment of pulmonic stenosis in dogs under cardiopulmonary bypass: outcome in nine dogs: Surgical treatment of pulmonic stenosis, *Journal of Small Animal Practice*. 59 (2018) 38–44. doi:10.1111/jsap.12793.
- [51] S.E. Hardt, A. Eicken, F. Berger, S. Schubert, M. Carminati, G. Butera, J. Grohmann, R. Höhn, J.E. Nielsen-Kudsk, D. Hildick-Smith, M. Settergren, J.D. Thomson, N. Geis, L. Søndergaard, Closure of patent foramen ovale defects using GORE® CARDIOFORM septal occluder: Results from a prospective European multicenter study: GSO European Study, *Catheterization and Cardiovascular Interventions*. 90 (2017) 824–829. doi:10.1002/ccd.26993.

- [52] M. Yamagishi, Right Ventricular Outflow Reconstruction Using a Polytetrafluoroethylene Conduit With Bulging Sinuses and Tricuspid Fan-shaped Polytetrafluoroethylene Valve, Operative Techniques in Thoracic and Cardiovascular Surgery. 21 (2016) 211–229. doi:10.1053/j.optechstcvs.2017.05.002.
- [53] T. Miyazaki, M. Yamagishi, Y. Maeda, S. Taniguchi, S. Fujita, H. Hongu, H. Yaku, Long-term outcomes of expanded polytetrafluoroethylene conduits with bulging sinuses and a fan-shaped valve in right ventricular outflow tract reconstruction, The Journal of Thoracic and Cardiovascular Surgery. 155 (2018) 2567–2576. doi:10.1016/j.jtcvs.2017.12.137.
- [54] J.S. Gammie, K. Bartus, A. Gackowski, M.N. D’Ambra, P. Szymanski, A. Bilewska, M. Kusmierczyk, B. Kapelak, J. Rzucidlo-Resil, N. Moat, A. Duncan, R. Yadev, S. Livesey, P. Diprose, G. Gerosa, A. D’Onofrio, D. Pitterello, P. Denti, G. La Canna, M. De Bonis, O. Alfieri, J. Hung, P. Kolsut, Beating-Heart Mitral Valve Repair Using a Novel ePTFE Cordal Implantation Device, Journal of the American College of Cardiology. 71 (2018) 25–36. doi:10.1016/j.jacc.2017.10.062.
- [55] U. Klinge, B. Klosterhalfen, Modified classification of surgical meshes for hernia repair based on the analyses of 1,000 explanted meshes, Hernia. 16 (2012) 251–258. doi:10.1007/s10029-012-0913-6.
- [56] M. Tatterton, S.-P. Wilshaw, E. Ingham, S. Homer-Vanniasinkam, The use of antithrombotic therapies in reducing synthetic small-diameter vascular graft thrombosis, Vascular and Endovascular Surgery. 46 (2012) 212--222.
- [57] J. Chlupac, E. Filova, L. Bacakova, Blood vessel replacement: 50 years of development and tissue engineering paradigms in vascular surgery, Physiological Research. 58 (2009) S119.
- [58] P. Zilla, D. Bezuidenhout, P. Human, Prosthetic vascular grafts: wrong models, wrong questions and no healing, Biomaterials. 28 (2007) 5009--5027.
- [59] R.A. and Hoshi, The blood and vascular cell compatibility of heparin-modified ePTFE vascular grafts, Biomaterials. 34 (2013) 30--41.
- [60] R. Pulli, W. Dorigo, P. Castelli, V. Dorrucchi, F. and Ferilli, Midterm results from a multicenter registry on the treatment of infrainguinal critical limb ischemia using a heparin-bonded ePTFE graft, Journal of Vascular Surgery. 51 (2010) 1167--1177.e1. doi:http://dx.doi.org/10.1016/j.jvs.2009.12.042.

- [61] J. Yang, D. Motlagh, J.B. Allen, A.R. Webb, M.R. Kibbe, O. Aalami, M. Kapadia, T.J. Carroll, G.A. Ameer, Modulating Expanded Polytetrafluoroethylene Vascular Graft Host Response via Citric Acid-Based Biodegradable Elastomers, *Advanced Materials*. 18 (2006) 1493–1498. doi:10.1002/adma.200600230.
- [62] M. Liisberg, M. Stenger, C. Behr-Rasmussen, J. Stubbe, J.S. Lindholt, Experimental comparative study of thrombogenicity of two differently luminal heparinized ePTFE vascular prosthetics, *Annals of Medicine and Surgery*. 35 (2018) 76–81. doi:10.1016/j.amsu.2018.09.037.
- [63] C. Uhl, C. Grosch, C. Hock, I. Töpel, M. Steinbauer, Comparison of Long-term Outcomes of Heparin Bonded Polytetrafluoroethylene and Autologous Vein Below Knee Femoropopliteal Bypasses in Patients with Critical Limb Ischaemia, *European Journal of Vascular and Endovascular Surgery*. 54 (2017) 203–211. doi:10.1016/j.ejvs.2017.05.001.
- [64] A.B. Lumsden, N.J. Morrissey, R. Staffa, J. Lindner, L. Janousek, V. Treska, P. Stadler, M. Moursi, M. Storck, K. Johansen, M. Schermerhorn, R. Powell, J. Panneton, W. Zhou, J. Naoum, E. Lipsitz, C. Buckley, C. Timaran, W. Jordan, R.C. Darling, Z. Silhart, C. Buckley, P. Armstrong, M. Belkin, N. Morrissey, F. Porreca, N. Cayne, Randomized controlled trial comparing the safety and efficacy between the FUSION BIOLINE heparin-coated vascular graft and the standard expanded polytetrafluoroethylene graft for femoropopliteal bypass, *Journal of Vascular Surgery*. 61 (2015) 703-712.e1. doi:10.1016/j.jvs.2014.10.008.
- [65] R.A. Oldinski, C.N. Cranson, S.P. James, Synthesis and characterization of a Hyaluronan-polyethylene copolymer for biomedical applications, *Journal of Biomedical Materials Research Part B: Applied Biomaterials*. 94 (2010) 441–446.
- [66] I. Niechajev, Facial reconstruction using porous high-density polyethylene (medpor): long-term results, *Aesthetic Plastic Surgery*. 36 (2012) 917–927.
- [67] M. Lestelius, B. Liedberg, P. Tengvall, In vitro plasma protein adsorption on ω -functionalized alkanethiolate self-assembled monolayers, *Langmuir*. 13 (1997) 5900–5908.
- [68] S. Kidoaki, T. Matsuda, Adhesion forces of the blood plasma proteins on self-assembled monolayer surfaces of alkanethiolates with different functional groups measured by an atomic force microscope, *Langmuir*. 15 (1999) 7639–7646.
- [69] A. Kheradvar, E.M. Groves, L.P. Dasi, S.H. Alavi, R. Tranquillo, K.J. Grande-Allen, C.A. Simmons, B. Griffith, A. Falahatpisheh, C.J. Goergen, Emerging trends in heart valve engineering: part I. Solutions for future, *Annals of Biomedical Engineering*. 43 (2015) 833–843.

- [70] X.. Zhang, S. Elkoun, A. Ajji, M.. Huneault, Oriented structure and anisotropy properties of polymer blown films: HDPE, LLDPE and LDPE, *Polymer*. 45 (2004) 217–229. doi:10.1016/j.polymer.2003.10.057.
- [71] R. Simon-Walker, J. Cavicchia, D.A. Prawel, L.P. Dasi, S.P. James, K.C. Popat, Hemocompatibility of hyaluronan enhanced linear low density polyethylene for blood contacting applications, *Journal of Biomedical Materials Research Part B: Applied Biomaterials*. 106 (2017) 1964–1975.
- [72] S. Banerjee, S. Ray, S. Maiti, K.K. Sen, U.K. Bhattacharyya, S. Kaity, A. Ghosh, Interpenetrating polymer network (IPN): a novel biomaterial, *Int. J. Appl. Pharm.* 2 (2010) 28–34.
- [73] Y.S. Lipatov, T.T. Alekseeva, Phase-separated interpenetrating polymer networks, in: *Phase-Separated Interpenetrating Polymer Networks*, Springer, 2007: pp. 1–227.
- [74] L.P. Dasi, A.Y. KOUPAEI, M.K. HEITKEMPER, Prosthetic heart valve with tri-leaflet design for use in percutaneous valve replacement procedures, WO2019006383A2, 2019. <https://patents.google.com/patent/WO2019006383A2/en?inventor=megan+heitkemper&assignee=prasad+dasi&oq=prasad+dasi+megan+heitkemper> (accessed March 18, 2019).
- [75] D. Vigetti, E. Karousou, M. Viola, S. Deleonibus, G. De Luca, A. Passi, Hyaluronan: Biosynthesis and signaling, *Biochimica et Biophysica Acta (BBA) - General Subjects*. 1840 (2014) 2452–2459. doi:10.1016/j.bbagen.2014.02.001.
- [76] M.K. Cowman, S. Matsuoka, Experimental approaches to hyaluronan structure, *Carbohydrate Research*. 340 (2005) 791–809. doi:10.1016/j.carres.2005.01.022.
- [77] K. Haxaire, I. Braccini, M. Milas, M. Rinaudo, S. Perez, Conformational behavior of hyaluronan in relation to its physical properties as probed by molecular modeling, *Glycobiology*. 10 (2000) 587–594. doi:10.1093/glycob/10.6.587.
- [78] M.K. Cowman, Hyaluronan and Hyaluronan Fragments, in: *Advances in Carbohydrate Chemistry and Biochemistry*, Elsevier, 2017: pp. 1–59. doi:10.1016/bs.accb.2017.10.001.
- [79] A. Almond, A. Brass, J.K. Sheehan, Oligosaccharides as Model Systems for Understanding Water–Biopolymer Interaction: Hydrated Dynamics of a Hyaluronan Decamer, *The Journal of Physical Chemistry B*. 104 (2000) 5634–5640. doi:10.1021/jp000402t.

- [80] I. Hargittai, M. Hargittai, Molecular structure of hyaluronan: an introduction, *Structural Chemistry*. 19 (2008) 697–717. doi:10.1007/s11224-008-9370-3.
- [81] N.T. Seyfried, G.F. McVey, A. Almond, D.J. Mahoney, J. Dudhia, A.J. Day, Expression and Purification of Functionally Active Hyaluronan-binding Domains from Human Cartilage Link Protein, Aggrecan and Versican: FORMATION OF TERNARY COMPLEXES WITH DEFINED HYALURONAN OLIGOSACCHARIDES, *Journal of Biological Chemistry*. 280 (2005) 5435–5448. doi:10.1074/jbc.M411297200.
- [82] L. HuangS, M. Yoneda, K. Kimatag, A Serum-derived Hyaluronan-associated Protein (SHAP) Is the Heavy Chain of the Inter α -Trypsin Inhibitor, (n.d.) 6.
- [83] S. Dogné, B. Flamion, N. Caron, Endothelial Glycocalyx as a Shield Against Diabetic Vascular Complications: Involvement of Hyaluronan and Hyaluronidases, *Arteriosclerosis, Thrombosis, and Vascular Biology*. 38 (2018) 1427–1439. doi:10.1161/ATVBAHA.118.310839.
- [84] P.A. Galie, A. van Oosten, C.S. Chen, P.A. Janmey, Application of multiple levels of fluid shear stress to endothelial cells plated on polyacrylamide gels, *Lab on a Chip*. 15 (2015) 1205–1212. doi:10.1039/C4LC01236D.
- [85] M.Y. Pahakis, J.R. Kosky, R.O. Dull, J.M. Tarbell, The role of endothelial glycocalyx components in mechanotransduction of fluid shear stress, *Biochemical and Biophysical Research Communications*. 355 (2007) 228–233. doi:10.1016/j.bbrc.2007.01.137.
- [86] S. Mochizuki, H. Vink, O. Hiramatsu, T. Kajita, F. Shigeto, J.A.E. Spaan, F. Kajiya, Role of hyaluronic acid glycosaminoglycans in shear-induced endothelium-derived nitric oxide release, *American Journal of Physiology-Heart and Circulatory Physiology*. 285 (2003) H722–H726. doi:10.1152/ajpheart.00691.2002.
- [87] M.A. Dragovich, D. Chester, B.M. Fu, C. Wu, Y. Xu, M.S. Goligorsky, X.F. Zhang, Mechanotransduction of the endothelial glycocalyx mediates nitric oxide production through activation of TRP channels, (n.d.) 8.
- [88] S. Grundmann, S.H. Schirmer, L.H.P. Hekking, J.A. Post, M.G. Ionita, D. de Groot, N. van Royen, B. van den Berg, H. Vink, M. Moser, C. Bode, D. de Kleijn, G. Pasterkamp, J.J. Piek, I.E. Hoefer, Endothelial glycocalyx dimensions are reduced in growing collateral arteries and modulate leucocyte adhesion in arteriogenesis, *J Cell Mol Med*. 13 (2009) 3463–3474. doi:10.1111/j.1582-4934.2009.00735.x.

- [89] C. Tolg, H. Yuan, S.M. Flynn, K. Basu, J. Ma, K.C.K. Tse, B. Kowalska, D. Vulkanesku, M.K. Cowman, J.B. McCarthy, E.A. Turley, Hyaluronan modulates growth factor induced mammary gland branching in a size dependent manner, *Matrix Biology*. 63 (2017) 117–132. doi:10.1016/j.matbio.2017.02.003.
- [90] B. Sadowitz, K. Seymour, V. Gahtan, K.G. Maier, The Role of Hyaluronic Acid in Atherosclerosis and Intimal Hyperplasia, *Journal of Surgical Research*. 173 (2012) e63–e72. doi:10.1016/j.jss.2011.09.025.
- [91] M.H. Ramadan, J.E. Prata, O. Karácsony, G. Dunér, N.R. Washburn, Reducing Protein Adsorption with Polymer-Grafted Hyaluronic Acid Coatings, *Langmuir*. 30 (2014) 7485–7495. doi:10.1021/la500918p.
- [92] L.P. da Silva, R.P. Pirraco, T.C. Santos, R. Novoa-Carballal, M.T. Cerqueira, R.L. Reis, V.M. Correlo, A.P. Marques, Neovascularization Induced by the Hyaluronic Acid-Based Spongy-Like Hydrogels Degradation Products, *ACS Applied Materials & Interfaces*. 8 (2016) 33464–33474. doi:10.1021/acsami.6b11684.
- [93] F. Gao, Y. Liu, Y. He, C. Yang, Y. Wang, X. Shi, G. Wei, Hyaluronan oligosaccharides promote excisional wound healing through enhanced angiogenesis, *Matrix Biology*. 29 (2010) 107–116. doi:10.1016/j.matbio.2009.11.002.
- [94] K.L. Aya, R. Stern, Hyaluronan in wound healing: Rediscovering a major player, *Wound Repair and Regeneration*. 22 (2014) 579–593. doi:10.1111/wrr.12214.
- [95] N. Nagy, T. Freudenberger, A. Melchior-Becker, K. Röck, M. ter Braak, H. Jastrow, M. Kinzig, S. Lucke, T. Suvorava, G. Kojda, A.A. Weber, F. Sörgel, B. Levkau, S. Ergün, J.W. Fischer, Inhibition of Hyaluronan Synthesis Accelerates Murine Atherosclerosis: Novel Insights Into the Role of Hyaluronan Synthesis, *Circulation*. 122 (2010) 2313–2322. doi:10.1161/CIRCULATIONAHA.110.972653.
- [96] J.W. Fischer, Role of hyaluronan in atherosclerosis: Current knowledge and open questions, *Matrix Biology*. (2018). doi:10.1016/j.matbio.2018.03.003.
- [97] C. de la Motte, J. Nigro, A. Vasanji, H. Rho, S. Kessler, S. Bandyopadhyay, S. Danese, C. Fiocchi, R. Stern, Platelet-Derived Hyaluronidase 2 Cleaves Hyaluronan into Fragments that Trigger Monocyte-Mediated Production of Proinflammatory Cytokines, *The American Journal of Pathology*. 174 (2009) 2254–2264. doi:10.2353/ajpath.2009.080831.

- [98] V.K. Krishnamurthy, A.J. Stout, M.C. Sapp, B. Matuska, M.E. Lauer, K.J. Grande-Allen, Dysregulation of hyaluronan homeostasis during aortic valve disease, *Matrix Biology*. 62 (2017) 40–57. doi:10.1016/j.matbio.2016.11.003.
- [99] T.-W. Chuang, K.S. Masters, Regulation of polyurethane hemocompatibility and endothelialization by tethered hyaluronic acid oligosaccharides, *Biomaterials*. 30 (2009) 5341–5351. doi:http://dx.doi.org/10.1016/j.biomaterials.2009.06.029.
- [100] A. Ruiz, K.R. Rathnam, K.S. Masters, Effect of Hyaluronic Acid Incorporation Method on the Stability and Biological Properties of Polyurethane-Hyaluronic Acid Biomaterials, *J Mater Sci Mater Med*. 25 (2014) 487–498. doi:10.1007/s10856-013-5092-1.
- [101] N.-H. Chi, M.-C. Yang, T.-W. Chung, N.-K. Chou, S.-S. Wang, Cardiac repair using chitosan-hyaluronan/silk fibroin patches in a rat heart model with myocardial infarction, *Carbohydr Polym*. 92 (2013) 591–597. doi:10.1016/j.carbpol.2012.09.012.
- [102] F. Wu, J. Li, K. Zhang, Z. He, P. Yang, D. Zou, N. Huang, Multifunctional Coating Based on Hyaluronic Acid and Dopamine Conjugate for Potential Application on Surface Modification of Cardiovascular Implanted Devices, *ACS Applied Materials & Interfaces*. 8 (2016) 109–121. doi:10.1021/acsami.5b07427.
- [103] J. Li, F. Wu, K. Zhang, Z. He, D. Zou, X. Luo, Y. Fan, P. Yang, A. Zhao, N. Huang, Controlling Molecular Weight of Hyaluronic Acid Conjugated on Amine-rich Surface: Toward Better Multifunctional Biomaterials for Cardiovascular Implants, *ACS Applied Materials & Interfaces*. 9 (2017) 30343–30358. doi:10.1021/acsami.7b07444.
- [104] M. Eslami, N.E. Vrana, P. Zorlutuna, S. Sant, S. Jung, N. Masoumi, R.A. Khavari-Nejad, G. Javadi, A. Khademhosseini, Fiber-reinforced hydrogel scaffolds for heart valve tissue engineering, *Journal of Biomaterials Applications*. 29 (2014) 399–410. doi:10.1177/0885328214530589.
- [105] C.B. Rodell, A.L. Kaminski, J.A. Burdick, Rational Design of Network Properties in Guest–Host Assembled and Shear-Thinning Hyaluronic Acid Hydrogels, *Biomacromolecules*. 14 (2013) 4125–4134. doi:10.1021/bm401280z.
- [106] A.C. Gaffey, M.H. Chen, A. Trubelja, C.M. Venkataraman, C.W. Chen, J.J. Chung, S. Schultz, C.M. Sehgal, J.A. Burdick, P. Atluri, Delivery of progenitor cells with injectable shear-thinning hydrogel maintains geometry and normalizes strain to stabilize cardiac function after ischemia, *The Journal of Thoracic and Cardiovascular Surgery*. (2018). doi:10.1016/j.jtcvs.2018.07.117.

- [107] D.S. Puperi, R.W. O’Connell, Z.E. Punske, Y. Wu, J.L. West, K.J. Grande-Allen, Hyaluronan Hydrogels for a Biomimetic Spongiosa Layer of Tissue Engineered Heart Valve Scaffolds, *Biomacromolecules*. 17 (2016) 1766–1775. doi:10.1021/acs.biomac.6b00180.
- [108] A. Ruiz, C.E. Flanagan, K.S. Masters, Differential support of cell adhesion and growth by copolymers of polyurethane with hyaluronic acid, *Journal of Biomedical Materials Research Part A*. 101 (2013) 2870–2882. doi:10.1002/jbm.a.34597.
- [109] H.P. Felgueiras, L.M. Wang, K.F. Ren, M.M. Querido, Q. Jin, M.A. Barbosa, J. Ji, M.C.L. Martins, Octadecyl Chains Immobilized onto Hyaluronic Acid Coatings by Thiol–ene “Click Chemistry” Increase the Surface Antimicrobial Properties and Prevent Platelet Adhesion and Activation to Polyurethane, *ACS Applied Materials & Interfaces*. 9 (2017) 7979–7989. doi:10.1021/acsami.6b16415.
- [110] M. Zhang, Surface modification of ultra high molecular weight polyethylene with hyaluronan for total joint replacement application, 2004.
- [111] Harold Casey Dean, Development of a BiopolyTM Micro-composite For Use In Prosthetic Heart Valve Replacements, Colorado State University, **Master of Science**, 2011.
- [112] N.R. Lewis, Hyaluronic acid enhancement of expanded polytetrafluoroethylene for small diameter vascular grafts, Colorado State University, 2014.

Chapter 2: Fabrication and Characterization of HA-ePTFE

2.1 Introduction & Preliminary Work

Previous research has demonstrated that IPN formation was achieved through solvent swelling of polymers and thus the technique was repeated for ePTFE [1]. The goal was to swell ePTFE using xylenes to enhance it with HA, but the process did not create a persistent HA layer on ePTFE. Much of the HA was removed when reverting the chemically modified HA (silylated HA-cetrimonium complex or SHACTA) back to the polysaccharide native form [2]. Moreover, xylene soaking significantly increased the roughness of the surface of ePTFE by increasing the depth and volume of the internal regions, and possibly affecting the performance of the synthetic graft.

2.1.1 Preliminary Wicking Study

Therefore, preliminary work was performed to analyze the solvent intake of medical grade ePTFE graft (Bard IMPRA© 70S10) to search for an alternative solvent. ePTFE samples were soaked in solvent (15 mg/ml) for one hour at 50°C, which are parameters for HA-synthetic polymer IPN fabrication from other work [1,3]. The samples were then dried under vacuum at 50°C for at least 24 hours. ePTFE samples gained weight after soaking in xylenes, acetone, and ethanol as shown in Table 2-1. The solvent intake for ePTFE in xylenes, acetone, and ethanol were $22.9 \pm 2.42 \%$, $20.8 \pm 6.42 \%$, $18.2 \pm 4.74 \%$, respectively; they are not statistically different ($n=3$, $\alpha = 0.95$). Despite significant weight change from the solvent study, there was not a significant increase in size of the ePTFE graft after soaking in solvent. This could mean that the fluoropolymer was not

swollen by the solvents, and the organic solvents were wicking into the polymer, penetrating the micropores of the ePTFE [2].

The preliminary wicking study (Table 2-1) was repeated in water, where no intake of water by ePTFE was observed. In fact, the samples could not sink into water partially due to its hydrophobic nature [4]; they had to be anchored to the bottom of the scintillation vial containing water to ensure full submergence. This is not surprising as ePTFE is often the preferred material for making membrane filters as a water barrier, due to its high porosity and hydrophobicity [5]. Figure 2.1 shows the microstructure of ePTFE, and Figure 2.2 shows an example of ePTFE commercial product.

Table 2-1: The solvent intake capability of ePTFE. Solvent intake was calculated as the percentage increase from the initial weight to the weight after solvent intake. Dry weight was measured to verify no degradation from solvent exposure. There was no statistical difference among the treatment groups. (n=3, $\alpha=0.95$).

Solvent	Sample #	Solvent Intake (%)
Xylenes	1	21.1
	2	22.0
	3	25.7
Acetone	1	28.7
	2	18.7
	3	15.7
Ethanol	1	19.9
	2	22.0
	3	12.9

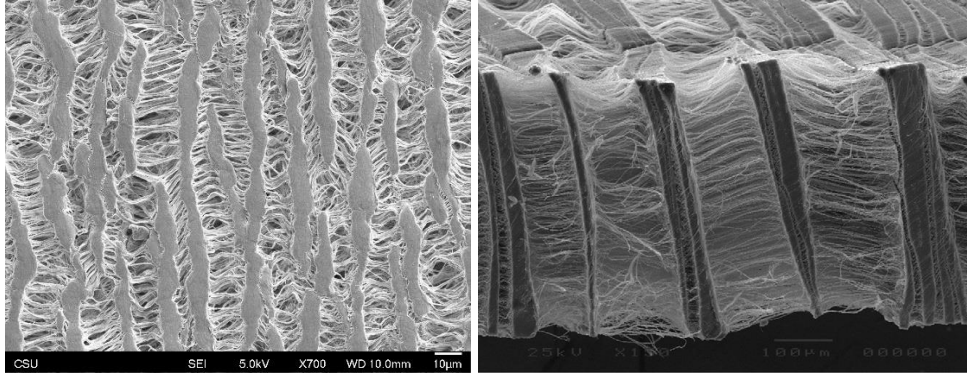


Figure 2.1: Top down (left image) and cross section (right image) micrographs of two different ePTFE materials. The internodal length can vary greatly from 10 (left image) to 100 micron (right image), but they almost always cover the entire depth making the polymer highly porous and permeable. The right image was reproduced with permission [6] © Elsevier Ltd.

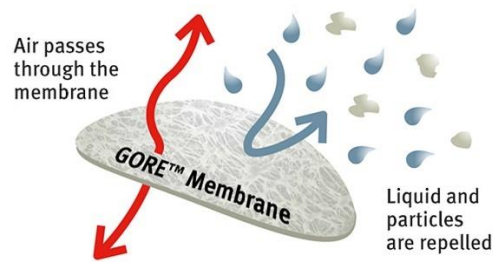


Figure 2.2: GORE® Membrane (right) is an example of commercial materials made from ePTFE to be vapor permeable yet waterproof, thanks to their high porosity and hydrophobicity.

2.1.2 Preliminary HA-ePTFE Fabrication

From the results of the wicking study, the microstructure of ePTFE may be exploited. HA could fill the voids within the microfibril regions of ePTFE, like the organic solvent wicking as demonstrated in the preliminary wick study. Therefore, this preliminary experiment was performed to test this hypothesis. Since solvent intake is achievable by using less aggressive solvents than xylenes, such as alcohols, HA (750 kDa) (Lifecore Biomedical) was modified to be soluble in ethanol. The modified HA/ethanol solution was then used for treating the inner lumen of ePTFE

graft (Impra[®] Bard). Different concentrations of HA/ethanol were tested along with two different delivery methods, soaking and spraying. The study was also repeated with water instead of ethanol as the solvent. The detailed procedure is described below:

- 1) HA-CTA fabrication followed procedures described elsewhere [7]. Briefly, sodium hyaluronate at 750 kDa (Lifecore Biomedical) and cetyltrimethylammonium bromide (CTAB) (Fisher Scientific) were each dissolved in deionized water (DiH₂O). The CTAB solution was slowly added to the HA solution while stirring to form a hyaluronan-cetyltrimethylammonium (HA-CTA) precipitate. The reaction scheme is shown in Figure 2.3. The HA-CTA precipitate was washed with DiH₂O to remove CTAB residue. The purified HA-CTA was granulated, dried, and stored in desiccator under vacuum until further usage.
- 2) HA-CTA, which is soluble in ethanol [7], was dissolved in the solvent at various concentrations (1.0, 0.75, 0.4 w/v %). The treatment involves soaking ePTFE graft samples in HACTA/ethanol at 50°C for one hour similar to previous work [1]. Samples were treated at different concentrations of HACTA/ethanol and either soaked in the solution as described or spray coated via an air brush (Powermate) (Figure 2.4) at 20 psi using 1.3 ml/cm² the HACTA/ethanol solution on a 2-cm long vascular graft that has a 1 cm-diameter (1.27 ml/cm²)
- 3) The treatment was also repeated but using HA/DiH₂O instead of HACTA/ethanol to compare to determine if wicking is a factor in the HA treatment. As shown in the wicking study, water does not wick into ePTFE, whereas ethanol does. HACTA is not soluble in water, therefore fresh HA was dissolved in DiH₂O.
- 4) The treated grafts were dried under vacuum at 50°C to fully remove ethanol and DiH₂O.
- 5) After drying, the ePTFE samples were submerged in dried acetone containing hexamethylene diisocyanate (HDI) (Bayer Materials Science) to crosslink HA (Figure 2.5), fixing the

polysaccharide in ePTFE. 2 v/v % HDI concentration was picked based on previous work, which showed that lower concentrations led to sparse HA network that is not durable and higher concentrations consume too many polar groups of HA creating a hydrophobic biopolymer [7].

- a. Acetone was used because it could solvate HDI but neither HACTA nor HA [7]; this allows the crosslinker to wick into ePTFE delivering HDI to the HA or HACTA without dissolving the HA or HACTA layer.
 - b. As described in the literature [8], acetone was dried by incubating in boric anhydride (Sigma) at 10% w/v for at least 72 hours; the solvent was then distilled in a nitrogen purged environment removing any trace of boric anhydride and water content. The water content of the dried acetone was verified to be below 500 parts per million (ppm) as recommended by the HDI manufacturer to prevent significant reaction of water with the crosslinker; this was done using a water testing kit (01-WTK-WATERSB ver. 1.2; Sandy Brae Laboratories, Inc). All glassware vessels exposed to HDI and acetone were treated with hexamethyldisilazane (HMDS) (Sigma) to replace the hydroxyl groups on silicate glass with organosilyl groups, preventing reaction of the glassware with the crosslinker. The reaction scheme is shown in Figure 2.6 [9].
 - c. The entire crosslinking experiment was performed in a nitrogen purged glove bag to prevent moisture contamination.
- 6) After 1 hour of crosslinking, samples were dried in a vacuum oven at 50°C for at least an hour.
 - 7) The CTA complex was removed by sonicating the treated ePTFE sample in 0.2 M NaCl DiH₂O/ethanol (1:1) solutions for four hours, allowing the sonicator to heat up to 45°C. Uncrosslinked HA compounds were further removed by incubating the treated ePTFE in

DiH₂O/ethanol (3:2) solution for at least 8 hours, before a final wash by sonicating in DiH₂O for 30 minutes. The CTA removal process is based on previous work [2,10].

- 8) Toluidine blue O (TBO) helped determine the presence of HA. TBO molecule is known to bind to the carboxyl group on HA, and the dye is often used for colorimetric analysis [11]. Samples were soaked in 0.1% TBO solution containing 8 M of urea for 10 minutes. Afterward, excess TBO not bound to HA was rinsed away by soaking samples in DiH₂O for 10 minutes

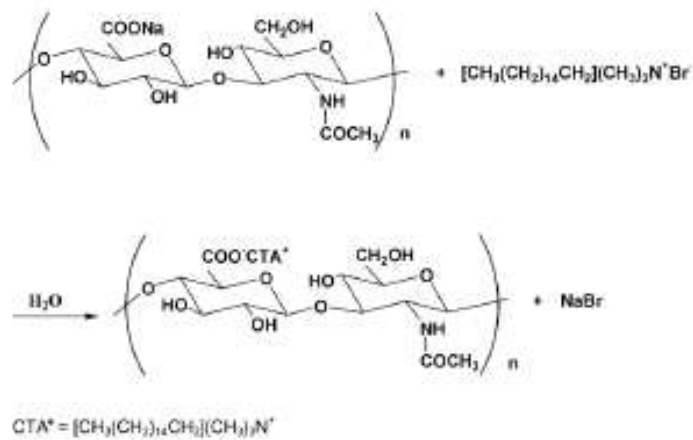


Figure 2.3: Reaction scheme of NaHA and CTAB to form HACTA.



Figure 2.4: Image of the airbrush used for the HA treatment.

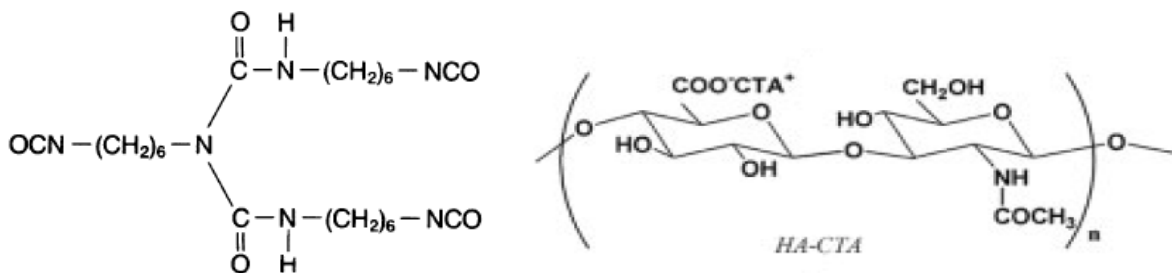


Figure 2.5: Left image shows the structure of HDI biuret used for crosslinking HACTA (right image). The reaction between isocyanates of HDI and hydroxyl groups of HA-CTA follow the regular reaction mechanism of isocyanates and polyols to form urethane linkages [12].

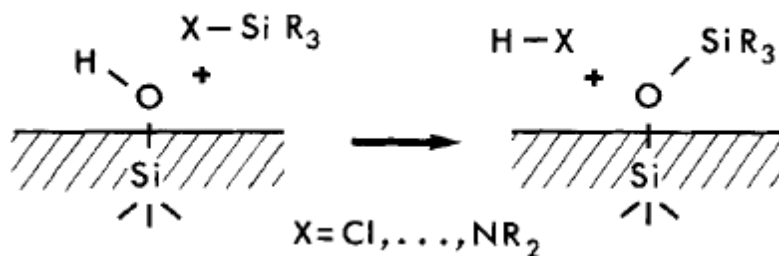


Figure 2.6: Reaction schematic was reproduced with permission [9] © John Wiley and Sons. Glassware were coated with HMDS and cured at 137°C for at least 4 hours. The silylation reaction takes place at the surface of the silicate glass between its hydroxyl groups and the reactive group of HMDS ($X=NH$ and $R=CH_3$). Removing the hydroxyl groups on borosilicate glassware prevents reaction between the silicate surface and the HDI crosslinker.

The TBO results in Table 2-2 demonstrate that there is more HA on ePTFE at 0.4 % (w/v) HACTA/ethanol treatment than 0.75 and 1.0 %. This may be because the lower concentration and lower viscosity solution allows better wicking of the biopolymer into ePTFE. Traces of HA were observed at the edges of samples treated with the 0.75 and 1.0 %, where rough edges were more likely to trap HA. The higher concentrations also created solutions that were too viscous to be used for spraycoating. Therefore, only 0.4% solution was utilized in all future studies, and this concentration treatment was able to create a confluent layer of HA on the inner lumen of ePTFE. The data (Table 2-3) shows that more HA is present on the surface of ePTFE in HACTA/ethanol

treatment than the NaHA/DiH₂O one. Overall, the TBO results demonstrate that wicking of the solvent is important for the deliverance of HA into the micro pores of ePTFE, and hydrophobic ethanol appears to be better at wicking into the hydrophobic ePTFE than water.

Table 2-2: TBO results from the preliminary HA-ePTFE fabrication process utilizing HACTA/ethanol.

	Untreated	1.0 %	0.75 %	0.4%
Dipping	N/A			
Spray coating		N/A	N/A	
Untreated				

Table 2-3: TBO results from the preliminary HA-ePTFE fabrication process utilizing HA/DiH₂O.

	Dipping	Spray coating
0.4%		

Because HA is present on both HACTA/ethanol and NaHA/DiH₂O treatment with both spray coating and soaking at 0.4 %, further assessment was performed to compare the treatment processes. The static water contact angles of the surfaces of the treated ePTFE samples were taken using a goniometer (260-F4 Ramé-Hart Instrument). Hydrophilicity, which is the hallmark of HA, is an indicator of a successful HA treatment process. Table 2-4 shows both soaking treatments have contact angles that are not statistically different from untreated ePTFE, despite TBO staining showing a layer of HA. This could be due to the high roughness of ePTFE, and/or that these treatments did not sufficiently cover the ePTFE surface with HA. Spraying of NaHA/DiH₂O was

also not adequate to wet the ePTFE with the HA solution. The high surface tension of water along with the low surface tension of ePTFE prevented interaction between the liquid and solid; this may explain why, even under pressure, the water from the spraying jet beaded up once it touched the surface of ePTFE, as shown Figure 2.7. The only successful treatment was the HACTA/ethanol spray coating technique, where a hydrophilic layer was formed on ePTFE, and the resulting contact angle was significantly lower than the untreated ePTFE. Overall, pressure alone was not enough to penetrate HA into ePTFE, and the solvent mattered too. Water was not able to deliver as much HA into ePTFE as ethanol, where the solvent could wick into ePTFE.

Table 2-4: Water contact angle data of HA-ePTFE samples from the HA-ePTFE fabrication process. Data represent mean \pm standard deviation with $n = 4$. ($p < 0.5$ relative to untreated).*

	Untreated	NaHA/DiH ₂ O	HACTA/ethanol
Dipping	N/A	127 \pm 4.03	111 \pm 12.8
Spray coating		116 \pm 6.65	26.5 \pm 4.80*
Untreated	126 \pm 5.00		



Figure 2.7: ePTFE graft that was spray coated with NaHA/DiH₂O. The water can be seen beading up on the inner lumen of ePTFE because of water high surface tension, and that prevents the liquid from wetting and soaking into ePTFE.

Based on all the results from preliminary work, the fabrication process involving spray coating HACTA/ethanol onto ePTFE is effective at enhancing the synthetic polymer with HA. Nevertheless, the process can be further improved and the finished product, i.e. HA-ePTFE, must be further characterized to analyze the effect of the fabrication process on the vascular graft. For example, the shrinkage of the ePTFE graft was observed after spray coating, and this may affect the material performance. To this end, the parameters of the spray coating process were varied. Characterizations were performed on both HA treated and untreated ePTFE for comparison.

2.2 Materials & Methods

2.2.1 Fabrication & Surface Characterization of HA-ePTFE

The HA-ePTFE fabrication process followed the procedure of spray coating 0.4 w/v% of HACTA/ethanol onto ePTFE as described in the preliminary work, and it is shown in Figure 2.8. The treatment parameters were varied to determine their effects on the fabrication process. Figure 2.9 shows the refinement process for enhancing ePTFE with HA. The volume of HA-CTA/ethanol solution used in spray coating increased incrementally, and surface wettability was the metric for determining the best spray coating volume. Shrinkage of HA-ePTFE graft had occurred during coating and the spraying pressure of the airbrush gun was investigated to ameliorate this problem. Further surface analysis verified the formation of a confluent HA layer on the ePTFE, which is discussed in the next section. The crosslinking procedure (step 4 in Figure 2.8) was not studied since previous work has investigated the HDI crosslinking process [7].



Figure 2.8: Schematic of the HA-ePTFE fabrication process.

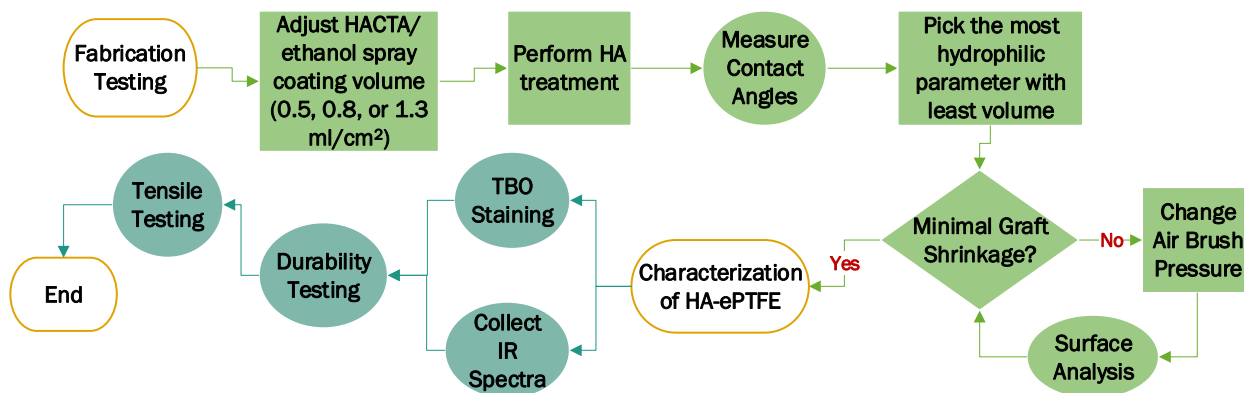


Figure 2.9: Schematic of the refinement process for fabricating HA-ePTFE. Green and blue nodes belong to the first and second aims, respectively.

Surface hydrophilicity, which is indicative of HA presence, was assessed by measuring water contact angles of HA-ePTFE. Although collecting water contact angle by performing sessile droplet was performed in the preliminary work because it is a common technique in surface chemistry, the captive bubble technique was chosen because it allowed for the HA-ePTFE samples to be constantly hydrated while water contact angle was measured. A hydrated HA surface is more physically relevant for data collection since HA is known to swell and rearrange in an aqueous environment. Figure 2.10 depicts both sessile droplet and captive bubble methods. Rather than applying a liquid droplet (water) on surface of interest like in sessile droplet, the captive bubble technique involves hanging the sample inverted and applying a gas (air) bubble to the surface of

the sample. In both cases, the contact angle along the liquid-solid interface was measured. The water contact angle is inversely correlated to the work of adhesion (W_a), as shown in [equation \(3\)](#), by combining the Young's contact angle [equation \(1\)](#) with the Young-Dupré [equation \(2\)](#) [4,13]. W_a is the required work to separate the liquid (water) from the solid surface, and it is often used for gaging the strength of the solid-liquid phase [13]. Thus, a higher W_a , or a lower contact angle (θ), is expected for a hydrophilic surface. The surface tension at the liquid-vapor interface (γ_{LV}) is a constant for air and water (72 mN/m), and room temperature during data collection was approximately 20 to 25°C where its influence on surface tension was negligible [14].

$$\gamma_{SV} - \gamma_{SL} = \gamma_{LV} \cos \theta \quad (1)$$

$$W_a = \gamma_{LV} + \gamma_{SV} - \gamma_{SL} \quad (2)$$

$$\gamma_{LV} (\cos \theta + 1) = W_a \quad (3)$$

In addition, measuring the static contact angles using the captive bubble method, the receding and advancing angles were also calculated. As shown in Figure 2.10, these metastable angles represent the highest and lowest contact angles a surface can achieve under dynamic conditions, and the static contact angle is often the intermediate of these two values. The difference in the advancing and receding contact angles, or hysteresis, may also reveal the heterogeneity of the surface both physically and chemically [14,15].

The captive bubble method discussed in this dissertation utilizes a goniometer (260-F4 Ramé-Hart Instrument). HA-treated and untreated ePTFE samples (n=3) were soaked for at least one hour in DiH₂O to swell the HA before testing. Samples were cut from the tubular grafts, flattened, and carbon taped on a glass slide with the inner lumen facing outward. The glass slide, along with the sample, was submerged and suspended in DiH₂O. An air bubble was introduced to the surface and

the static contact angle was measured immediately. As depicted in Figure 2.10, receding angle was measured by expanding the air bubble until a stable measurement was reached, and advancing angle was measured by minimizing the air bubble until a constant value was obtained. Reported angles were measured between the solid-liquid interface.

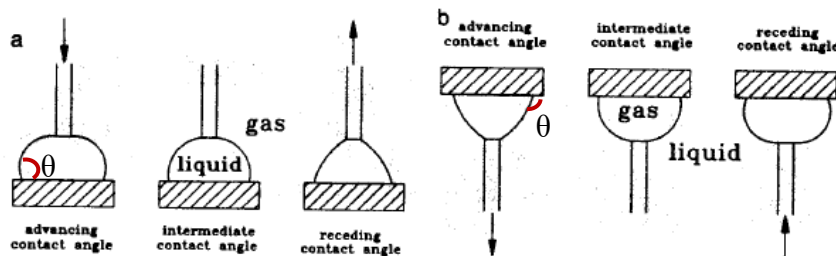


Figure 2.10: Reproduced with permission [14] © Elsevier Ltd, the illustration shows measurements of contact angles using sessile droplet (a) and captive bubble techniques (b). Red theta (θ) represents contact angle of the interface in each method for determining surface wettability.

Attenuated total reflectance-Fourier transform infrared spectroscopy (ATR-FTIR) (Nicolet iS50) was used to qualitatively analyze the functional groups on the surface of plain and HA-treated ePTFE. Untreated and HA-ePTFE grafts were cut and flayed open. The inner lumen of the graft was placed face down on the ATR diamond of the spectrometer and 32 scans were performed. Absorption spectra were collected over a range of 500-4000 cm^{-1} at a resolution of 2 cm^{-1} after 32 scans. Samples were coated with 10 nm of gold and imaged at 5 kV under a scanning electron microscope (SEM) (JEOL JSM 6500F) for qualitative assessment. TBO staining, as described in preliminary work, was also used for qualitative assessment.

2.2.2 Mechanical Stability of HA on ePTFE

To assess the mechanical stability of HA on ePTFE, a hyper-physiological constant shear (55 dyne/cm^2) was applied to the HA-ePTFE. Untreated ePTFE was the negative control. HA-ePTFE

samples (n=3) were cut, flattened, placed inside silicone tubing (Masterflex L/S® 16), and mounted in a flow loop system that circulated DiH₂O via a gear pump (Cole Parmer) at 37°C as shown in Figure 2.11. The inner lumen of the HA-ePTFE faced outward to ensure the water flowing applied 55 dyne/cm². Such a high shear stress was picked to simulate accelerated wear on the sample. The water reservoir containing 1% penicillin/streptomycin (Gibco®) was replaced daily to prevent contamination. Wall shear stress (τ) was determined using the Hagen-Poiseuille equation (4) after making the following assumptions [16]:

- 1) The DiH₂O from the reservoir is a Newtonian fluid.
- 2) The cross-sectional area of the silicone tubing is cylindrical.
- 3) The tubing is straight, and its wall is inelastic.
- 4) The water flow is steady and laminar.

Assumption 1, 2, and 3 can be made based on data from literature [17] and knowing the specifications of Masterflex tubing. The flow loop was designed with water flowing in a straight path around where the sample is located as shown in figure 4. To ensure a steady and laminar flow in accordance with assumption 4, the Reynolds number was calculated using equation (5) and kept below 2300 [18]. This was done by picking the appropriate tubing size (0.16 cm radius) and water flow rate. To prevent any possible turbulent flow, the silicone tubing was anchored to the bench top and the ePTFE sample was threaded tightly and sitting flat in the tubing.

The Hagen-Poiseuille Equation:

$$\tau = \frac{4\eta Q}{\pi r^3} \quad (4)$$

Q (23 cm³/s) is the flow rate and r (0.16 cm) is the radius of the silicone tubing. The dynamic viscosity (η) of water was determined to be 0.69 mPa·s at 37°C [19].

The Reynolds Equation:

$$Re = \frac{\rho v L}{\eta} \quad (5)$$

The Reynolds number (Re) was calculated by knowing the density (ρ) (0.99 kg/m^3) and dynamic viscosity (η) ($0.69 \text{ mPa}\cdot\text{s}$) of water at 37°C [19], and measuring the proper characteristic distance (L) ($\approx 12 \text{ cm}$) and velocity of water (v) (300 cm/s); v was controlled by adjusting the flow rate ($\approx 23 \text{ cm}^3/\text{s}$) at the given tubing radius size ($r = 0.16 \text{ cm}$).

After exposing samples to a constant shear stress in the flow loop for seven days, the amount of HA remaining on samples were determined by thermogravimetric analysis (TGA) with samples and controls in a thermogravimetric analyzer (TA 2950) at a heating rate of $10^\circ\text{C}/\text{min}$ under air purge from 25°C up to 700°C . Weights of individual samples were between 5 and 8 mg. To determine the decomposition temperature range of HA, weight (%) vs. temperature thermographs of plain ePTFE and freshly made HA-ePTFE grafts were compared. The loss in weight observed in HA-ePTFE that was not seen on the curve of ePTFE was indicative of HA amount.

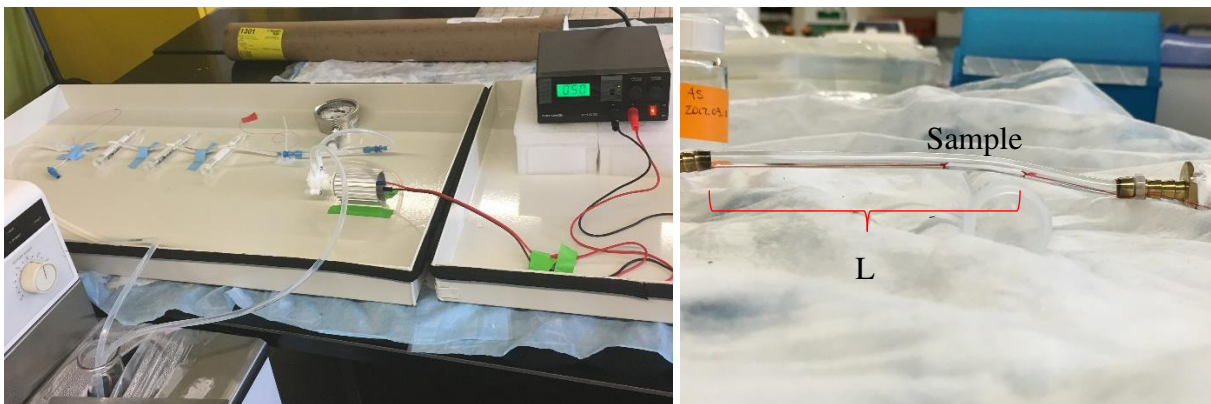


Figure 2.11: The flow loop system is shown in the left image. The right image zooms into the region of the sample. L is the characteristic distance between the sample and the nozzle where entering liquid maintains a constant flow in a straight path. Sample can be seen lying flat within the silicone tubing exposing to water flow.

2.2.3 Circumferential Tensile Testing

Monotonic tensile testing was performed in accordance to the ISO/ANSI 7198 for determining whether HA treatment affected the tensile properties of the ePTFE graft. Samples were hydrated in DiH₂O for one hour. The tubular graft was cut into 10 mm longitudinal lengths (cylindrical rings) (N=10), threaded on pins, and mounted on an Instron 4442 with a 5 kN load cell. The preload of 1 N was applied for one minute. The tubular specimen was then elongated at 100 mm/min until it ruptured. Load and displacement were recorded to calculate the elastic modulus, engineering tensile stress, yield stress, and engineering strain at failure. The duration of the experiment, starting when samples were mounted onto pins and ending when the samples ruptured, was no more than ten minutes to ensure the HA would not dehydrate significantly. The engineering stress (σ) and strain (ϵ) were calculated as follows:

$$\sigma = \frac{F}{2tL} \quad \epsilon = \frac{\Delta l}{l_0} \quad (6)$$

F is force, t is the graft thickness, L is the longitudinal length of the sample, Δl is the change in radial length, and l_0 is the initial radial length. The dimensions are labeled in the schematic of Figure 2.12 . The Young's modulus was calculated from the slope of the linear elastic region, which was the initial 10% of strain. Yield stress was determined using a 0.2% strain offset along the elastic region.

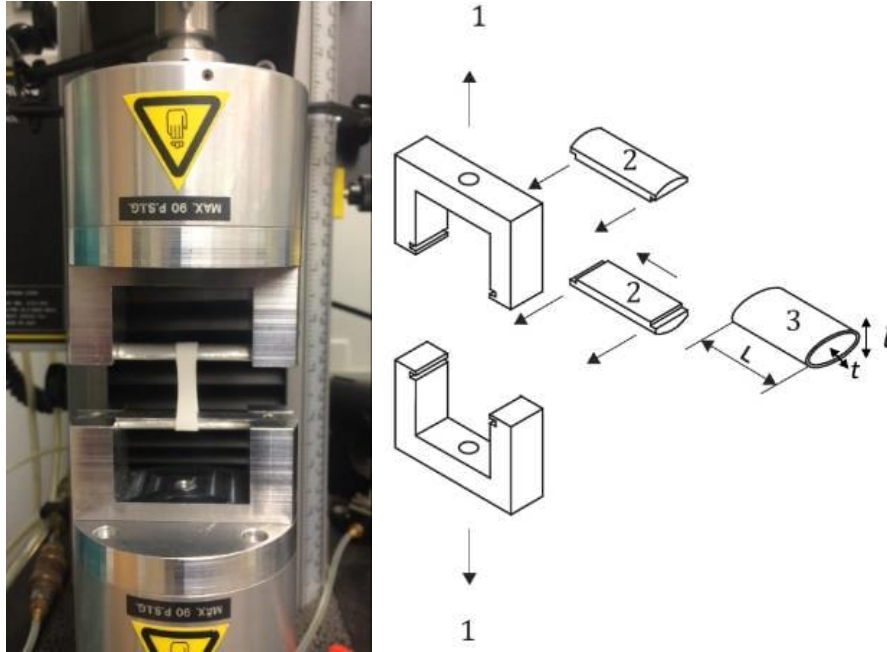


Figure 2.12: Image of tensiometer used to perform circumferential tensile testing (left). The tubular ePTFE graft is threaded by two pins that are connected to the load cells of the tensiometer. The right side is the schematic of the tensile apparatus adopted from ISO 7198. 1) tensile test 2) split bar 3) ePTFE tubular sample with dimensions labeled (L =longitudinal length, t = graft thickness, l = radial length).

2.2.4 Statistical Analysis

Statistical analysis was performed using ANOVA with post hoc Tukey's test. The Anderson-Darling and Levene's test were also used to verify normal distributions and equal variances. All statistical analysis was performed using Minitab 17 (p value =0.05). The initial sample size was either four or three in all the experiments. Power analysis (GPower 3.1) was then performed after each study to verify the required sample size (effect size = 0.8).

2.3 Results & Discussion

2.3.1 Fabrication and Surface Characterization of HA-ePTFE

The HA-ePTFE grafts showed a significant decrease in all contact angles compared to the plain ePTFE control group (Figure 2.13). The respective static, receding, and advancing angles of untreated group are $97 \pm 11^\circ$, $57 \pm 11^\circ$, and $140 \pm 5.5^\circ$. Although all HACTA/ethanol treatments (0.5, 0.8, and 1.3 ml/cm²) markedly reduced water contact angles of ePTFE, there were significant differences among the data groups. As expected, contact angle decreases with higher amount of HA because HA is known for its high-water retention [20]. For example, the 0.5 ml/cm² treatment did not provide enough HA to completely cover the surface of ePTFE as demonstrated by the significantly high advancing contact angle ($69 \pm 7.4^\circ$) compared to 0.8 ml/cm² ($33 \pm 5.0^\circ$) and 1.3 ml/cm² ($52 \pm 6.1^\circ$) treatments. The hysteresis, which is the difference between advancing and receding contact angles, appears also to be high for the 0.5 ml/cm² treatment comparing to the 0.8 and 1.3 ml/cm² treatments. Hysteresis is correlated to chemical and topographical heterogeneity [15], which may explain the insufficient HA layer on the surface of ePTFE treated with the 0.5 ml/cm². With an incomplete layer of hydrophilic HA on the hydrophobic ePTFE, the heterogenous surface could have created a large hysteresis. Overall, the contact angle goniometry results show that HA enhancement significantly decreases the water contact angles of ePTFE, changing it from hydrophobic to hydrophilic. This is expected because HA is known for its high surface tension and water retention, while ePTFE has low surface tension and water retention [4,20,21].

The 0.8 ml/cm² treatment seems to create the hydrophilic surface with the lowest contact angles, even lower than that of the 1.3 ml/cm² treatment. The 1.3 ml/cm² treatment may have formed an extremely thick, but unstable, coating of HA on ePTFE; this would cause HA removal during sonication (last step in Figure 2.8), leading to an unevenly treated HA layer and an increase in the

advancing contact angle. Nevertheless, the static and receding contact angles were not significantly different between 0.8 ml/cm² and 1.3 ml/cm². Based on wettability results in Figure 2.13, the 0.8 ml/cm² HACTA/ethanol treatment was chosen for the fabrication process in the next series of studies.

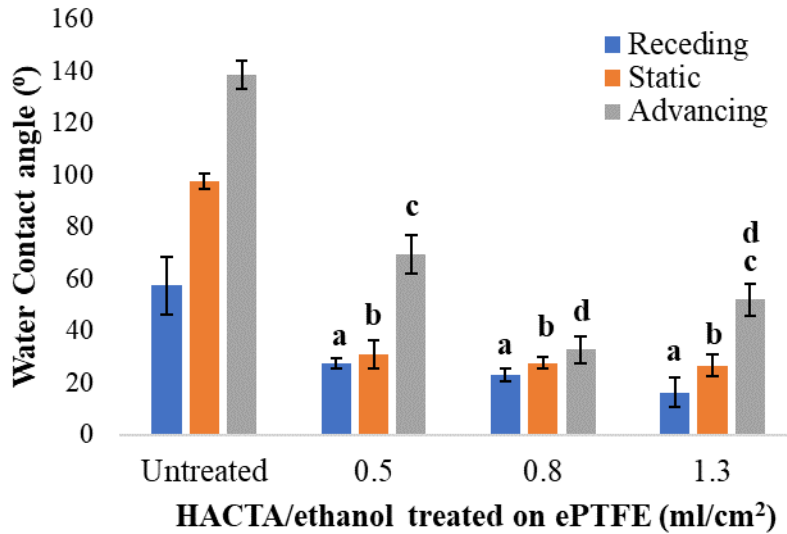


Figure 2.13: Water Contact angles of HA-ePTFE that was sprayed with different volumes of 0.4% HACTA/ethanol solutions. All samples were sprayed at 20 psi. Columns sharing the same letter means no statistical difference (p value < 0.05 , $n=4$). Data represent mean \pm standard deviation.

The results in Figure 2.14 demonstrate that increasing pressure of the air brush significantly lowers the shrinkage of the ePTFE graft while still maintaining a very hydrophilic surface in the inner lumen. When dry, ePTFE grafts were shrunk by $39 \pm 3.7\%$ if spraycoated with HACTA/ethanol at 20 psi, but they only shrank by $19 \pm 8.9\%$ when spraycoated at 25 psi. At both spraying pressures, the HA-ePTFE grafts re-expanded after hydration in DiH₂O for 1 hour; but the 25 psi samples recovered more, $9.5 \pm 3.1\%$ shrinkage compared to $28 \pm 1.1\%$ from the 20 psi batch. SEM images in Figure 2.15 compare the dry, untreated with 20 and 25 psi-treated surfaces. The

images further confirm that 25-psi treatment preserved the morphology of ePTFE by retaining the ridge and valley features on ePTFE that are created by the nodes and internodes. Although there is still inconsistency, as shown by random flat and hilly regions on SEM images of 25-psi surfaces, it is still a noticeable topographical difference compared to surfaces in the 20 psi images; this heterogeneity in 25 psi images may explain the larger water contact angle hysteresis for these samples than the 20 psi samples (Figure 2.14).

The results demonstrate that spray coating parameters can be adjusted to improve the use of airbrush for coating HA onto ePTFE. The pressure of the airbrush during spraying was increased to reduce shrinkage. Higher pressure spraying might have been able to quickly put more HA-CTA deeper into the internodes of ePTFE. The higher volume of internodal HA may have prevented contraction of the fibrils in the internodal regions. Based on Bernoulli's principle, applying a pressure of 25 psi instead of 20 psi along the air tube of the airbrush gun created a larger pressure gradient; this forms a higher velocity and a stronger spraying jet [22]. Although the flow rate was not methodically analyzed, it was observed that spraying the HACTA solution (0.8 ml/cm^2) at 25 psi took less than time at 20 psi (12 versus 25 minutes, respectively). The higher flow rate may have prevented shrinkage by packing more HA into the internodal regions of ePTFE. Pressures higher than 25 psi was also tested, but no reduction in shrinkage for ePTFE was observed. The samples treated a higher pressure neither appeared to have more HA nor lower water contact angles. This could be due to the limitation of the technique as everything was done manually, and spray coating with an airbrush at high pressure leads to more instability in handling. Based on the results, 25 psi was chosen for spray coating.

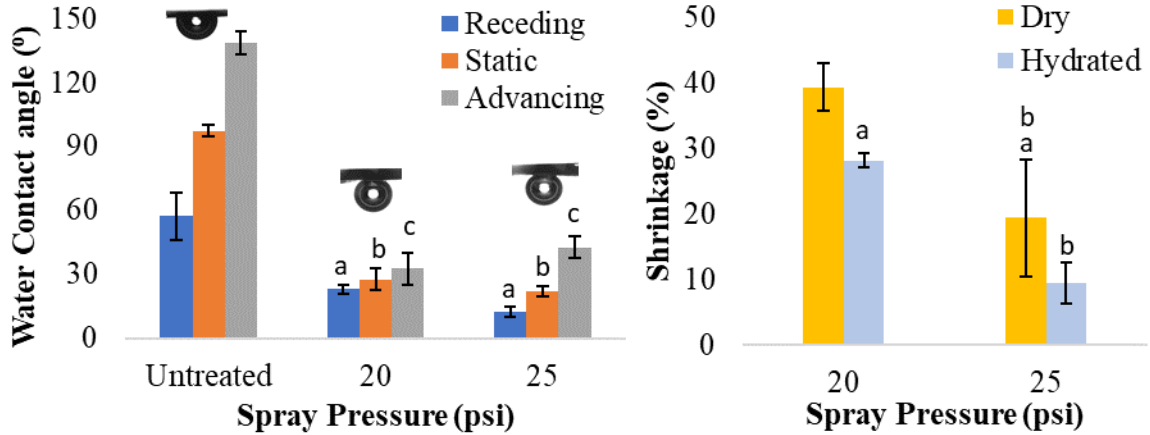


Figure 2.14: Water Contact angles of HA-ePTFE (left) and the shrinkage of ePTFE graft in longitudinal direction (right) that was sprayed at different pressures of HACTA/ethanol solutions. Images of air bubbles for measuring static water contact angles are above their respective treatment groups. All samples were sprayed with 0.8 ml/cm² of HACTA/ethanol. Columns sharing the same letter means they are not statistically different (p value < 0.05, $n=4$). Data represent mean \pm standard deviation.

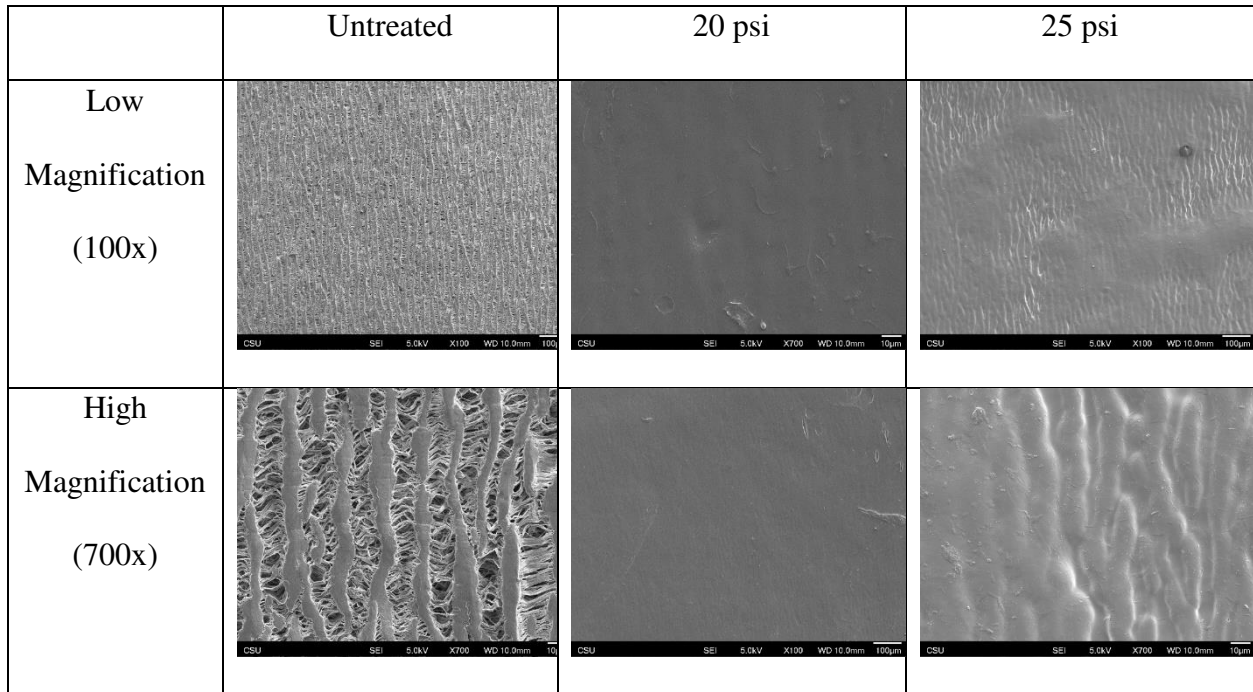


Figure 2.15: SEM images of untreated ePTFE and HA-ePTFE spray coated at 20 and 25 psi at low (bottom row) and high (top row) magnifications. Though there is not a clear consistency, the 25-psi treated HA-ePTFE surface (3rd column) appear to retain the ridges and valleys like those of the ePTFE surfaces (1st column), which are created by the nodes and internodes. 20-psi treated HA-ePTFE seems to form a flat surface.

FTIR spectra (Figure 2.16) confirm the presence of HA on the treated samples using the refined HA enhancement process (spraying coating 0.8 ml/cm² of HACTA/ethanol at 25 psi). The two significant peaks appearing on the plain ePTFE at 1220 and 1150 cm⁻¹ represent the stretching vibration of -CF₂- on the backbone of the ePTFE carbon chain. These peaks are no longer visible after the fluoropolymer is covered with HA. The chemical structures of HA appear in bands at 1650 and 1560 cm⁻¹ (C=O, and -NH- of the carboxylate groups), 2900 and 2800 cm⁻¹ (-CH₃- and -CH₂- stretching), and 3400 cm⁻¹ (OH of the glycoside rings). Presence of HA on the luminal surface is further confirmed by bands at 1400 cm⁻¹ (-COO- carboxylate symmetric stretch), 1320 and 1450 cm⁻¹ (C-CH and O-CH stretching), and 1060 cm⁻¹ (C-O-C bending). Surface chemical functionality is an important parameter in evaluating the interaction of blood with biomaterials. FTIR data show no fluorocarbon peaks. The visible peaks and their corresponding chemical groups are associated with HA presence, as shown from previous work [1]. The presence of HA is further validated by the TBO stained images in Figure 2.17.

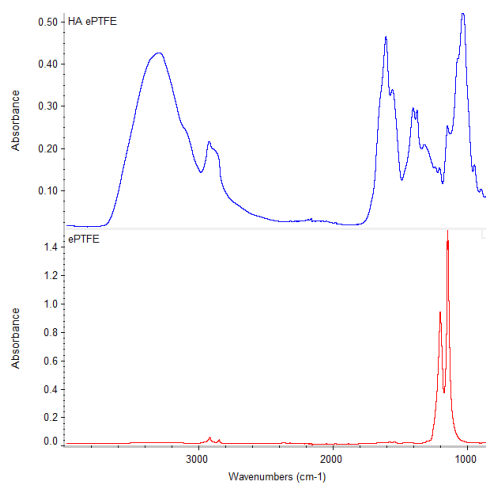


Figure 2.16: Representative FTIR spectra (left image) of plain ePTFE (bottom) and HA-treated ePTFE (top) confirm the presence of HA on the treated samples. Peaks at 1220 and 1150 cm⁻¹ (CF₂) (bottom) are the main intensive bands on ePTFE. Main bands indicative of HA (top) are 2900 (-CH₂), 3400 (-OH), 1650 and 1560 (-C=O, and -NH), 1400(-COO-), 1320 and 1450 (-C-CH and O-CH), and 1060 cm⁻¹ (-C-O-C-).



Figure 2.17: Pictures of HA-ePTFE (left) and ePTFE (right) after stained with TBO. It is evident that the treatment creates a confluent layer of HA on the inner lumen of ePTFE graft.

2.3.2 Mechanical Stability Results

The TGA results shown in Figure 2.18 are from the mechanical stability experiments. Approximately 1.56 ± 0.05 % of material burns off on HA-ePTFE that is not subjected to fluid shear, while 1.66 ± 0.38 % burns off HA-ePTFE under shear. The two groups are not statistically different from each other ($n=3$, $P=0.05$). Therefore, it does not appear that there is any loss of HA on the ePTFE after applying a hyper-physiological shear stress of 55 dyne/cm^2 . The fact that 0.04 ± 0.04 % (essentially none) of the untreated ePTFE burned off within the analyzed temperature range further confirms the material loss on treated samples is HA.

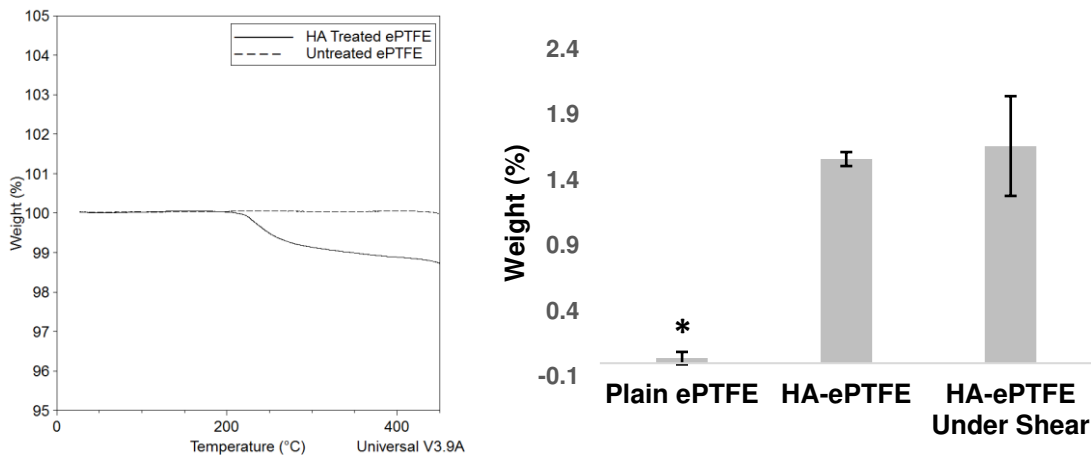


Figure 2.18: The thermogram (left) shows weight % burns off between 200 and 450°C for ePTFE and HA-ePTFE, and the bar graph (right) is the result from the flow study. Asterisk represents significant difference between plain ePTFE (negative control) and the HA treated ePTFE. The amount of HA on ePTFE before and after applying shear (55 dyne/cm²) for 7 days are not statistically different ($p < 0.05$). Data represent mean \pm standard deviation ($n=3$).

2.3.3 Circumferential Tensile Results

Figure 2.19 and Table 2-5 show data that were obtained from mechanical testing. Young's or elastic modulus is the ratio of applied stress to the corresponding strain in the elastic region, representing the ability of a material to withstand deformation in the non-plastic region of the stress strain curve. The elastic moduli for HA treated and untreated samples are 21.1 ± 0.8 and 21.2 ± 0.4 MPa, respectively, which are not statistically different. The tensile data also reveal that, while under tension, the HA-ePTFE graft can withstand the same amount of force as its untreated counterpart. The tensile strength of HA treated and untreated are 5.8 ± 0.4 and 6.7 ± 0.3 MPa; there was a slight, but not statistically significant, decrease after HA treatment. Tensile strength is the maximum stress a material experiences before failure. The tensile strength and strain at failure are indicative of the ability for the ePTFE to withstand external force and deform before ruptures (Figure 2.19). The strain at failure of HA-ePTFE appears slightly lower than the untreated result (5.5 ± 0.5 to 6.4 ± 0.6 MPa), but they are not statistically different ($p < 0.05$). The tensile strength

and strain at failure for both HA-treated and untreated ePTFE grafts are not statistically different, indicating the HA treatment did not change these mechanical properties. Another important parameter is yield stress, which is the stress exerted on ePTFE just before permanent deformation begins. Vascular grafts are required to deliver blood under varying pressures, leading to constant dilation and contraction [23]. The yield stress for ePTFE and HA-ePTFE are 2.33 ± 0.36 and 2.15 ± 0.11 MPa, showing that the HA enhancement does not statistically change the yield stress of the ePTFE vascular graft.

Despite shrinkage of ePTFE graft during the HA treatment that could have created a denser material, there were no changes in the tensile properties. It may be that, when HA-ePTFE is hydrated, the $9.5 \pm 3.1\%$ shrinkage did not significantly change the density enough to affect the mechanical properties. It was not surprising that the addition of HA did not affect the tensile properties. The biopolymer has a very low modulus and tensile strength relative to ePTFE, and it only contributes $1.56 \pm 0.05 \%$ to HA-ePTFE. By the rule of mixture, ePTFE predominantly influences the tensile properties [24].

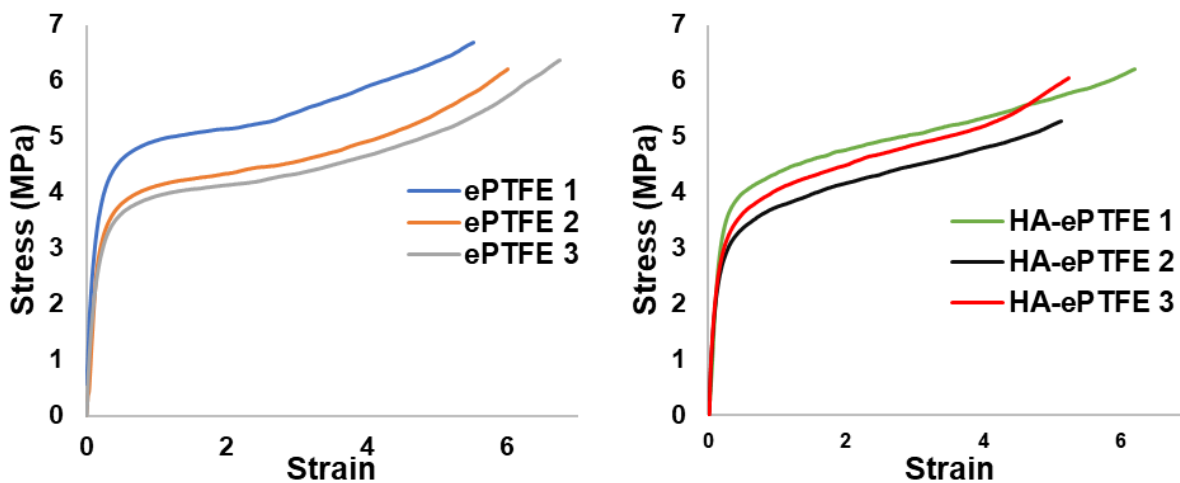


Figure 2.19: Stress and strain plots of ePTFE and HA-ePTFE grafts from the circumferential tensile test. The sample size was three.

Table 2-5: Elastic modulus, failure strain, tensile stress, and yield stress of HA-treated and untreated ePTFE from the circumferential tensile test showing no significant changes in the tensile properties of ePTFE after treatment with HA. (n=3, p<0.05). Data is presented as mean ± standard deviation.

	ePTFE	HA-ePTFE
Young's Modulus (MPa)	21.2 ± 0.39	21.2 ± 0.84
Yield Strength (MPa)	2.33 ± 0.36	2.15 ± 0.11
Tensile Strength (MPa)	6.69 ± 0.28	5.84 ± 0.41
Strain at Failure	6.36 ± 0.59	5.50 ± 0.48

2.4 Limitations & Future Work

Pressure and volume per unit area of the spray coating technique were investigated, but further optimization of the process can be made by adjusting other parameters. For example, viscosity of the HACTA/ethanol solution could vary to determine the best concentration. The concentration that was picked is 0.4 % (w/v) HACTA/ethanol because it was shown to be diluted enough to form a spray cone through the annular opening of the airbrush during spray coating. Another effect that could be influenced by viscosity and solution density is the spraying concentration, or the HACTA density in the spray cone immediately before the molecules bombarded ePTFE. Minimal HACTA residual was observed forming on the tip of the nozzle of the air brush was observed, and this may reduce the efficiency of the technique with time. Along with adjusting the viscosity and density, the efficiency could be improved by lowering the MW of HA. Indeed, low MW HA has been shown to be more effective by mitigating back diffusion as seen in electro spraying [25]. Optimizing the spraying parameters to improve consistency could also help accurately measure the flow rate and the deposition layer of HA on the ePTFE surface. Nevertheless, the experimental

data demonstrate an effective method in forming HA in the inner lumen of medical grade ePTFE graft that might be enough for cardiovascular applications.

It must be noted that the contact angle equations (1), (2), and (3) only apply to flat and chemically uniform surfaces [14], which may not be the case for ePTFE and HA-ePTFE as seen in figure 7.

The contact angle data is for evaluating wettability and cannot be used for accurately measuring surface energies. SEM images (Figure 2.15) show rougher surfaces on ePTFE than HA-ePTFE, but these were taken when the samples were dry. Further investigation is required to determine the topography of hydrated HA-ePTFE that is more representative of a physiological environment. Indeed, surface area and porosity could be altered by the HA layer, and further investigation is of great interest. Sophisticated surface characterization techniques such as scanning white light interferometry and atomic force microscopy could accurately map the swollen surface. They may also provide other topological features including surface roughness and stiffness.

Mechanical stability testing demonstrates that the HA layer can withstand hyper-physiological shear, as seen in the TGA results (Figure 2.18) [16]. Despite lasting for seven days, the applied shear stress in the flow study was more than three times the average physiological wall shear stress in blood vessels, which is approximately 15 dyne/cm^2 [16]. The HA layer on the ePTFE appeared to be mechanically stable despite having no chemical links between the isocyanate crosslinked HA and ePTFE. It is possible that the high porosity of ePTFE, due to its internodal space, may allow HA to penetrate and persist in the polymeric graft. Nevertheless, future work is required to better characterize the mechanical and biological stability of the HA on ePTFE. Examples include enzymatic degradation studies.

Although the HA-ePTFE graft never fully recovered to its original length even when hydrated (Figure 2.14), the shrinkage did not significantly change the elastic modulus, tensile strength, yield

stress, or strain at failure. Future work may be needed to prevent or reduce shrinkage, because this phenomenon could possibly affect other properties of the grafts. The mechanical properties of ePTFE play an influential role in determining its biomedical applications. These characteristics are often controlled during material fabrication. Examples are internodal distance and density, where specific requirements are met by adjusting the sintering, heating and stretching of the Teflon® [26]. Therefore, various ePTFE vascular grafts and patches exhibit different porosities and densities [27]. The HA-ePTFE process does not significantly alter the elastic modulus, tensile strength, yield stress, and strain to failure of the ePTFE (Table 2-5). Future work should involve evaluating whether the treatment affects other mechanical properties such as pressurized burst strength, compliance, and relaxed and pressurized internal diameter. Although the mentioned parameters aim toward tubular grafts for bypasses, the HA enhancement technique can be used for other ePTFE based devices. In those cases, properties such as kink radius, suture retention strength, and diaphragm pressurized burst strength must be considered. Compliance mismatch is another issue facing synthetic ePTFE vascular grafts especially small diameter grafts, because the material characteristics of the ePTFE are significantly different from that of the soft small blood vessel it replaces. These differences cause increasing wall stress at the implant site [28]. How HA-ePTFE can overcome such challenges needs to be addressed in follow up studies.

References

- [1] D.A. Prawel, H. Dean, M. Forleo, N. Lewis, J. Gangwish, K.C. Popat, L.P. Dasi, S.P. James, Hemocompatibility and hemodynamics of novel hyaluronan–polyethylene materials for flexible heart valve leaflets, *Cardiovascular Engineering and Technology*. 5 (2014) 70–81.
- [2] N.R. Lewis, Hyaluronic acid enhancement of expanded polytetrafluoroethylene for small diameter vascular grafts, Colorado State University, 2014.
- [3] R. Koch, Improving Hydrophilicity of Silicone Elastomer by IPN Formation with Hyaluronan, Colorado State University, 2016.
- [4] D. Mańko, A. Zdziennicka, B. Jańczuk, Surface tension of polytetrafluoroethylene and its wetting by aqueous solution of some surfactants and their mixtures, *Applied Surface Science*. 392 (2017) 117–125. doi:10.1016/j.apsusc.2016.09.020.
- [5] L. Eykens, K. De Sitter, C. Dotremont, L. Pinoy, B. Van der Bruggen, Membrane synthesis for membrane distillation: A review, *Separation and Purification Technology*. 182 (2017) 36–51. doi:10.1016/j.seppur.2017.03.035.
- [6] P. Zilla, D. Bezuidenhout, P. Human, Prosthetic vascular grafts: wrong models, wrong questions and no healing, *Biomaterials*. 28 (2007) 5009–5027.
- [7] M. Zhang, Surface modification of ultra high molecular weight polyethylene with hyaluronan for total joint replacement application, 2004.
- [8] D.R. Burfield, R.H. Smithers, Desiccant efficiency in solvent drying. 3. Dipolar aprotic solvents, *The Journal of Organic Chemistry*. 43 (1978) 3966–3968. doi:10.1021/jo00414a038.
- [9] F. Deyhimi, J.A. Coles, Rapid Silylation of a Glass Surface: Choice of Reagent and Effect of Experimental Parameters on Hydrophobicity, *Helvetica Chimica Acta*. 65 (1982) 1752–1759. doi:10.1002/hlca.19820650610.
- [10] H. Dean, Development of Biopoly® Materials for use in Prosthetic Heart Valve Replacements, Colorado State University, 2012.
- [11] Z. Ma, Z. Mao, C. Gao, Surface modification and property analysis of biomedical polymers used for tissue engineering, *Colloids and Surfaces B: Biointerfaces*. 60 (2007) 137–157.
- [12] A. Ravve, Principles of polymer chemistry, 3rd ed., Springer Science & Business Media, 2013.
- [13] M.E. Schrader, Young-Dupre Revisited, *Langmuir*. 11 (1995) 3585–3589. doi:10.1021/la00009a049.
- [14] J. Drelich, J.D. Miller, R.J. Good, The effect of drop (bubble) size on advancing and receding contact angles for heterogeneous and rough solid surfaces as observed with sessile-drop and captive-bubble techniques, *Journal of Colloid and Interface Science*. 179 (1996) 37–50.

- [15] L. Gao, T.J. McCarthy, Contact angle hysteresis explained, *Langmuir*. 22 (2006) 6234–6237.
- [16] T.G. Papaioannou, C. Stefanadis, Vascular wall shear stress: basic principles and methods, *Hellenic J Cardiol*. 46 (2005) 9–15.
- [17] N. Westerhof, N. Stergiopoulos, M.I.M. Noble, *Snapshots of Hemodynamics*, Springer US, Boston, MA, 2010. doi:10.1007/978-1-4419-6363-5.
- [18] W.O. Lane, A.E. Jantzen, T.A. Carlon, R.M. Jamiolkowski, J.E. Grenet, M.M. Ley, J.M. Haseltine, L.J. Galinat, F.-H. Lin, J.D. Allen, G.A. Truskey, H.E. Achneck, Parallel-plate Flow Chamber and Continuous Flow Circuit to Evaluate Endothelial Progenitor Cells under Laminar Flow Shear Stress, *Journal of Visualized Experiments: JoVE*. (2012) 3349. doi:10.3791/3349.
- [19] J. Kestin, M. Sokolov, W.A. Wakeham, Viscosity of liquid water in the range- 8 C to 150 C, *Journal of Physical and Chemical Reference Data*. 7 (1978) 941–948.
- [20] D. and Pasqui, Polysaccharide-based hydrogels: the key role of water in affecting mechanical properties, *Polymers*. 4 (2012) 1517--1534.
- [21] J. Li, A. He, C.C. Han, D. Fang, B.S. Hsiao, B. Chu, Electrospinning of Hyaluronic Acid (HA) and HA/Gelatin Blends, *Macromolecular Rapid Communications*. 27 (2006) 114–120. doi:10.1002/marc.200500726.
- [22] H. Lee, *Experimental Study of the Atomization Process for Viscous Liquids by Meniscus Perturbation and Micro Air Jet*, (n.d.) 79.
- [23] J.D. Kakisis, C.D. Liapis, C. Breuer, B.E. Sumpio, Artificial blood vessel: The Holy Grail of peripheral vascular surgery, *Journal of Vascular Surgery*. 41 (2005) 349–354. doi:10.1016/j.jvs.2004.12.026.
- [24] W.D. Callister, D.G. Rethwisch, *Materials science and engineering*, John Wiley & Sons NY, 2011.
- [25] Z. Tan, Partial reflection of hyaluronan molecules inside the Taylor-cone during electrospray, *World Congress on Engineering and Technology*. (2012) 84.
- [26] C.E. Banas, T.J. Edwin, Expanded polytetrafluoroethylene vascular graft with increased healing response, Google Patents, 2002. <https://www.google.com/patents/EP1185313A1?cl=en>.
- [27] V. Shankaran, D.J. and Weber, A review of available prosthetics for ventral hernia repair, *Annals of Surgery*. 253 (2011) 16--26.
- [28] D.N. Ghista, F. Kabinejadian, Coronary artery bypass grafting hemodynamics and anastomosis design: a biomedical engineering review, *Biomedical Engineering Online*. 12 (2013) 129.

Chapter 3: Fabrication and Characterization of HA-LLDPE

3.1 Introduction & Preliminary Work

Previous research has described the modification of HA into silyl-hyaluronan-cetyltrimethylammonium (SHACTA) to make the HA soluble in xylenes and other organic solvents [1]. SHACTA can penetrate or diffuse into LLDPE that is swollen in heated xylenes; once the SHACTA has been crosslinked and reverted to HA via hydrolysis, a sequential IPN is formed [2]. Unfortunately, this enhancement process often creates inconsistent HA confluency on the surface of the LLDPE; in the present work, a novel vapor crosslinking method is explored to mitigate this problem. Furthermore, the new crosslinking method can potentially increase HA presence on LLDPE, which is correlated with surface wettability [3]. The previous HA-LLDE fabrication technique can create an HA layer with a static water contact angle of $28 \pm 20^\circ$ [4], but data from literature has shown HA enhanced polymers can be more hydrophilic with lower static contact angles and smaller standard deviations [5,6].

It has been shown that vapor crosslinking has many benefits including maintaining the structures and improving the shelf life of biomaterials [7,8]. Moreover, vapor techniques can be better controlled and less prone to homopolymerization of crosslinking agents [7,9]. Although vapor crosslinking involving volatile fixatives such as glutaraldehyde and formaldehyde have long been implemented in the biomedical field [7], utilization of isocyanates vapor crosslinkers has not been investigated. The next section describes the HA enhancement of LLDPE similar to past research [2], but the herein process uses 2,4 toluene diisocyanate (TDI) for vapor crosslinking and a controlled draining method during SHACTA treatment.

3.1.1 Preliminary HA-LLDPE Fabrication

The following procedure describes the HA enhancement process of LLDPE in this dissertation.

Figure 3.1 shows the schematic of the process. The detailed protocol can be found in the appendix.

1. Complexation and silylation of HA were performed following previous work [1] and reaction scheme is shown in Figure 3.2. Protocols for the process are in the appendix. Briefly, sodium hyaluronate at 750 kDa (Lifecore Biomedical) and cetyltrimethylammonium bromide (CTAB) (Fisher Scientific) were each dissolved in room temperature deionized water (DiH_2O). The CTAB solution was slowly added to the HA solution while stirring to form a hyaluronan-cetyltrimethylammonium (HA-CTA) precipitate, which was then washed with DiH_2O to remove CTAB residue. The purified HA-CTA was granulated and dried under vacuum at 50°C . To synthesize the silyl HA-CTA, DMSO was added to HA-CTA under dry N_2 flow; the solution was stirred at 50°C until the HA-CTA was completely dissolved. The HA-CTA and DMSO solution temperature was increased to 75°C and hexamethyldisilazane (HMDS) was added under dry N_2 flow; the reaction was carried out for 48 hours with constant stirring. The resulting two-phase solution was separated, and the top layer containing the silylated HA-CTA (SHACTA) was washed five times with xylenes through rotary evaporation. The SHACTA was then dried at 50°C under vacuum and then stored under vacuum in a desiccator. The quality of SHACTA batches is discussed elsewhere, and the degree of silylation (DS) was demonstrated to be consistently high enough for SHACTA to be soluble in xylenes [1,10]. The DS for each SHACTA batch was measured using techniques described in literature [1]. Batches with DS of at least 3.2 were used for HA enhancement, because this DS was deemed high enough for the SHACTA to be soluble in xylenes [1].

2. Dowlex 2056 LLDPE (Dow Corning) blown extruded films were cleaned in acetone, immersed in xylenes for 12 hr, and then vacuum dried at 50 °C prior to further use. Figure 3.1 describes the general HA enhancement procedure using SHACTA, with details on SHACTA concentration and vapor crosslinking in the sections below.
3. Similar to previous work [11], LLDPE films were swollen in SHACTA/xylene solution for 1 hour to swell the polyethylene and allow for molecular penetration with the modified HA (step 1 in Figure 3.1).
 - a. Xylenes was dried by incubating in 4Å molecular sieves at 10% w/v for at least 72 hours. The solvent was then distilled in a nitrogen purged environment removing any trace of sieves and water content. The water content of the dried xylenes was verified to be below 500 ppm, and all glassware vessels exposed to 2,4 toluene diisocyanate (TDI) and xylenes were treated with hexamethyldisilazane (HMDS) (Sigma) as described in Section 2.1.2 [12]. Xylene distillation protocol is in the appendix.
4. After swelling, the film was then held upright in a fritted funnel by clipping onto a thin Teflon ring. The SHACTA solution was then added into the fritted funnel and allowed to drain from the vessel (Step 2 in Figure 3.1). Two different draining rates, 1.75 and 0.3 mm/min, were tested. Afterward, the SHACTA-treated LLDPE was dried for at least three hours in a vacuum oven (Step 3). Previous work has shown this is long enough to remove xylenes from the swollen LLDPE [10,11].
5. The SHACTA treated on LLDPE was vapor crosslinked for one hour by incubating the LLDPE film above a 2 (v/v) % TDI/xylene solution under heat (Step 4). Samples were then

dried for at least three hours to fully remove xylenes; they were then rinsed with acetone by swirling in the solvent for at least five minutes to remove any uncrosslinked TDI.

- a. Xylenes were dried, and all glassware were silylated same as step 3a.
 - b. The entire crosslinking experiment was performed in a nitrogen purged glove bag to prevent moisture contamination.
6. After crosslinking, samples were dried in vacuum oven at 50°C for at least three hours (Step 5). Previous work has shown this is long enough to remove xylenes from the swollen LLDPE [10,12].
 7. SHACTA was reverted to HA by sonicating the samples in 0.2 M NaCl DI water/ethanol (1:1) solutions for three hours and 0.2 M NaCl/DI water for one hour, allowing the sonicator to heat up to 40°C (Step 6). Excess uncrosslinked HA and its derivatives were further removed by incubating the treated LLDPE in a DI water/ethanol (3:2) solution for at least 2 hours, before a final wash by sonicating in DI water for 30 minutes. The process was adopted from previous work [10,13].
 8. To determine the HA surface density of the biomaterials, samples were soaked in 0.1% toluidine blue O (TBO) solution containing 8 M of urea for 10 min as described literature [14] and the appendix. Stained samples were submerged in 50% acetic acid solution for 30 minutes to release all the bound TBO from the material surface into the eluting solution. The absorbance of the eluting solution was determined through fluorescent spectrometry (FLUOstar Omega) (excitation at 630 nm). The TBO concentration in the eluting solution was quantified based on known standards. The quantity of HA per nominal surface area, or surface density, of the sample was calculated assuming that one TBO molecule consistently binds to one HA repeating unit. The MW of HA was 740 KDa, and the nominal

surface area of the samples was 102 mm². Samples were 70 μm thick and created from 8 mm diameter biopsy punches.

9. Captive bubble water contact angle goniometry was used to assess HA coverage on LLDPE; protocols for these techniques are in the appendix. Description of captive bubble goniometry is in section 2.1.2.

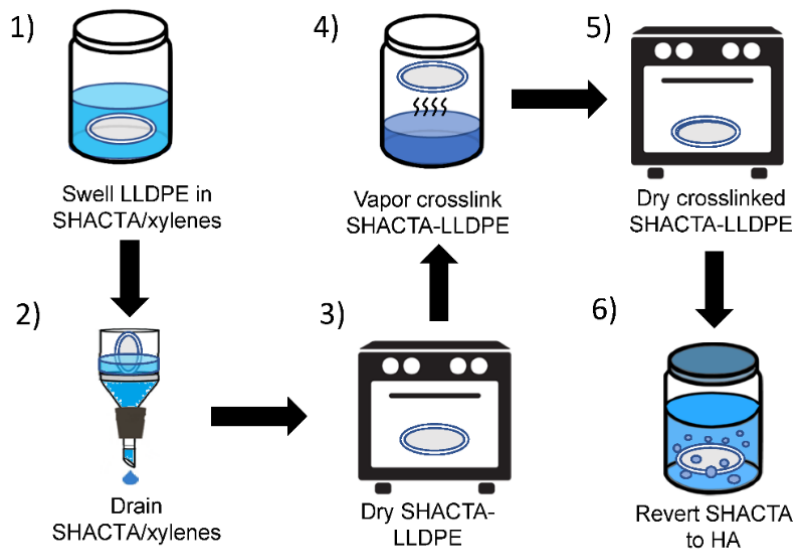


Figure 3.1: Schematic of the HA enhancement process for LLDPE.

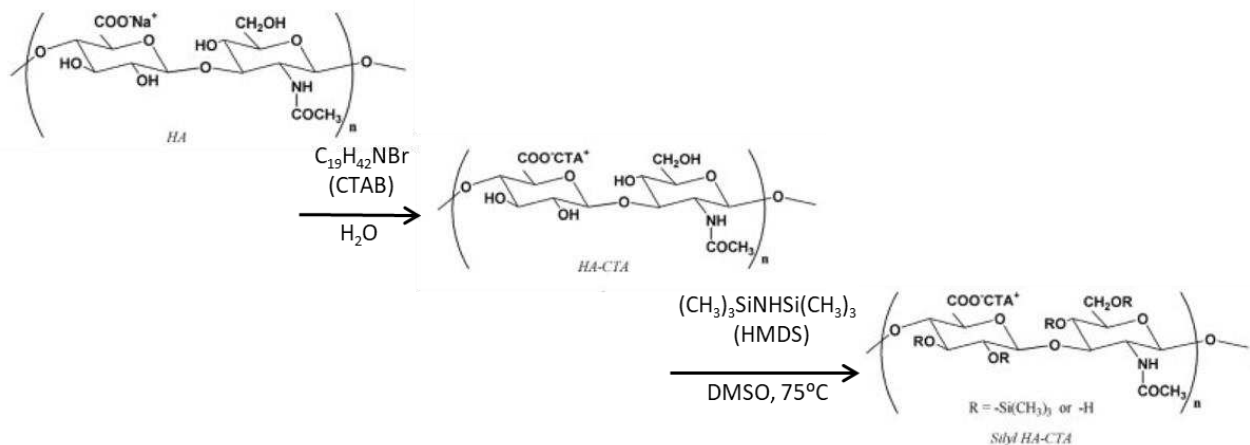


Figure 3.2: Chemical modification of carboxyl and hydroxyl groups HA using CTAB and HMDS.

3.1.2 Preliminary Results

Figure 3.3 shows TBO stained image of HA-LLDPE along with the HA surface density data from the preliminary study. The HA densities of HA-LLDPE for draining rate of 1.75 and 0.3 mm/min are $7.4\text{e-}7 \pm 2.8\text{e-}7$ and $4.2\text{e-}6 \pm 1.2\text{e-}6$ $\mu\text{mol}/\text{cm}^2$, respectively. The TBO stain is known to bind to HA through bonding at the carboxyl group [14]. An increasing concentration of TBO correlates to more HA coverage at the surface. Note that the LLDPE is originally colorless and clear. This is an effective method for approximating surface density of HA on treated samples. Assumptions were that every TBO molecule bonded to one HA repeating unit and the molecular weight of HA are the same on every sample.

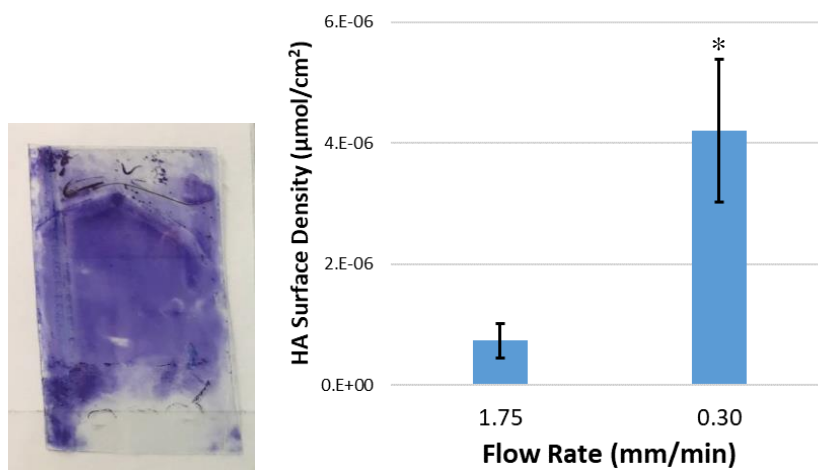


Figure 3.3: TBO stained image HA-LLDPE (left) of slow draining (0.30 mm/min). Dark blue to purple is representative of HA. Top and bottom portions of LLDPE has no HA because they were clipped during treatment. HA Surface density of LLDPE in two different draining rates, 1.75 and 0.30 mm/min are shown on the right. The lower rate has more than 4 times the HA on its surface than the faster rate. The asterisk means significant difference ($n=4$, p value < 0.05). Data represent mean \pm standard deviation.

The quantitative data of HA on LLDPE proves there is more incorporation of HA at a slower draining rate. Indeed, literature has shown LLDPE rearrangement is different depending on the

speed at which the polymer is being solvent casted from xylenes [15]. LLDPE films casted when the polymer is slowly pulled out of xylenes allows more time for the carbon backbone to be mobile. That extra swelling time while draining may allow more penetration of HA into the polymer network creating a more prominent layer of HA on LLDPE. Because 0.3 mm/min draining creates significantly more HA on the surface. This parameter was picked to fabricate HA-LLDPE for further characterization. LLDPE treated with HA showed a significant decrease in all contact angles compared to the untreated groups (Figure 3.4). The respective static, receding, and advancing angles of untreated LLDPE are $86 \pm 1.9^\circ$, $75 \pm 0.7^\circ$, and $104 \pm 3.8^\circ$. The angles for HA treated counterparts are $32 \pm 1.2^\circ$, $25 \pm 9.1^\circ$, and $57 \pm 19^\circ$, respectively.

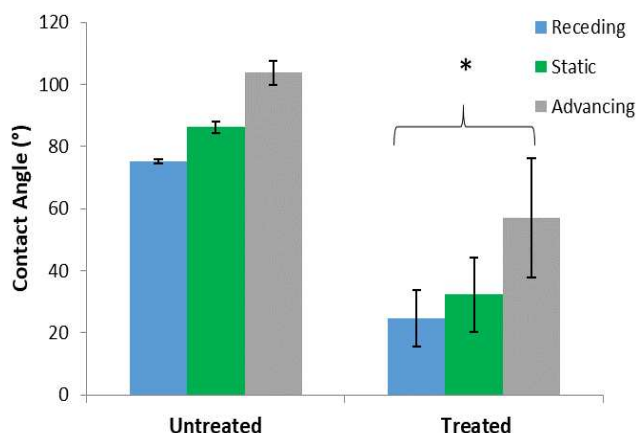


Figure 3.4: Goniometric data shows a significant decrease in all contact angles for treated samples compared to the plain LLDPE (left graph). Data represent mean \pm standard deviation. The asterisk symbolizes a significant difference between treated and untreated group for each and all angle types. ($n = 3$, $p < 0.05$)

Based on all the results from preliminary work, the fabrication process that involves slow draining SHACTA/xylenes (0.3 mm/min) and TDI/xylene vapor for crosslinking are effective at enhancing LLDPE with HA. Nonetheless, the process must be further studied to understand the effect of the

fabrication steps. To this end, the concentration of the SHACTA treatment and various parameters of the crosslinking steps were adjusted. Characterizations were performed on both HA treated and untreated LLDPE for comparison. The usage of 2,4 toluene diisocyanate (TDI) was analyzed for vapor crosslinking HA to form an IPN with LLDPE. The effect of SHACTA concentration during the interpenetration/diffusion stage of IPN formation was also explored. Surface properties of the HA-LLDPE IPN were studied, along with its tensile properties and cytocompatibility.

3.2 Materials and Methods

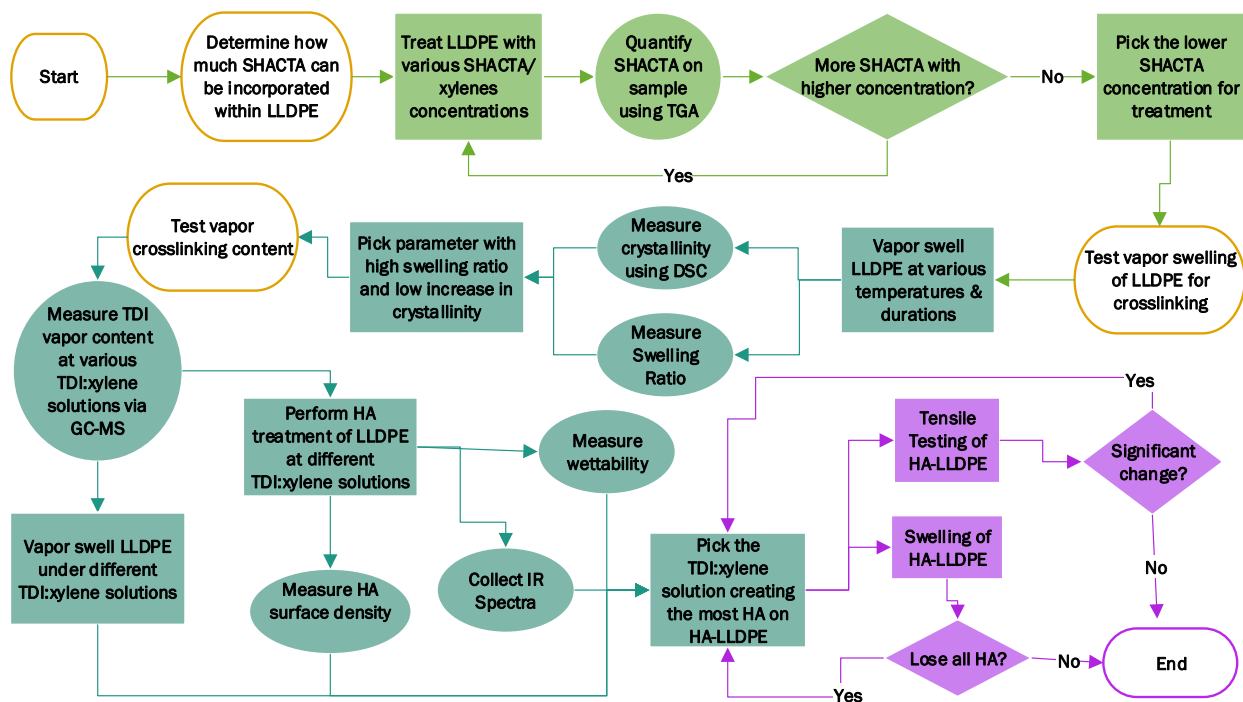


Figure 3.5: Schematic of the refinement process for fabricating HA-LLDPE.

Figure 3.1 describes the HA-LLDPE IPN fabrication process investigated in this paper. The effect of SHACTA concentration (step 1 of Figure 3.1) and its results are shown in Figure 3.7. The data from swelling of LLDPE by xylenes (step 3 of Figure 3.1) to promote interpenetration of TDI are

in Figure 3.8. After determining the appropriate parameters in step 1 and 3 in the fabrication process, the entire HA enhancement process was performed under various TDI vapor contents to test their effects. The most appropriate crosslinker vapor content was determined based on the wettability and HA surface density of the fabricated biomaterials. Tensile properties and IPN verification of the final biomaterial were then assessed. Figure 3.5 shows the refinement process for enhancing LLDPE with HA.

3.2.1 SHACTA Concentration Study

Different SHACTA/xylene concentrations (0.5, 1.0, 2.0, 3.0%) were tested to determine how much SHACTA can penetrate into LLDPE from this technique. SHACTA treated LLDPE (step 1 and 2 of Figure 3.1) was burned in a thermogravimetric analyzer (TGA) to determine the wt% composition of SHACTA. The decomposition temperatures of SHACTA were found by burning the material under N₂ purge from 25 to 600°C. It was determined that the main decomposition range of SHACTA was 125 and 300°C (80.0 ± 0.69 %, n = 4). Similar tests were performed with Virgin LLDPE and its decomposition temperatures were above 350°C while the small percent of LLDPE burns off at the major thermal decomposition range of SHACTA (1.01 ± 0.20 %). Understanding the decomposition kinetics of SHACTA and LLDPE, the SHACTA composition on SHACTA treated LLDPE was calculated.

3.2.2 Vapor Swelling Test

The swelling of LLDPE in the vapor crosslinking process (step 4 of Figure 3.1) was studied. The LLDPE film was cut into rectangular pieces (3.5 x 2.5 cm) and incubated above a 10 ml xylene solution in a 100 ml container at various durations (0.25, 0.5, 1.0, and 2.0 hours) and temperatures (50, 60, and 70°C). The dry (W_0) and swollen (W_s) weights of the samples were recorded. The

swollen ratio was calculated using equation 1, and the densities (ρ) of xylenes and LLDPE were determined to be 0.92 and 0.87 g/cm³, respectively.

$$\text{swelling ratio} = \frac{(W_s - W_0) / \rho_{xylenes}}{W_0 / \rho_{LLDPE}} \quad (1)$$

Because the HA enhancement process of LLDPE required swelling of the base polymer, it was important to verify whether this changed the percent crystallinity (% χ_c) of the polyethylene that may have led to molecular rearrangement and affect the material properties. A differential scanning calorimeter (TA Modulated DSC 2500) was used to heat the LLDPE from 40 to 180°C at a rate of 10°C/min under N₂ purge. % χ_c was calculated by dividing the heat of fusion (H_f) of the sample by H_f of 100 % crystalline polyethylene (288 J/g) and multiplying by 100 [16]. Ultimately, higher degree of swelling and lower degree of change in % χ_c for LLDPE are preferred.

3.2.3 The Effect of Crosslinking Vapor Content on HA-LLDPE IPN

To test the effect of the TDI vapor content on HA-LLDPE, various TDI concentrations (2%, 50%, 75%, 100%) were used in the HA treatment. All other parameters were kept constant based on the previous studies; these are the SHACTA concentration, the crosslinking time and temperature; they were chosen depending on the results from the SHACTA concentration study and vapor swelling test.

3.2.3.1 Measurement of TDI Vapor

Calculation of TDI vapor was determined using headspace gas chromatograph-mass spectrometry (GC-MS; Waters Quattro Micro GC). After incubating pure TDI until equilibrium at various temperatures, 10 μ l of the vapor in the headspace were injected into the GC capillary column (Restek Rtx-35) with initial and final temperatures of 100°C and 310°C, respectively. The ramping

rate was 20°C/min, and the carrier gas was helium. Peak areas of the chromatograms were calculated at the retention time of TDI (10 min) knowing that mass/ion (m/z) ratio of 174 belongs to TDI. A ladder (Figure 3.9) was created to correlate peak areas from chromatograms to vapor concentration using equations from literature [17,18].

3.2.3.2 Surface Characterization

Surface wettability was assessed by measuring water contact angles via the captive bubble technique using a goniometer (260-F4 Ramé-Hart Instrument); detailed description of the process is in section 2.2.1. Toluidine blue O (TBO) staining and quantitative assessment was done as described in section 3.1.1. Protocols for goniometry and TBO staining are in the appendix. Attenuated total reflectance-Fourier Transform Infrared Spectroscopy (ATR-FTIR) (Nicolet iS50) was used to qualitatively analyze the chemical groups on the virgin LLDPE and HA-LLDPE. Samples were face down on the ATR diamond for the spectrometer to run 32 scans.

3.2.4 IPN Verification of HA-LLDPE

To determine whether an IPN was formed between HA and LLDPE, after manufacturing and hydrolysis, as described in previous sections, HA-LLDPE samples were swollen by submerging in xylenes at 50°C for one hour. The goal was to expand the LLDPE film and assess how much of the physically interlocked, crosslinked HA would be released. After swelling, the HA-LLDPE samples were cleaned with paper wipes to remove xylenes, and their swollen weight was immediately measured; samples were then dried until future analysis. The swollen ratio along with surface characterization such as IR spectrometry, water contact angle, and HA surface density were recorded.

3.2.5 Tensile Testing

Mechanical properties of LLDPE was assessed according to ASTM D882-18[19] using a tensometer (Instron 5966) at 23 ± 4 °C and $50 \pm 5\%$ humidity. LLDPE and HA-LLDPE samples were soaked in DI water for at least a day to ensure HA was fully hydrated. The initial gauge length and the crosshead speed were set at 25 mm and 500 mm/min, respectively. Samples were tested in both the transverse (TD) and machine directions (MD) of the blown film ($n = 5$). Elastic modulus was determined as the best-fit slope of the elastic region of stress-strain curves. Yield stress and strain were calculated by finding the 0.2% strain offset of the elastic region. Toughness, or the energy required for rupturing, was the area under the stress and strain curve. Data from HA-LLDPE were compared with that of virgin LLDPE.

3.2.6 Statistical Analysis

All data were tested for normal distribution (Anderson-Darling test) and equal variances (Levene's test). One-way ANOVA was run along with a post hoc test. The Tukey test was used for homoscedastic data groups, while the Games-Howell test was used for heteroscedastic ones. All data analysis was performed on Minitab 17 for statistical differences (p value = 0.05). The initial sample size was either four or three in all the experiments. Power analysis (GPower 3.1) was then performed after each study to verify the required sample size (effect size = 0.8).

3.3 Results & Discussion

3.3.1 SHACTA Concentration Study

Figure 3.7 shows the results from the SHACTA concentration study. SHACTA mostly decomposes between 125 and 300°C ($80.0 \pm 0.69 \%$) (Figure 3.6), while only $1.01 \pm 0.20 \%$ LLDPE decomposes at this temperature range. The SHACTA composition of treated LLDPE can be seen burning off between 125 and 300°C, which was quantified based on the known amount that SHACTA and LLDPE decompose in this temperature range. The SHACTA contents for 0.5, 1.0, 2.0, and 3.0 % SHACTA/xylene treatments are 0.18 ± 0.09 , 0.72 ± 0.39 , 0.82 ± 0.37 , $1.01 \pm 0.48 \%$, respectively. The 0.5 % treatment creates the least amount of SHACTA content on LLDPE, statistically less than other treatments. Although there appears to be a positive correlation between treatment concentration and the resulting SHACTA content for 1.0, 2.0, and 3.0 %, the standard deviations are large. The large variances could result from the appearance of an uneven layer of crosslinked HA at the surface due to irregular entanglement of the bulky HA (750 KDa) within the LLDPE, which would likely be greater with higher HA concentration. It seems that treating LLDPE samples with 1.0 % SHACTA/xylene provides a sufficient amount of HA compared to higher concentrations. Raising the SHACTA treatment concentration above 1% does not appear to statistically increase the amount of HA on LLDPE. Therefore, the 1% SHACTA treatment concentration was chosen for the next set of studies. Concentrations higher than 3% were not tested because previous work has shown this to be too viscous that may affect HA diffusing into LLDPE [10].

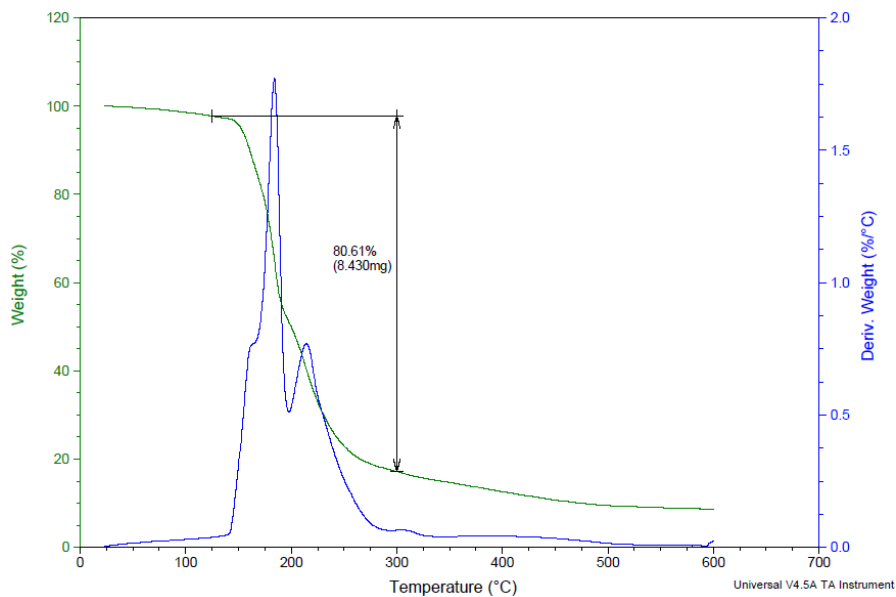


Figure 3.6: Representative thermogram of SHACTA. Approximately $80.0 \pm 0.69\%$ of SHACTA burns off between 125 and 300°C ($n=4$).

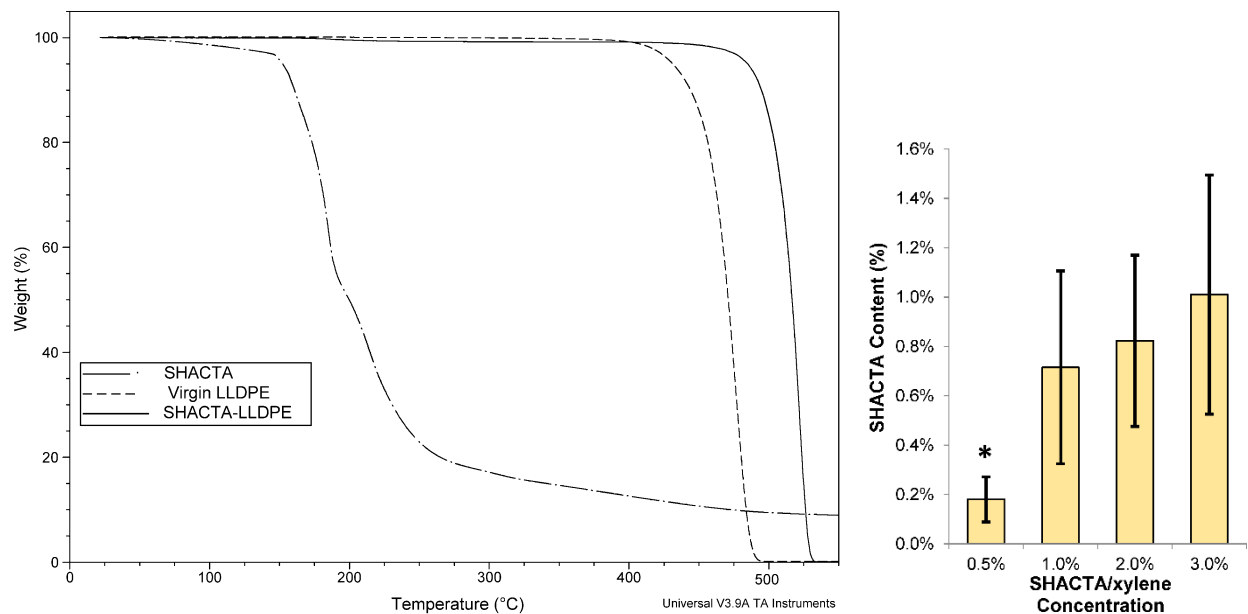


Figure 3.7: TGA curves show weight % burn off between 25 and 550°C (left graph) for SHACTA, LLDPE, and SHACTA treated LLDPE. The right graph shows the SHACTA content calculated from the thermal analyzer for various concentrations used in the SHACTA concentrations. Asterisk means significant difference from the other treatment groups (p value < 0.05 , $n = 4$). Data represent mean \pm standard deviation.

3.3.2 Vapor Swelling Test

The right graph of Figure 3.8 shows the swelling ratio of LLDPE at various temperatures and durations. The swelling rate of LLDPE in xylene vapor seems to increase with temperature but is independent of time in the 2-hour study. Statistical analysis reveals no significant difference for 50 and 60°C data, but most of the 70°C data are significantly higher than that of the lower two temperatures. Exceptions to this finding are swelling ratios for 0.5 hr at 60°C and 1.0 hr at 70°C; these two treatment groups are not statistically different from all the others, which can be attributed to their large standard deviations. Similar trends can be observed in the %crystallinity data (left graph of Figure 3.8) where 70°C groups are significantly higher than those in 50 and 60°C. All treatments created polyethylene films with significantly greater %crystallinity than the virgin form. The %crystallinity of 70°C treatment samples are not remarkably bigger than the virgin samples. For example, the %crystallinity of LLDPE vapor swollen at 70°C for 1 hour was 37 ± 1.4 % compared to the %crystallinity of virgin LLDPE 30 ± 2.1 % (mean \pm standard deviation). Nevertheless, the 70°C treatment samples did feel stiffer after the experiment, showing that the materials became more rigid from the change in crystallinity. The increasing rigidity may affect the performance of the LLDPE flexible heart valve leaflets. Based on these results, the parameter that gives the highest swelling ratio without noticeable increase in crystallinity is 0.5 hr at 60°C; this was chosen for the next set of studies.

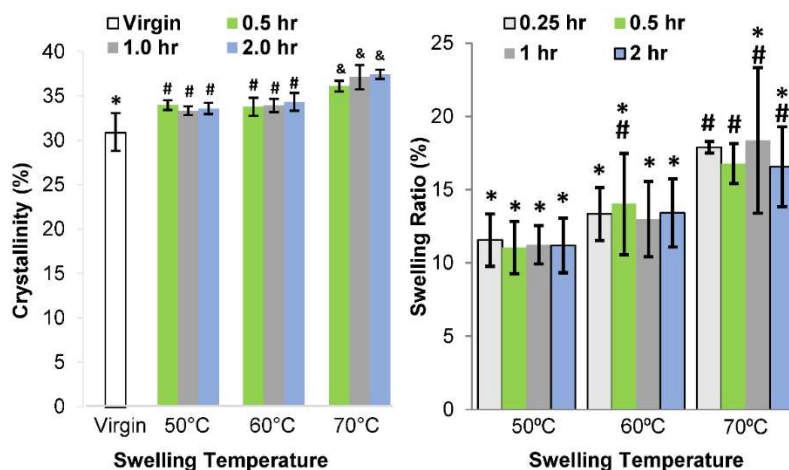


Figure 3.8: The swelling ratio (left graph) and % crystallinity (right graph) of LLDPE in xylene vapor at various temperatures and durations. Groups that do not share a symbol are significantly different from each other ($\alpha = 0.95$, $n = 8$). Data is presented as mean \pm standard deviation.

3.3.3 The Effect of Crosslinking Vapor Content on HA-LLDPE IPN

The GC-MS data in Figure 3.9 and Figure 3.10 were used to calculate TDI vapor. The top graph of Figure 3.10 shows the activity coefficients of TDI vapor at 50 and 60°C when mixed with xylenes at different molar fractions. The vapor content was calculated using the standard curve in Figure 3.9. The regression curves helped determine the activity coefficients of TDI at any molar fraction in xylenes, showing no noticeable differences between the two temperatures. The TDI vapor contents (parts per million or ppm) were calculated by plugging these activity coefficients into equation 3, which is based on Henry's Law [17,20].

$$\text{Vapor Content (ppm)} = \gamma_i \frac{x_i P}{P_t} \times 10^6 \quad (3)$$

The vapor content of TDI is proportional to the product of the activity coefficient (γ_i), the molar fraction of TDI (x_i) in the solution, and the partial pressure of TDI (P) divided by the total pressure (P_t). γ is molar fraction dependent, while both P and P_t are temperature dependent. The GC-MS

standards are displayed in the bottom graph of Figure 3.10; Their regression equations were used to calculate the TDI vapor content at any molar fraction in xylenes.

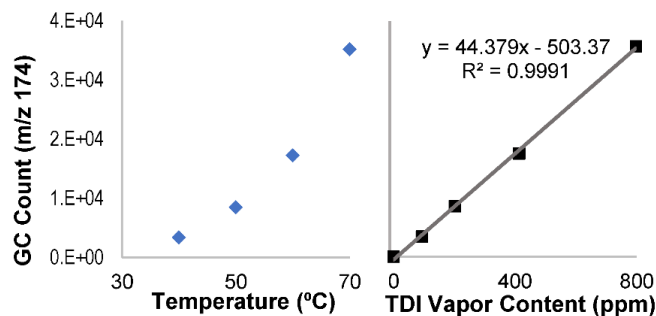


Figure 3.9: GC detection count of pure TDI was recorded at different temperatures as shown by the left graph. Using known Antoine equation parameters [18], the TDI vapor content was calculated for each temperature, and a linear regression was created to correlate GC count to TDI vapor content (right graph). The first data point on the regression curve is a blank where no TDI vapor was present for the chromatographer to detect.

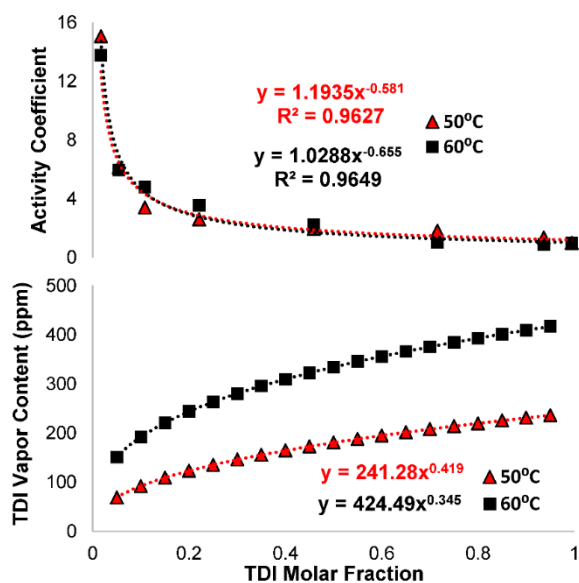


Figure 3.10: The activity coefficients (top graph) of TDI at various molar fractions in xylenes were determined by using the regression equation in Figure 3.9 and plugging the vapor content values into equation 2. The regression equations of activity coefficients were then used to calculate TDI vapor content (bottom graph) when different concentration in xylenes by plugging the derived activity coefficients into equation 2. The data are temperature dependent and only accounted for 50°C (red curve) and 60°C (black curve).

After deriving equations for calculating the amount of TDI vapor that can interact with SHACTA during crosslinking, a swelling study of LLDPE was performed at five different concentrations of TDI in xylenes to assess their effect on the material. The duration and temperature parameters (60°C for 30 minutes) were chosen based on the swelling kinetic test results. Figure 3.11 shows that as TDI composition increases and xylenes decreases, the swelling ratio of LLDPE decreases. The swelling ratios of LLDPE were 14.4 ± 1.81 , 13.8 ± 1.85 , 8.69 ± 1.26 , 7.36 ± 1.21 , 3.69 ± 1.25 for 2, 25, 50, 75, and 100% of TDI/xylenes (v/v%), respectively; their TDI vapor contents are shown in the bottom of the x-axis. TDI alone slightly swelled LLDPE, as shown by the swelling ratio of the pure TDI group (100:0).

The swelling study confirms that xylene concentration affects the swelling rate and expansion of the LLDPE polymeric network, which may influence the HA crosslinking during the IPN formation with LLDPE. But reducing xylene vapor for polymeric interpenetration also means more TDI vapor is available for crosslinking. Surface characterization was performed to find the best balance between xylene to increase swelling and TDI to promote crosslinking. The parameters that improved wettability and HA surface coverage the most were selected. One of the concentration treatment groups (50:50) was not tested because it did not provide a significant amount of swelling of LLDPE nor TDI vapor content compared to other groups such as 75:25.

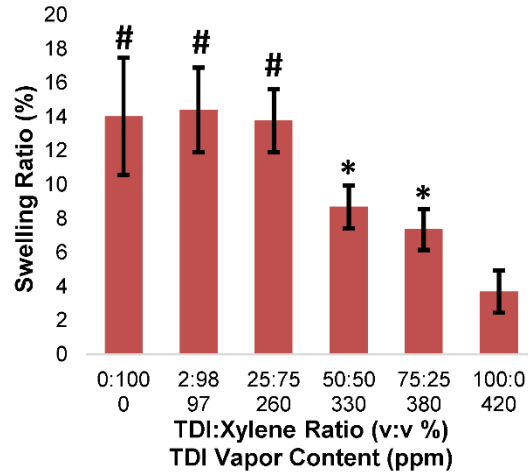


Figure 3.11: The swelling ratio of LLDPE films that were sitting above solutions of different TDI to xylene ratio. The polymer was swollen for 30 minutes at 60°C. Columns sharing the same symbol are not significantly different from each other ($\alpha=0.95$, $n = 4$). Data are presented as mean \pm standard deviation.

A hallmark of HA is hydrophilicity [21], which is shown in the contact angle data (Figure 3.12). The static contact angle is indicative of water droplets at equilibrium, whereas receding and advancing contact angles represent wettability in a dynamic state [22]. Water contact angles are low when HA is present, as shown in the IR spectra and the HA surface density (Figure 3.13 & Figure 3.14); this suggests that HA is responsible for creating the hydrophilic surface on the IPN. Apart from 100:0 and 0:100 treatment groups, all HA-LLDPE samples have significantly lower water contact angles than virgin LLDPE (Figure 3.12). Based on these data, all crosslinking treatments containing both TDI and xylenes (2:98, 25:75, 75:25) significantly increased the surface hydrophilicity of LLDPE, changing it from hydrophobic to hydrophilic; there is no significant difference among them (p value < 0.05). Despite having the highest amount of crosslinking vapor to interact with HA, 100% TDI solution (100:0) did not markedly increase the hydrophilicity of LLDPE as much as other crosslinking compositions. This could result from less swelling of

LLDPE. Nevertheless, the significant decrease in static and receding contact angles means increasing hydrophilicity.

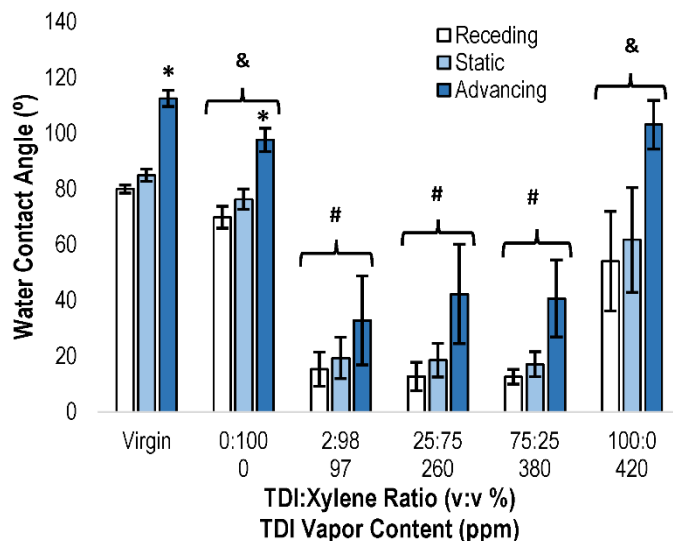


Figure 3.12: Dynamic and static water contact angles of virgin LLDPE and HA-LLDPE that were vapor crosslinked above solutions of different TDI to xylene ratio. Samples were treated with 1% (w/v) SHACTA and vapor crosslinked for 30 minutes at 60°C. Columns sharing the same symbols are not statistically different from their respective water contact angle types in other treatment groups (p value < 0.05, $n = 4$). Data are presented as mean \pm standard deviation.

Figure 3.13 shows the IR spectra of Virgin LLDPE and HA-LLDPE in the vapor crosslinking concentration experiments. The chemical structures of HA appear in bands 1250 cm^{-1} (C-O stretching), and 1060 cm^{-1} (C-O-C bending). The functional groups of TDI are represented by the aromatic amide observed at 1660 cm^{-1} , and the C=C aromatics at 1540 and 1600 cm^{-1} . These IR bands only appear on spectra of HA-LLDPE vapor crosslinked above solutions containing both TDI and xylenes. The IR spectra of HA-LLDPE with 100% TDI (100:0) crosslinking solution and 100% xylenes look similar that of Virgin LLDPE, which has scissoring and twisting of CH_2 at 1460 cm^{-1} and 1370 cm^{-1} , respectively. No peaks indicating the existence of HA and TDI are found on these spectra.

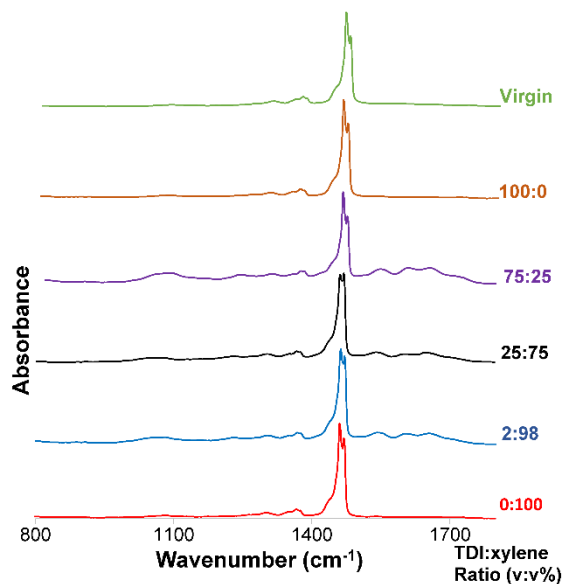


Figure 3.13: IR spectra of Virgin LLDPE and HA-LLDPE that were vapor crosslinked above solutions of different TDI to xylene ratio. Samples were treated with 1% (w/v) SHACTA and vapor crosslinked for 30 minutes at 60°C. The functional groups of HA and TDI can be seen on 75:25, 25:75, and 2:98 compositions; but they're not detected on Virgin, 100:0, and 0:100.

The IR spectra also infers that crosslinking density is independent of crosslinking solution concentration. Figure 3.13 shows that IR peaks of 2% TDI are much more prominent than those in 25%. It could be that the swollen SHACTA, which was highly entangled during crosslinking, sterically hindered TDI from crosslinking many of the available functional groups. Steric hindrance has been shown to affect crosslinking reactions of hyaluronan, especially in its high molecular weight form, by preventing the lateral diffusion of guest molecules [23,24]. 2% TDI in xylenes at 60°C (97 ppm) might be sufficient to vapor crosslink all the unhindered functional groups. The least amount of TDI used also means less worries about any excess TDI to avoid toxicity issues.

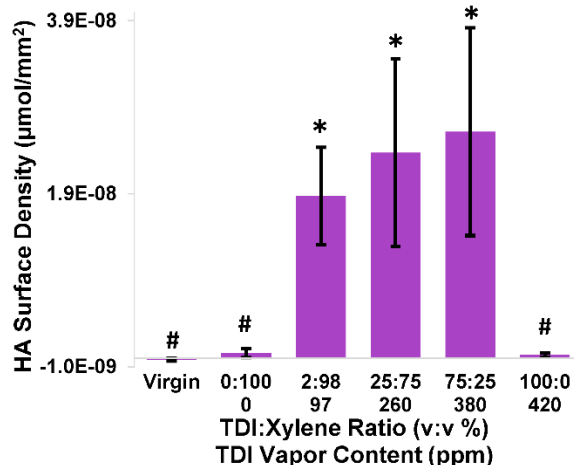


Figure 3.14: HA surface densities of virgin LLDPE and HA-LLDPE that were vapor crosslinked above solutions of different TDI to xylene ratio. Samples were treated with 1% (w/v) SHACTA and vapor crosslinked for 30 minutes at 60°C. Columns sharing the same symbol are not statistically different from each other (p value < 0.05 , $n = 4$). Data are presented as mean \pm standard deviation.

TBO staining results in Figure 3.14 reveal significantly more HA on the surface of 75:25, 25:75, and 2:98 HA-LLDPE groups than on virgin, 100:0, and 0:100 HA-LLDPE. Based on these results, there appears to be no HA on LLDPE samples that were vapor crosslinked using either pure TDI or xylenes. This observation coincides with the contact angle goniometry and IR spectroscopy data, where increasing TDI vapor does not increase HA presence on the surface. Crosslinking solution containing 2% TDI (to form 97 ppm TDI vapor at 60°C) creates an HA layer that is statistically as dense as any higher TDI concentration in xylenes. Overall, the results from the vapor swelling and concentration experiment demonstrate that a 2% TDI/xylenes is sufficient to effectively crosslink the SHACTA within LLDPE.

Another interesting discovery is that there is no correlation between wettability and swelling ratio. Similarly, there is no correlation between HA surface density and swelling ratio. Although there appears to be a slight increase in HA surface density with decreasing swelling ratio (increasing crosslinker), it is not statistically significant. Even with 97 ppm TDI vapor, there was enough TDI

to create a hydrophilic HA surface density that was not statistically different from those at any higher crosslinker concentration. One may argue that increasing TDI vapor content implies increasing xylene vapor, lowering the swelling of LLDPE, and affecting IPN formation and HA surface coverage. The tradeoff could be the reason for similar HA surface density at various composition of TDI/xylenes. Nevertheless, the vapors from the 25:75 and 2:98 TDI/xylene crosslinking solution swelled LLDPE to a comparable size, yet the TDI vapor content for the prior is more than twice of the latter (260 vs. 97 ppm). Because the resulting water contact angles and HA surface densities of the two treatment groups are not statistically different, the degree of LLDPE swelling and the crosslinker solution composition may not have an influence on HA surface density and wettability.

TDI was chosen for crosslinking HA because of its high reactivity and volatility, as demonstrated by the GC-MS data. Interestingly, when no xylenes were present to swell LLDPE during vapor crosslinking, an HA-LLDPE IPN was not created. TDI vapor (420 ppm) was present, which did adhere to the LLDPE and contribute to the increasing weight and change in swelling ratio (Figure 3.11). During hydrolysis, much of the adhering HA on LLDPE might have cleaved off along with the trimethylsilyl groups and the CTA molecules. Thus, any coating of crosslinked HA on LLDPE could have cleaved off. This would reaffirm the idea that an IPN is formed when xylenes swell the LLDPE to penetrate the polymer with TDI for HA crosslinking. The HA-LLDPE IPN is sufficiently durable to withstand hydrolysis (step 6 in Figure 3.1). Without xylenes during vapor crosslinking, only a superficial coating of TDI-crosslinked HA is formed on the non-swollen LLDPE; the coating could not withstand the mechanical agitation during sonication of hydrolysis. Overall, the surface properties of HA-LLDPE demonstrate that vapor crosslinking technique is effective for creating an interpenetrating polymer network consisting of HA and LLDPE. These

results are the first to demonstrate that an isocyanate vapor crosslinker can be used to form an IPN between a naturally derived polymer and a synthetic one. Despite the vast difference in chemical properties of HA and LLDPE, such as their miscibility, an IPN was consistently created. The large standard deviations in the HA surface densities in Figure 3.14 could be from the SHACTA treatment, which also shows a large distribution of SHACTA on the IPN (Figure 3.7).

3.3.4 IPN verification of HA-LLDPE

In the IPN verification study, the HA-LLDPE was fabricated based on the chosen parameters from the previous experiments (2% SHACTA/xylenes, 30 min at 60C vapor crosslinking, and 2% TDI/xylenes). The results from Figure 3.15 show that the water contact angle data and IR data does not change after the HA-LLDPE film was swollen in xylenes. Functional groups of TDI crosslinked HA are still present, and the biomaterial is hydrophilic, with water contact angles not statistically different from freshly made HA-LLDPE (n=4, p value < 0.05). However, the HA density on LLDPE decreases, as shown by the TBO stained data, by $73 \pm 13\%$. It is possible that there is an HA layer on the surface that is loosely entangled and not crosslinked with the HA anchored in the LLDPE, and the swelling process dissolved away this weakly bound layer on the IPN [25]. Despite this reduction, HA is still visible on the samples. The greatest reduction in HA surface density appears in the 4th sample in the column of Figure 3.15c, but even it still retained a hydrophilic surface, while the presence of HA is confirmed in FTIR results. The swollen ratio of the HA-LLDPE films in xylenes during reswelling was $15.6 \pm 1.32\%$, which apparently was enough to remove a layer of the HA. Nevertheless, the IPN remained durable enough to retain HA at the surface, as shown by the IR spectra and water contact angles. A portion of the HA anchored

on the LLDPE was physically interlocked within the LLDPE chains, preventing full dissolution of the HA.

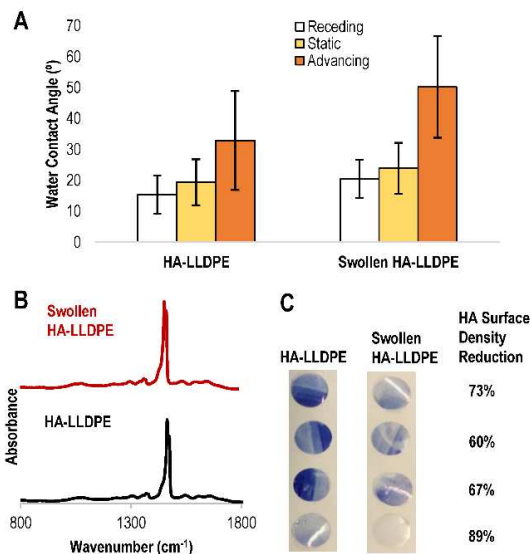


Figure 3.15: Swelling results showing the water contact angles (A) and IR spectra (B) of HA-LLDPE before and after swollen remains statistically the same ($n=4$). Data are presented as mean \pm standard deviation. There was a decrease in HA surface density as shown in the TBO stained result (C) of four different HA-LLDPE samples. The average decrease in HA surface density is $73 \pm 13\%$.

3.3.5 Tensile Testing

Figure 3.16 shows the tensile testing results for HA-LLDPE samples whose treatment parameters have been determined from the previous experiments (1% SHACTA treatment, 2% TDI/xylenes, and crosslinked for 0.5 hr at 60°C). Statistical analysis shows no significant difference in elastic modulus, toughness, yield stress, tensile strength, yield point, and elongation at break between the HA-LLDPE and virgin LLDPE. The exceptions are MD HA-LLDPE versus TD Virgin LLDPE (7.85 ± 0.27 vs. 7.15 ± 0.09 MPa) yield stress, and elongation at break of TD HA-LLDPE versus MD Virgin LLDPE (597 ± 83.5 vs. 445 ± 40.8 %). The mechanical testing demonstrates that

introduction of HA into LLDPE does not significantly change the tensile properties. This makes sense as HA constitutes a small fraction of the IPN (<1.2 %) when treated with 1.0% SHACTA/xylenes as seen in Figure 3.7. By the rule of mixtures, LLDPE is expected to have a majority if not the sole influence on the tensile properties [26].

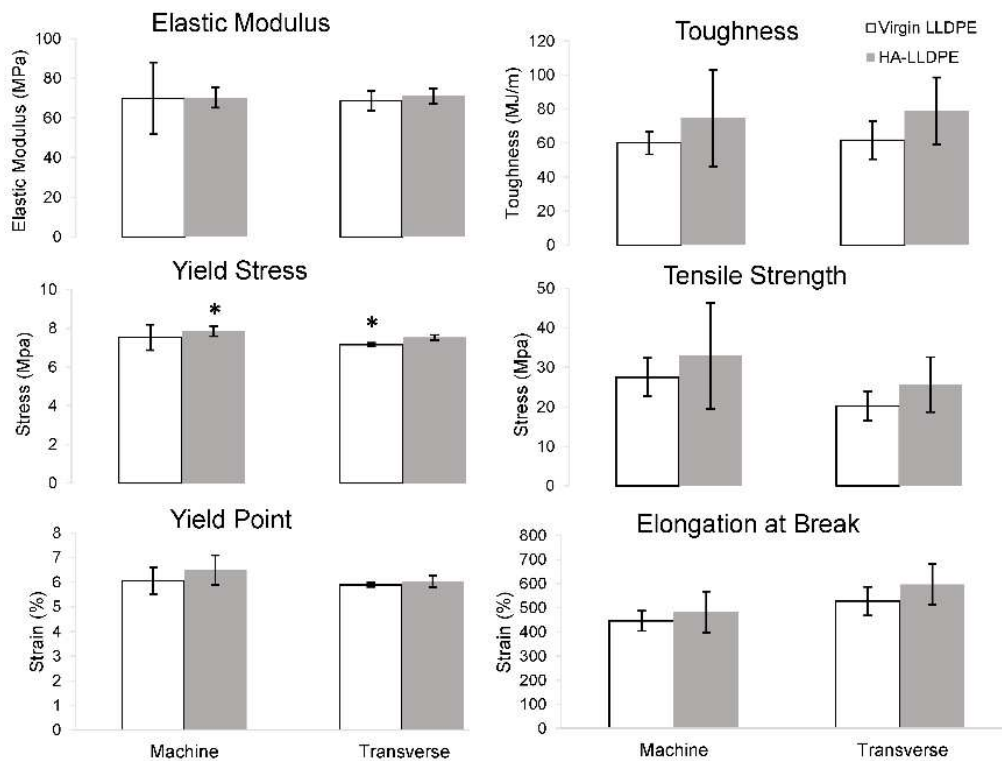


Figure 3.16: Young’s modulus, toughness, tensile stress, yield stress, yield point, and elongation at break of LLDPE and HA-LLDPE were calculated from the tensile test. Uniaxial tensile testing was performed on both machine (M D) and transverse (TD) direction with respect to how the LLDPE film was blown molded. Columns having an asterisk are significantly different from each other ($n=5$, $p<0.05$). Data are presented as mean \pm standard deviation.

3.4 Limitations and Future Work

The studies in this chapter focused on adjusting various parameters for vapor crosslinking SHACTA integrated with Dowlex 2056 LLDPE films but tailoring the crosslinking process to

different HA molecular weight or another type of LLDPE may require reanalysis of material properties. One could follow the steps in Figure 3.5 with the new LLDPE and/or HA components to find the best parameters for making a durable IPN. The molecular weight distribution and percent crystallinity of the LLDPE resins vary depending on the grade, and this can influence the thermoplastic polymer during manufacturing. LLDPE films are typically blow extruded, and the process configuration for each LLDPE could affect the thickness of the film, its crystallinity, and swollen ratio when soaked in xylenes [10]. The mechanical testing data in Figure 3.16 shows the transverse and machine directions of Dowlex 2056 do not exhibit significantly different tensile properties, but this is not always true of blow extruded LLDPE [27]. Therefore, the orientation of LLDPE films could affect their performance [27,28]. Tensile testing to compare transverse and machine must be revisited if the SHACTA vapor crosslinking method is repeated for another type of LLDPE film.

Preliminary work revealed that the slower draining rate (0.3 mm/min) of SHACTA/xylenes (step 1 of Figure 3.1) produced higher HA surface density; no further work was conducted because the goal of creating a confluent HA layer on LLDPE was achieved. But more research, perhaps by testing various draining rates, could offer further insights regarding the relationship between the draining rate and HA coverage. Another aspect of the study that could be refined is the draining rate measurement, which was determined by knowing the height of the SHACTA/xylene solution in the fritted funnel and the total time it took to fully drain the solution. A more accurate method of measuring the draining rate is recommended for future investigation of the draining effect.

Despite the HA enhancement process capable of consistently creating an HA rich surface on LLDPE, the HA surface distribution is not homogeneous (Figure 3.15c). As revealed by the TBO stained image, the HA surface coverage follows a unique specific pattern where the density

decreases incrementally from one end of the film to another; this pattern is seen by the different shades TBO stain ranges from purple to light blue on HA-LLDPE. The varying HA density on LLDPE could also be the reason for the large variability of HA surface density in Figure 3.14. Either the SHACTA treatment step, the vapor crosslinking step, or both contributed to this unique HA surface density pattern. Further analysis should aim at learning how HA is entangled within and on LLDPE. Swelling HA-LLDPE, like in the IPN verification experiment, could be a way to remove the entangled HA on the surface of LLDPE that is not anchored in LLDPE.

Because of equipment limitation, the GC-MS in this work was not able to calculate the vapor content of xylenes; this was not important in the conducted studies, because the behavior of TDI was of interest. But measuring xylene vapor content at different degree of LLDPE swelling ratio could reveal their relationship to predict the swelling rate of LLDPE in any xylene vapor.

Overall, the experiments from this chapter show that an HA-LLDPE IPN can be formed by vapor crosslinking HA with TDI. The series of material fabrication tests show that 1% SHACTA concentration treatment and vapor crosslinking above 2% TDI/xylenes at 60°C for 30 minutes can create an HA-LLDPE with a hydrophilic surface. A hydrophilic material can form a water film that has been shown to prevent thrombotic protein adhesion while allowing cellular adhesion [29]. Future studies will analyze HA-LLDPE IPN to determine topographical changes due to the HA entanglement. For example, atomic force microscopy has been used to characterize mechanical properties of glycosaminoglycans on glycocalyx-mimicking biomaterials by mapping the modulus and correlating modulus features to the adsorbed substituents such as chitosan, hyaluronan, heparin, and chondroitin sulfate [30]. Accelerated flow tests could also be performed to analyze the mechanical durability of HA-LLDPE IPN, especially for biomedical applications [5]. Future studies should consider characterizing the HA-LLDPE IPN molecular structure. Techniques such

as transmission electron microscopy, ion microscopy, and two-photon excitation microscopy, which are able to track aromatic amino acids within proteins [31], could help reveal the patterns of the TDI crosslinked HA within LLDPE at the molecular level. Despite the ubiquity of HA surface coverage, as shown by TBO coverage everywhere on the sample (before and after swelling), the HA density varies on the surface. How or if this affects the performance of the biomaterial must be further studied.

References

- [1] M. Zhang, S.P. James, Silylation of hyaluronan to improve hydrophobicity and reactivity for improved processing and derivatization, *Polymer*. 46 (2005) 3639–3648.
- [2] D.A. Prawel, H. Dean, M. Forleo, N. Lewis, J. Gangwish, K.C. Popat, L.P. Dasi, S.P. James, Hemocompatibility and hemodynamics of novel hyaluronan–polyethylene materials for flexible heart valve leaflets, *Cardiovascular Engineering and Technology*. 5 (2014) 70–81.
- [3] F. Xu, J.C. Nacker, W.C. Crone, K.S. Masters, The haemocompatibility of polyurethane–hyaluronic acid copolymers, *Biomaterials*. 29 (2008) 150–160. doi:10.1016/j.biomaterials.2007.09.028.
- [4] R. Simon-Walker, J. Cavicchia, D.A. Prawel, L.P. Dasi, S.P. James, K.C. Popat, Hemocompatibility of hyaluronan enhanced linear low density polyethylene for blood contacting applications, *Journal of Biomedical Materials Research Part B: Applied Biomaterials*. 106 (2017) 1964–1975.
- [5] H.T. Bui, A.R. Friederich, E. Li, D.A. Prawel, S.P. James, Hyaluronan enhancement of expanded polytetrafluoroethylene cardiovascular grafts, *Journal of Biomaterials Applications*. 33 (2018) 52–63.
- [6] M. Zhang, R. King, M. Hanes, S.P. James, A novel ultra high molecular weight polyethylene–hyaluronan microcomposite for use in total joint replacements. I. Synthesis and physical/chemical characterization, *Journal of Biomedical Materials Research Part A*. 78 (2006) 86–96.
- [7] I.V. Yannas, J.F. Kirk, Method for the preparation of collagen-glycosaminoglycan composite materials, 4448718, 1984.
- [8] V. Leszczak, L.W. Place, N. Franz, K.C. Popat, M.J. Kipper, Nanostructured Biomaterials from Electrospun Demineralized Bone Matrix: A Survey of Processing and Crosslinking Strategies, *ACS Appl. Mater. Interfaces*. 6 (2014) 9328–9337. doi:10.1021/am501700e.
- [9] N. Barbani, P. Giusti, L. Lazzeri, G. Polacco, G. Pizzirani, Bioartificial materials based on collagen: 1. Collagen cross-linking with gaseous glutaraldehyde, *Journal of Biomaterials Science, Polymer Edition*. 7 (1996) 461–469.
- [10] H. Dean, Development of Biopoly® Materials for use in Prosthetic Heart Valve Replacements, Colorado State University, 2012.
- [11] D.A. Prawel, H. Dean, M. Forleo, N. Lewis, J. Gangwish, K.C. Popat, L.P. Dasi, S.P. James, Hemocompatibility and hemodynamics of novel hyaluronan–polyethylene materials for flexible heart valve leaflets, *Cardiovascular Engineering and Technology*. 5 (2014) 70–81.
- [12] F. Deyhimi, J.A. Coles, Rapid Silylation of a Glass Surface: Choice of Reagent and Effect of Experimental Parameters on Hydrophobicity, *Helvetica Chimica Acta*. 65 (1982) 1752–1759. doi:10.1002/hlca.19820650610.

- [13] N.R. Lewis, Hyaluronic acid enhancement of expanded polytetrafluoroethylene for small diameter vascular grafts, Colorado State University, 2014.
- [14] Z. Ma, Z. Mao, C. Gao, Surface modification and property analysis of biomedical polymers used for tissue engineering, *Colloids and Surfaces B: Biointerfaces*. 60 (2007) 137–157.
- [15] M.F. Butler, A.M. Donald, Deformation of spherulitic polyethylene thin films, *Journal of Materials Science*. 32 (1997) 3675–3685.
- [16] F.M. Mirabella, A. Bafna, Determination of the crystallinity of polyethylene/ α -olefin copolymers by thermal analysis: Relationship of the heat of fusion of 100% polyethylene crystal and the density, *Journal of Polymer Science Part B: Polymer Physics*. 40 (2002) 1637–1643. doi:10.1002/polb.10228.
- [17] H.K. Frensdorff, R.K. Adams, Vapor pressure of 2,4-tolylene diisocyanate, *J. Chem. Eng. Data*. 20 (1975) 13–15. doi:10.1021/je60064a003.
- [18] Benzene, 2,4-diisocyanato-1-methyl-, in: NIST Chemistry WebBook, National Institute of Standard and Technology, n.d. <https://webbook.nist.gov/cgi/cbook.cgi?ID=C584849&Mask=4&Type=ANTOINE&Plot=on#Refs>.
- [19] D20 Committee, Test Method for Tensile Properties of Thin Plastic Sheeting, ASTM International, n.d. doi:10.1520/D0882-18.
- [20] H. Hori, I. Tanaka, Equilibrated vapor concentrations for bicomponent organic solvents, *Journal of Occupational Health*. 40 (1998) 132–136.
- [21] D. Pasqui, M. De Cagna, R. Barbucci, Polysaccharide-based hydrogels: the key role of water in affecting mechanical properties, *Polymers*. 4 (2012) 1517–1534.
- [22] D.A. Olsen, P.A. Joyner, M.D. Olson, THE SLIDING OF LIQUID DROPS ON SOLID SURFACES, *The Journal of Physical Chemistry*. 66 (1962) 883–886. doi:10.1021/j100811a029.
- [23] C.E. Schanté, G. Zuber, C. Herlin, T.F. Vandamme, Improvement of hyaluronic acid enzymatic stability by the grafting of amino-acids, *Carbohydrate Polymers*. 87 (2012) 2211–2216. doi:10.1016/j.carbpol.2011.10.050.
- [24] L. Xu, V. Selin, A. Zhuk, J.F. Ankner, S.A. Sukhishvili, Molecular Weight Dependence of Polymer Chain Mobility within Multilayer Films, *ACS Macro Letters*. 2 (2013) 865–868. doi:10.1021/mz400413v.
- [25] M. Zhang, Surface modification of ultra high molecular weight polyethylene with hyaluronan for total joint replacement application, 2004.
- [26] W.D. Callister, D.G. Rethwisch, *Materials science and engineering*, John Wiley & Sons NY, 2011.

- [27] R.K. Krishnaswamy, M.J. Lamborn, Tensile properties of linear low density polyethylene (LLDPE) blown films, *Polymer Engineering & Science*. 40 (2000) 2385–2396. doi:10.1002/pen.11370.
- [28] X.. Zhang, S. Elkoun, A. Aji, M.. Huneault, Oriented structure and anisotropy properties of polymer blown films: HDPE, LLDPE and LDPE, *Polymer*. 45 (2004) 217–229. doi:10.1016/j.polymer.2003.10.057.
- [29] P. Parhi, A. Golas, E.A. Vogler, Role of proteins and water in the initial attachment of mammalian cells to biomedical surfaces: a review, *Journal of Adhesion Science and Technology*. 24 (2010) 853–888.
- [30] M. Hedayati, M.J. Kipper, Atomic force microscopy of adsorbed proteoglycan mimetic nanoparticles: Toward new glycocalyx-mimetic model surfaces, *Carbohydrate Polymers*. 190 (2018) 346–355. doi:10.1016/j.carbpol.2018.02.023.
- [31] M. Lippitz, W. Erker, H. Decker, K.E. van Holde, T. Basché, Two-photon excitation microscopy of tryptophan-containing proteins, *PNAS*. 99 (2002) 2772–2777. doi:10.1073/pnas.052662999.

Chapter 4: Thrombogenic Potential of HA-ePTFE and HA-LLDPE

4.1 Introduction

This chapter discusses the *in vitro* assays that were performed on hyaluronan enhanced linear low density polyethylene (HA-LLDPE) and expanded polytetrafluoroethylene (HA-ePTFE). The studies were done with a focus on hemocompatibility analysis, and more specifically, the thrombogenic potential of HA-LLDPE and HA-ePTFE. Cytocompatibility analysis is often the first screening to determine whether a material is appropriate for biomedical applications [1]. Indeed, cytocompatibility tests such as cytotoxic assays are the first to be required in most biocompatibility screening of biomaterials [2]. Common testing methods are (3-(4,5-dimethylthiazol-2-yl)-2,5-diphenyltetrazoliumbromid (MTT), (2,3-bis(2-methoxy-4-nitro-5-sulfophenyl)-5-[(phenylamino)carbonyl]-2H-tetrazolium hydroxide) (MTS), lactate dehydrogenase (LDH) assays [3,4]. In addition to cytocompatibility testing, thrombogenic analysis was picked because thrombosis is often the first adverse effect triggered upon blood-material interaction [1]. This is often done by assessing blood clotting potential of the material of interest [5,6]. Platelet activation experiment is also relevant, because platelets are important mediators in primary hemostasis and blood coagulation [7].

The following sections describe the *in vitro* assays performed on HA-LLDPE and HA-ePTFE. The first study evaluated cytocompatibility through measuring the LDH activity of mammalian cells incubated with the HA enhanced synthetic polymers. The second study analyzed the whole blood clotting potential of the polymer samples similar to work reported in literature [8]. The third study assessed platelet activation after incubation with platelet rich plasma. All ePTFE samples came

from medical grade grafts (Impra Bard). HA-ePTFE fabrication followed the method described in chapter 2, where 5 ml of HACTA/ethanol were spraycoated on the ePTFE samples at 25 psi. The LLDPE samples were cut from a roll of Dowlex 2056 film (Dow Chemical), with samples freshly cut from the film denoted as virgin LLDPE. HA enhancement of LLDPE follows the protocol described in chapter 3 with the following parameters: 1% SHACTA/xylene treatment, 30 minutes of vapor crosslinking at 60°C, and 2% (v/v) TDI/xylene crosslinking solution.

4.2 Materials and Methods

4.2.1 Cytocompatibility Assay

4.2.1.1 Contact Assay of Biomaterials with Human Dermal Fibroblasts

To screen whether the HA treated materials are cytotoxic, *in vitro* LDH assays were performed. LDH is a metabolic enzyme that is found in the cytoplasm and crucial for energy production in both glycolysis and the Krebs cycle. LDH is released in the extracellular space during apoptosis and necrosis, which is correlated with cell death [9]. Figure 4.1 depicts the reaction mechanism behind LDH assay, which involves adding a chemical mixture into the medium that contains the mammalian cells of interest. The main components of the assay chemical mixture are lactate, nicotinamide adenine dinucleotide (NAD⁺), tetrazolium salt, and diaphorase. After the mixture is introduced into the cell medium, lactate hydrolyzes into pyruvate if LDH is present, and NAD⁺ is reduced into NADH because of the hydrolysis. With diaphorase as a catalyst, NADH reacts with tetrazolium salt, and the latter is transformed into red formazan. Using a spectrophotometer, the concentration of red formazan can be quantified at 490 nm. The absorbance value is correlated to the LDH concentration in the medium.

In the present study, the LDH assay was conducted in accord with protocol of the LDH kit (Pierce LDH Kit, 88654). 8 mm diameter disc size of ePTFE and LLDPE were made using biopsy punches (Acuderm). ePTFE and LLDPE samples were sterilized using 70% ethanol and hydrated for at least 24 hours in phosphate buffered saline (PBS) before putting in the well plates. Each sample was incubated with 20,000 Human dermal fibroblasts (HDF) in a 24-well tissue culture polystyrene (TCPS) plate for 24 hours. Positive control had lysis buffer added to HDF grown in plain TCPS to quantify the total LDH activity, which was deemed the total possible cell death. HDF grown in TCPS neither incubated with samples nor lysis buffer was the negative control, where any detected LDH activity corresponded to spontaneous release of LDH and the concentration constituted by the growth media. Reported cytotoxicity level was the difference of absorbance (Abs) between experimental data and negative control normalized by the difference between the positive control and negative control, as shown in the following equation.

$$\frac{Abs_{sample} - Abs_{negative\ control}}{Abs_{positive\ control} - Abs_{negative\ control}} \times 100\% = Cytotoxicity\ level$$

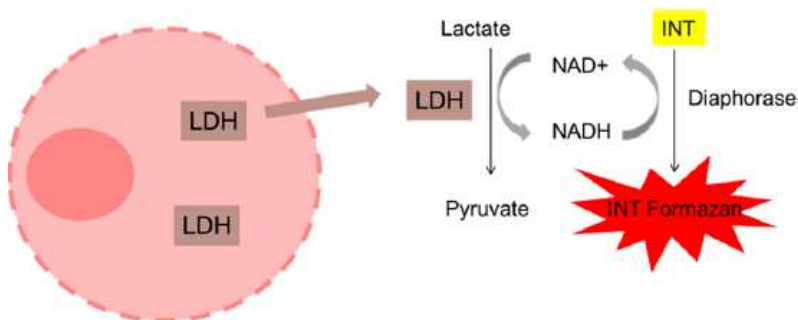


Figure 4.1: Picture describing the reactions in the LDH assay. Reprinted (adapted) with permission from [10] © 2019 American Chemical Society.

4.2.1.2 Leaching Study of HA-LLDPE

The cytocompatibility of HA-LLDPE eluent was also assessed over 28 days. 8 mm diameter disc size of LLDPE were made using a biopsy punch (Acuderm). Samples were incubated in growth media composed of 89% α -modified eagle media (α -MEM), 10% fetal bovine serum (FBS), and 1% penicillin/streptomycin (pen/strep). This study was done to analyze the toxicity of any chemicals from the HA-LLDPE that would leach out into the media. The growth media were incubated with samples for three different durations (7, 14, and 28 days). Cytotoxic potential was quantified by determining the LDH activity (Cayman, No.601170) of 1×10^4 adipose derived stem cells (ADSCs) cultivated for one day in the sample eluate media. ADSCs incubated with eluates of tissue culture polystyrene (TCPS) were used as a negative control (i.e., no cell death was expected). For a positive control, lysis buffer was added to the ADSCs to induce cell death, releasing all LDH from the ADSCs into the extracellular environment. LDH concentration was measured by using a plate reader (FLUOstar Omega) (excitation at 490 nm). Reported cytotoxicity level was the difference of absorbance (Abs) between experimental data and negative control normalized by the difference between the positive control and negative control, as shown in the following equation.

$$\frac{Abs_{sample} - Abs_{negative\ control}}{Abs_{positive\ control} - Abs_{negative\ control}} \times 100\% = Cytotoxicity\ level$$

4.2.2 Whole Blood Clotting Assay

Thrombogenicity was evaluated by studying blood-material interaction [8]. Briefly, 8 mm diameter discs of LLDPE and ePTFE were made using biopsy punches (Acuderm) and then

hydrated in DI water for 1 hour prior to the experiment. Human blood was collected from healthy donors by a certified phlebotomist (Colorado State University Health Network). The donors had not taken any medication, including aspirin, for at least two weeks. Blood was collected by venipuncture directly into a 3-mL plastic tube (BC Vacutainer®) and used immediately. ePTFE and LLDPE samples (n=3) were placed in tissue culture polystyrene (TCPS) 24-well plates (Greiner CELLSTAR®). Blood droplets (10 μ L) were pipetted onto the surface of each sample and the TCPS wells. TCPS was used as a control because its surface is known to promote blood clotting [11]. Blood was left to clot for 30 and 60 minutes on the samples in the ePTFE study. For the LLDPE study, blood only clotted for 15 and 30 minutes. One thousand μ L of DI water was added to each well and the solutions were gently agitated on a plate shaker (Titer) for 30 seconds to free non-clotted blood. The samples rested for five minutes allowing further free hemoglobin that was not trapped in the blood clot to be released into DI water. Two μ L of whole blood was also mixed with 200 μ L of DI water and used as a reference representing absorbance (i.e., free hemoglobin) of blood with no clotting. Two hundred and two μ L of the blood solution from the ePTFE samples and the TCPS wells were transferred into a 96-well plate for absorbance analysis using a plate reader (FLUOstar Omega) at 540 nm. Absorbance was inversely correlated to blood clotting where hemoglobin is trapped in the clot. A detailed protocol is in Appendix A.12.

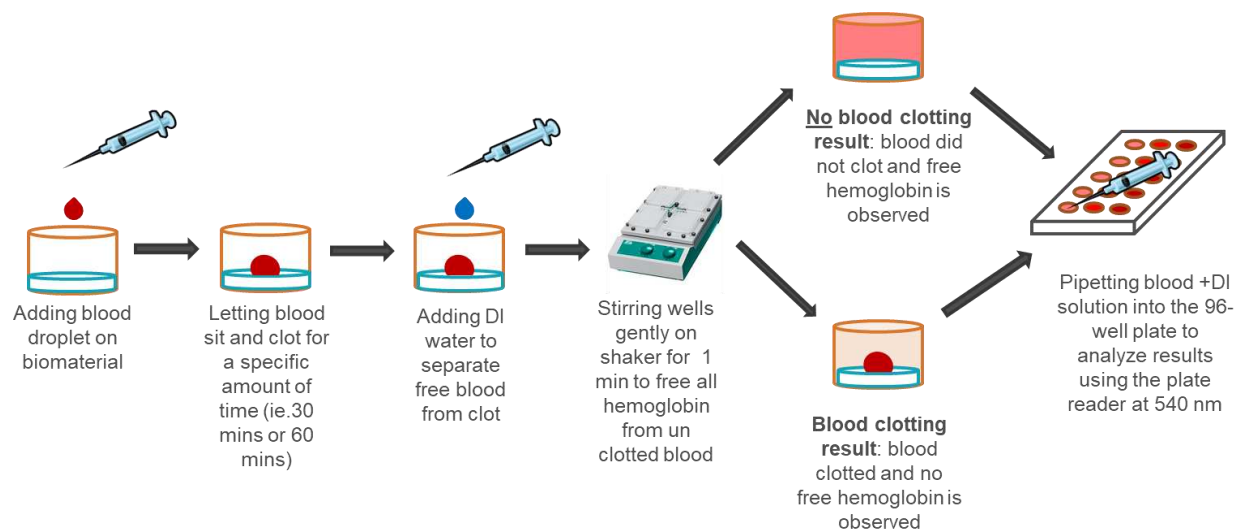


Figure 4.2: Schematic of the whole blood clotting test.

4.2.3 Platelet Activation Assay

Platelets are one of the first cells to be involved in the clotting cascade and studying their behavior on biomaterials is important in hemocompatibility assessment. Briefly, test samples were made into 8 mm diameter pucks using a biopsy punch (Acuderm). TCPS “pucks” (8 mm diameter) were punched from Greiner CELLSTAR® materials and used as a positive control. Untreated and HA-treated grafts, and TCPS pucks (n=3), were sterilized with 70% ethanol, dried, then placed in TCPS 24-well plates. One mL of DI water was added to each well to allow the HA to hydrate for one hour, then removed just prior to the actual experiment. Whole blood was collected, as described above in the whole blood study, into ethylenediaminetetraacetic acid (EDTA) coated vials (BD Vacutainer®) to prevent coagulation. Blood was centrifuged at 150 g for 15 minutes to separate plasma from blood. One mL of plasma was pipetted into each sample-containing well and the well plate was stirred on a shaker at 100 RPM for 2 hours inside a cell-culturing incubator (37°C, 5% CO₂). Afterward, plasma was gently aspirated, and samples were rinsed twice with phosphate buffered saline. Platelets adhering to the samples were fixed according to a previously published

method [8]. Briefly, samples were submerged in a 3% (v/v) glutaraldehyde, 0.1 M sucrose, and 0.1 M sodium cacodylate aqueous solution for 45 minutes, then placed in a secondary fixative solution containing only sodium cacodylate and sucrose for at least one hour. Platelets were dehydrated by incubating the samples in consecutive ethanol/DI water solutions (35, 50, 70, 95, and 100% ethanol) for 10 minutes each. The samples were then placed in a desiccator under vacuum for at least 24 hours. The protocol for platelet activation and fixing can be found in Appendix A.13 and A.14.

Samples containing glutaraldehyde fixed platelets were coated with 10 nm of gold and imaged at 5 kV under a scanning electron microscope (SEM) (JEOL JSM 6500F). SEM images were taken in five different areas per fixed sample at different magnifications (2500x and 2000x for ePTFE and LLDPE samples, respectively). Platelets were counted based on their morphology using ImageJ (NIH). Platelet activation chronology was quantified by dividing their morphology into the following six stages using a previously published method [7,12,13]: 1) round: discoid shape representing platelets that were not activated. 2) dendritic: early pseudopodal showing cellular extension. 3) spreading dendritic: pseudopodal shaped cells that are slightly flattening with signs of tethering, but the hyaloplasm has not spread between pseudopodia. 4) spreading: one or more pseudopodia flattened, and hyaloplasm spread between pseudopodia. 5) fully Spreading: firm cellular adhesion with hyaloplasm extensively spread, and there are no distinct pseudopodia, but granulation is observed. 6) aggregation: platelet activation and mediating factor secretion recruit more platelets, which promotes thrombus formation.

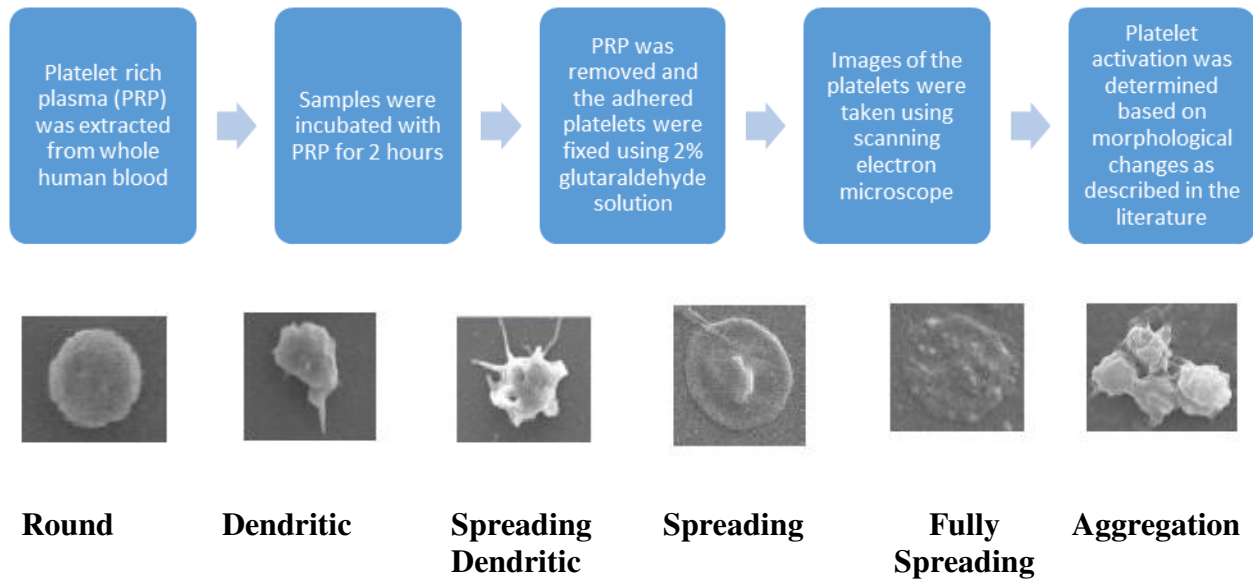


Figure 4.3: Top portion shows steps in the platelet activation test. Bottom portion shows the plate morphologies of the six activation stages.

Platelet coverage of biomaterial from the activation study was also quantified. After human plasma was removed from the 2-hour incubation, the adhered platelets were stained in a 10-nM concentration of calcein AM solution (Thermo Scientific 3224) for 40 minutes in an incubator (37°C, 5% CO₂). Calcein AM can permeate the cytoplasm of platelets and react with esterase in the cytosol producing calcein serving as a fluorescent indicator. Samples were imaged using a fluorescent microscope (Zeiss Axiovision), excitation/emission: 493/514 nm. 5 images were collected for each sample in each treatment group (n=3). Percent coverage of platelet were determined based on area coverage of the fluorescent stained region via ImageJ. Because ePTFE auto fluoresces, their materials were not included in the study. Protocol for calcein staining can be found in Appendix A.15.

4.2.4 Statistical Analysis

All studies were repeated twice to ensure reproducibility, and all blood used in the studies came from one donor. Normal distribution (Anderson-Darling test) and equal variance (Levene's test) were verified. Statistical analysis for all studies was performed using one-way ANOVA with a post hoc Tukey's test (p value < 0.05). All tests in this chapter were performed on Minitab 17.

In the ePTFE platelet activation study, a two-way ANOVA was used to analyze platelet activation with activation category as factor one and the treatment group as factor two. The initial sample size was either four or three in all the experiments. Power analysis (GPower 3.1) was then performed after each study to verify the required sample size (effect size = 0.8). In the LLDPE platelet activation study, the mood median test (p value < 0.05) was performed to compare each platelet activation stage among the treatment groups. The nonparametric mood median test was picked because the platelet activation data in the LLDPE study were not normally distributed. Briefly, mood median test sorted the raw data in ascending order and then found the middle number, M . The test then listed how many data points were greater than M and then counted how many data points were smaller than or equal to M in a contingency table. Afterward, a chi-square test was performed based on the data from the contingency table.

4.3 Results & Discussion

4.3.1 Cytocompatibility Assay

4.3.1.1 Contact Assay of Biomaterials with Human Dermal Fibroblasts

There was no significant difference in LDH concentration between untreated ePTFE, HA-enhanced ePTFE and TCPS (Figure 4.4, right side). Similar results were found when tested for LDH activity in LLDPE and HA-LLDPE (Figure 4.4, left side). The presence of LDH in this assay

correlates with dead cells and there was no increase in LDH activity between the negative control (TCPS) and the treatment groups. Therefore, HA-ePTFE, HA-LLDPE, and their untreated counterparts did not exhibit a significant toxicological effect on HDF. The results prove that cell viability was not affected by the HA treatment. Although human dermal fibroblasts may not exist in the cardiovascular system, this study demonstrates that the biomaterials are not cytotoxic to at least one type of mammalian cells.

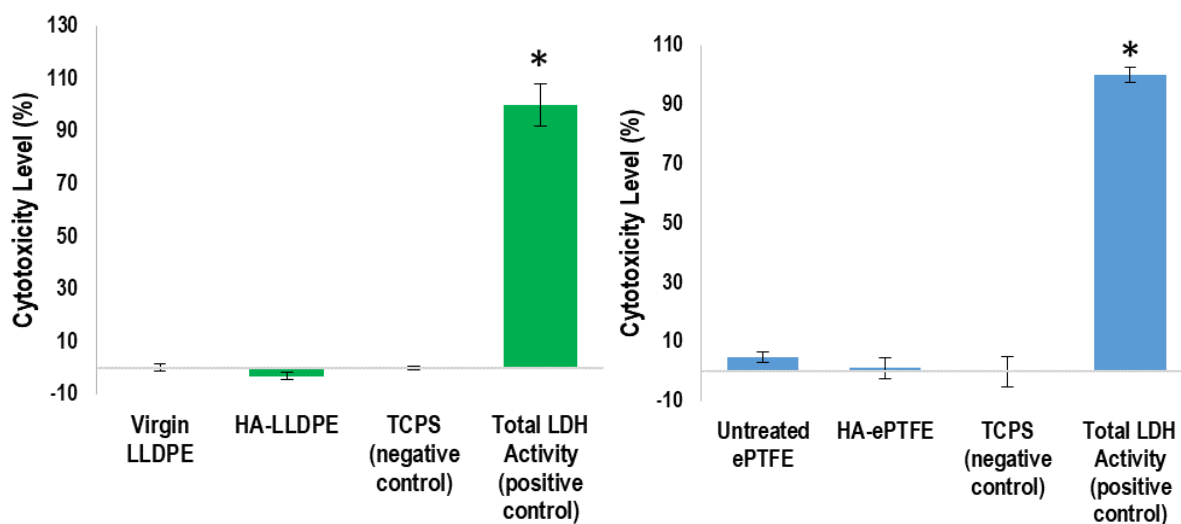


Figure 4.4: LDH data for LLDPE (left) and ePTFE (right). Treated samples did not exhibit a significant toxicological effect on HDF from that of the plain (virgin LLDPE and untreated ePTFE). They were not significantly different from the negative (TCPS), which is not cytotoxic for mammalian cells ($n=5$, $\alpha=0.05$). Total Activity represents total LDH released for 100% cell death, where there was significant difference compared with other groups (*). Data are presented as mean \pm standard deviation.

4.3.1.2 Leaching Study of HA- LLDPE

Cytocompatibility data from the leaching study is shown in Figure 4.5 for Virgin LLDPE and HA-LLDPE samples (1% SHACTA treatment, 2% TDI/xylenes, and crosslinked for 0.5 hr at 60°C). There was no significant difference in LDH concentration among Virgin LLDPE, HA-

LLDPE, and TCPS for both 7 and 14-day time points. Therefore, Virgin LLDPE and HA-LLDPE did not exhibit a significant toxicological effect on ADSCs. No chemicals released by the samples over 7, 14 and 28 days were cytotoxic. The significant increase in LDH for the positive controls (lysed cells) verifies that the LDH assay can detect LDH released upon cell death.

The cytocompatibility study demonstrates that vapor crosslinked HA-LLDPE IPN can be used for biomedical applications without affecting the viability of adipose derived stem cells. Although the toxicity level appears below average in some data (e.g. HA-LLDPE in figure 4.4 and 4.5), this does not mean the samples induced a decrease in toxicity. The shown data are presented as mean \pm standard deviation, and any negative value could be from inconsistent concentration of LDH in the growth media contributed by the supplemented serum. Nevertheless, the data analysis demonstrated that sample data are not statistically different from the negative control.

Earlier generation materials have been shown to be useful and safe in cardiovascular applications [14–16]. The key difference is the use of TDI for vapor crosslinking in the most recent materials. TDI was picked because of its high reactivity, volatility, and known durability in polyurethane synthesis [17]. The crosslinked TDI does not harm ADSC cells, which are representative of a general mammalian cell population. It must be noted that TDI crosslinked polyurethane was utilized in breast implant foam, and improper cleaning after crosslinking led to unreacted TDI residue remaining in the implants [18]. This resulted in adverse reactions between the unreacted TDI and water, forming the toxic chemical toluene diamine (TDA) after implantation. In the current process, meticulous care has been implemented to ensure any unreacted TDI was fully removed. Crosslinked samples were rinsed multiple times in acetone, sonicated for few hours in salt solutions heating up to 40°C, and incubated in alcohol/water for at least another two hours.

These steps had been designed to revert SHACTA to HA, but the aggressive process may have helped to remove any unreacted TDI.

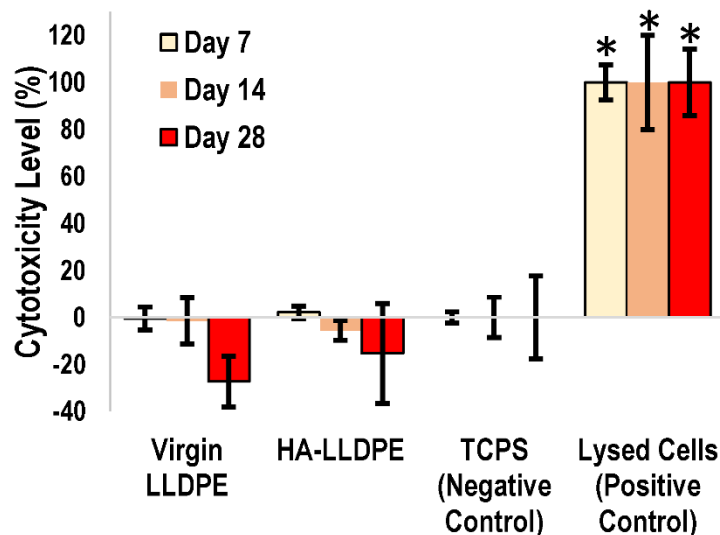


Figure 4.5: Cytocompatibility data from the leaching study. ADSCs cultivated with eluates exposed to samples for three different durations (7, 14, and 28 days). Columns having an asterisk are significantly different from other data groups within the same duration. ($n=5$, $p<0.05$). Data are presented as mean \pm standard deviation.

4.3.2 Whole Blood Clotting

The images in Figure 4.6 show how HA treatment affects blood clotting over time for ePTFE samples. In the first 30 minutes, there appears to be a noticeable amount of blood clotted at the center of the untreated ePTFE (left image, second row), while there was extremely little clot on the TCPS and HA-treated samples (left image, first and third row, respectively). The color of the solutions in these two groups look slightly darker than the untreated ePTFE, suggesting more coagulation on the untreated ePTFE samples. After 60 minutes, large clots formed in the TCPS and untreated ePTFE wells (right image, first and second row, respectively). Maximal clotting appears to occur on TCPS, where all the blood concentrated in the coagulated region leaves the

color of the solution virtually clear. Similar behavior is observed on untreated ePTFE samples, but to a lesser extent. The HA-ePTFE only shows a minor blood clot at the center of its samples (right image, third row). The color of its solution remains approximately the same after 30 minutes, which implies that most of the blood eluted into the solution without clotting. Figure 4.7 shows the colorimetric data obtained from the plate reader. The amount of free hemoglobin after 30 minutes was significantly different between TCPS and that of whole blood, but there were no differences among TCPS, HA-ePTFE, and untreated ePTFE. After 60 minutes, there was a significant decrease in free hemoglobin on all the samples except for the HA-treated ePTFE; only minor blood clots are seen at the center of these samples, which indicates that HA treatment significantly reduces blood clotting on the surface of HA-ePTFE graft after 60 minutes.

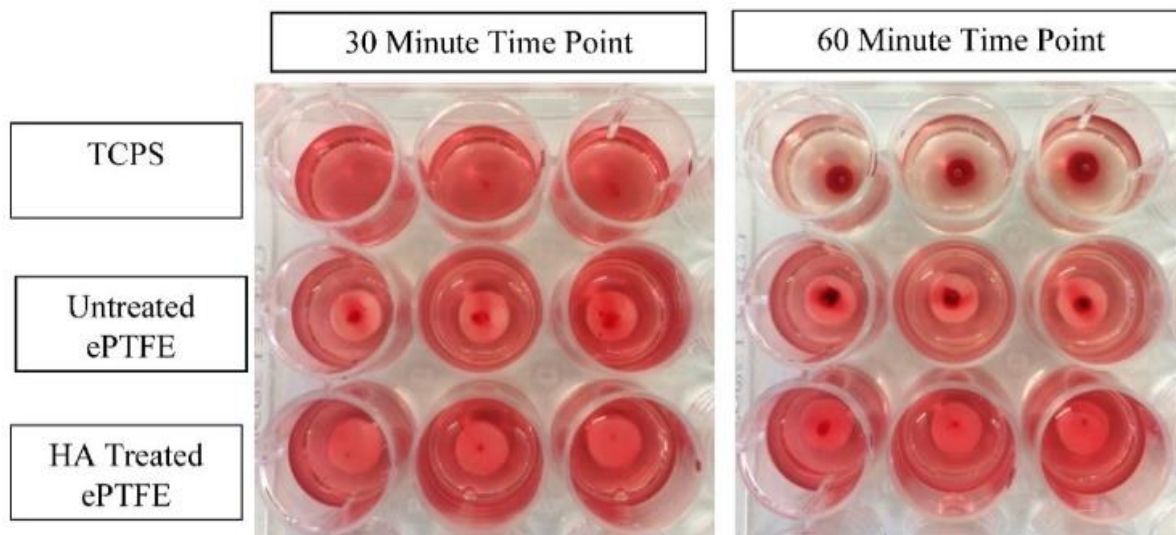


Figure 4.6: Images of whole blood clotting showing significantly less clotting behavior for HA-ePTFE samples than plain ePTFE. Left image shows 30 min time point and right image is of 60 min time point. Top row is TCPS, middle row is untreated ePTFE, and bottom row is HA-ePTFE (n=3).

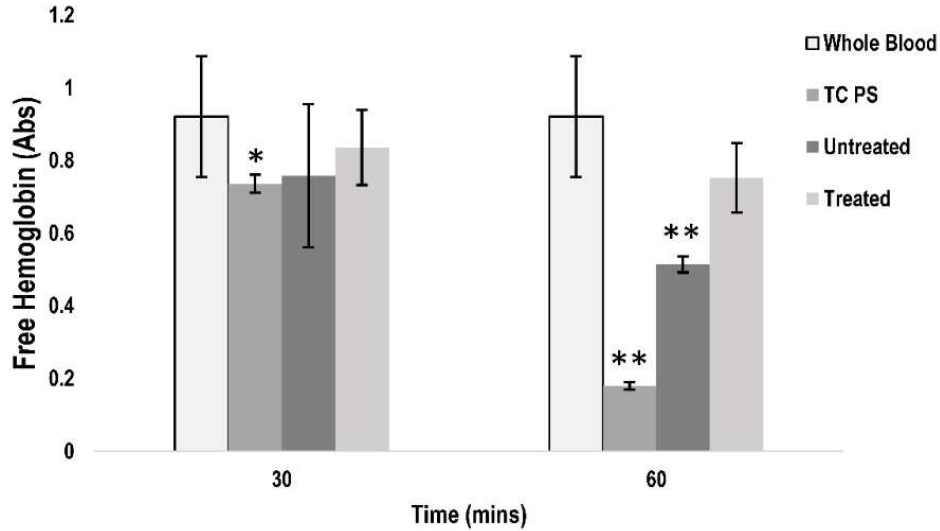


Figure 4.7: The colorimetric data obtained from the plate reader. The amount of free hemoglobin after 30 minutes was significantly different between TCPS and that of whole blood, but there were no differences among TCPS, HA-ePTFE, and untreated ePTFE. After 60 minutes, there was a significant decrease in free hemoglobin on all the samples except for the HA-ePTFE; only minor blood clots are seen at the center of these samples, which indicates that HA treatment significantly reduces blood clotting on the surface of HA-ePTFE graft after 60 minutes. Asterisk and double asterisks represent significant difference with whole blood and all treatment groups in both time points, respectively. ($n=3$, p value < 0.05). All data are presented as mean \pm standard deviation.

Figure 4.8 shows the blood clotting data from the LLDPE samples. At the 15-minute time point, blood did not seem to clot on both virgin and HA-LLDPE compared to TCPS. This is supported by the fact that there is not a statistical difference for free hemoglobin of virgin LLDPE, HA-LLDPE, and whole blood. After the 30-minute time point, there was noticeable clotting for both virgin and HA-LLDPE, and there was a significant difference with the 15-minute timepoint data. HA-LLDPE appears to have clotted less than virgin LLDPE, but it was not statistically significant (p value > 0.05). Images of LLDPE samples were not taken, because the black tape under the clear LLDPE masked the color of the clot, posing as a challenge for visual assessment. LLDPE samples were adhered to the TCPS well via black carbon tape to prevent samples from floating. Black tape was used instead of clear ones because its adhesiveness is water resistant.

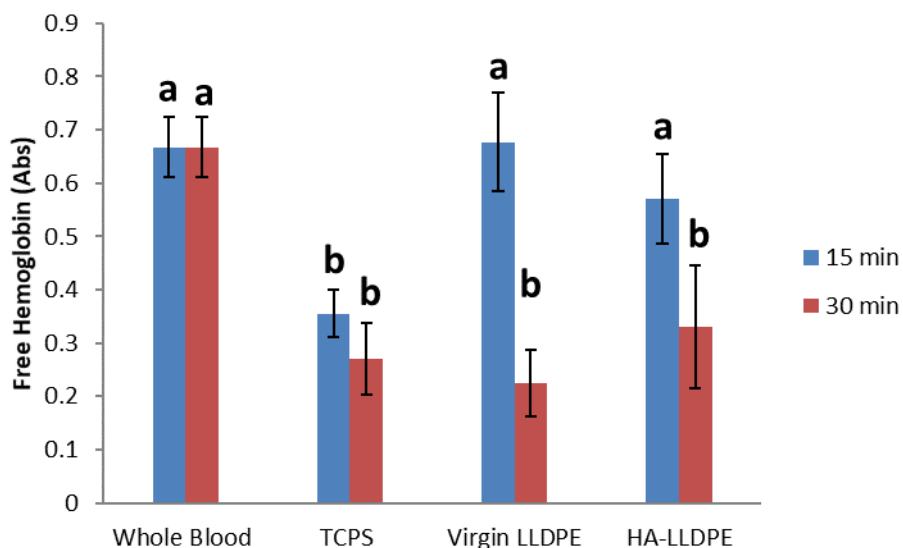


Figure 4.8: The colorimetric data obtained from the plate reader from the blood clotting on LLDPE samples. The amount of free hemoglobin after 15 minutes was significantly different between TCPS (positive control) and that of whole blood (negative control), HA-LLDPE, and virgin LLDPE. After 30 minutes, there was a significant decrease in free hemoglobin on all the samples. Although HA-LLDPE appears to have more free hemoglobin (less clotting) than LLDPE, their data are not significantly different from each other ($n=4$, $\alpha = 0.95$). Samples sharing the same letter are not significantly different from each other. All data are presented as mean \pm standard deviation.

The whole blood study demonstrated a marked decrease in clotting for HA-ePTFE, supporting the argument for HA-ePTFE anti-thrombogenic properties. The results seem to agree with data reported in literature for HA enhanced polymers [15]. Hydrophilic surfaces are known to repel proteins such as fibrinogen [19], which is important during coagulation [20]. Although the whole blood study was a simple experiment, previous work involving protein adsorption and endothelial studies has shown the method to be a good indicator of thrombogenic potential [21]. It is interesting that HA-LLDPE did not exhibit significant decrease in clotting after 30 minutes when comparing to virgin LLDPE and the control (TCPS). Perhaps the HA layer on the surface is thin, and it could have dried within the first 30 minutes. The study was performed in an open atmosphere that could have caused the HA rich surface of LLDPE to dehydrate. The blood data in the ePTFE study shows

much less clotting for HA-ePTFE than HA-LLDPE, which could be influenced by the thicker layer of HA on the HA-ePTFE. More HA means higher water intake allowing to withstand dehydration longer.

4.3.3 Platelet Activation Assay

Platelets on substrates were imaged using SEM to qualitatively assess cell morphology and spreading (Figure 4.9). The TCPS is nearly completely covered with platelets, often clumping together; some cells appear have spreading pseudopodia. Higher magnification reveals many of the platelets either granulated after spreading or clumped together. A similar trend appears on plain ePTFE samples, but there was much less cellular adhesion on the plain ePTFE than TCPS. Despite this, almost all cells on plain ePTFE are layered on each other, forming large clumps. HA-treated ePTFE shows fewer cells on their surfaces compared to TCPS, and most platelets appear rounded and much less activated. Comparable results are observed on the LLDPE samples. More cells adhered and aggregated on virgin LLDPE than HA-LLDPE. When comparing the HA treatment, there appears to be more platelets on HA-LLDPE than HA-ePTFE.

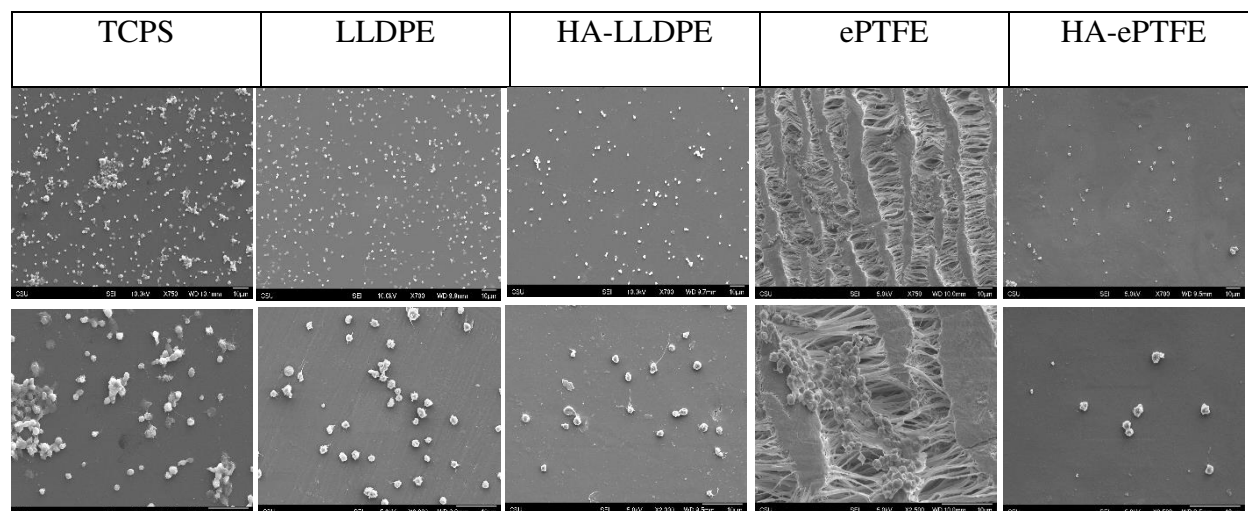


Figure 4.9: Low (top row) and high (bottom row) magnification SEM images of TCPS (1st column), Untreated LLDPE (2nd column), HA treated LLDPE (3rd column), plain ePTFE (4th column), and HA treated ePTFE (5th column) from the platelet activation study show significantly less platelet activation on HA treated groups. Platelets are round and least activated on treated surfaces. Cells can be seen aggregating and spreading on TCPS and the plain groups.

Quantification of platelet activation of ePTFE samples in Figure 4.10 reveal three different patterns in platelet-material interaction on each surface. HA-ePTFE demonstrates significantly fewer platelets reaching a later activation stage (>3) than other groups. Nearly half of the cells on HA-treated ePTFE are either rounded ($18 \pm 7.4\%$) or in their early dendritic form ($34 \pm 1.4\%$). Other morphologies also appeared, but in lesser amounts: spreading dendritic ($18 \pm 0.8\%$), spreading ($3.3 \pm 2.4\%$), fully spreading ($5.7 \pm 4.0\%$), and aggregation ($21 \pm 12\%$). No single stage was dominant, and the overall distribution was dispersed. The number of platelets on TCPS gradually increased in each stage from round ($3.3 \pm 2.7\%$), dendritic ($12 \pm 7.1\%$), spreading dendritic ($6.0 \pm 3.0\%$), spreading ($9.2 \pm 2.9\%$), fully spreading ($19 \pm 11.0\%$), to aggregation ($51 \pm 3.8\%$). In contrast to HA-ePTFE, majority of platelets have reached the final stage of aggregation on untreated ePTFE ($84 \pm 1.1\%$).

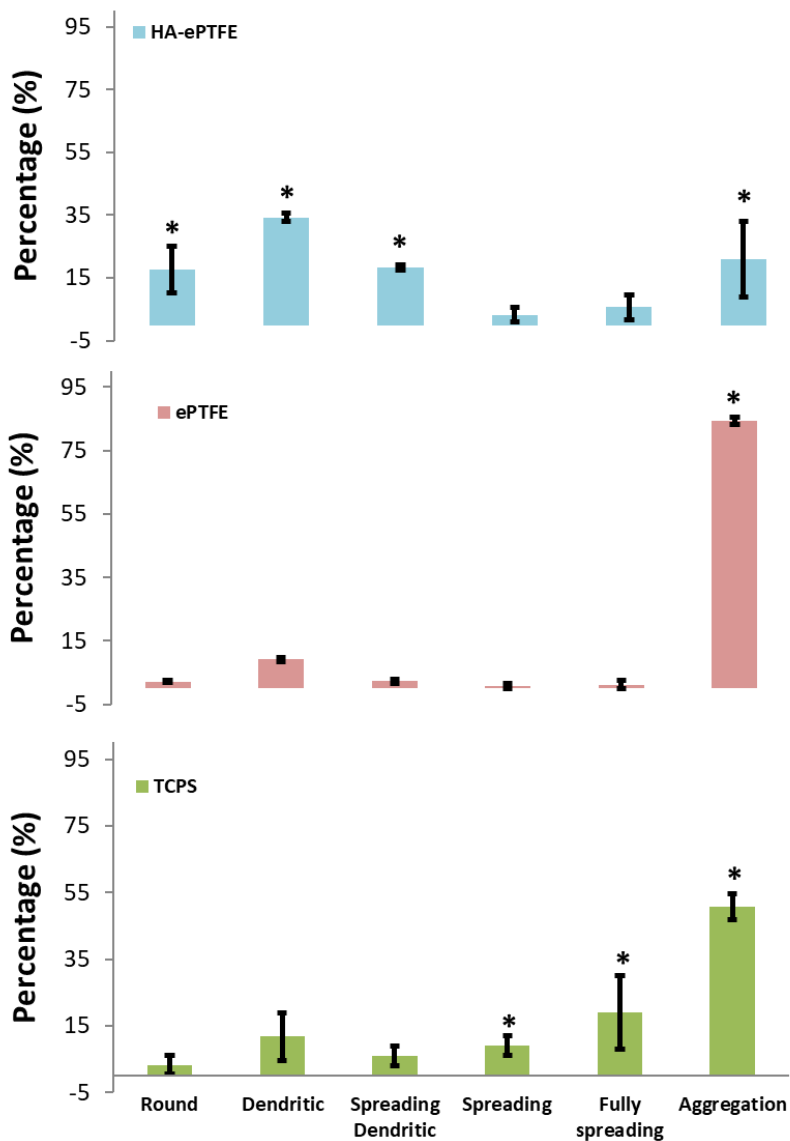


Figure 4.10: Quantitative analysis of the platelet activation study for HA-ePTFE, ePTFE, and TCPS. Asterisk (*) means significant difference from other groups within the same activation step. (n=3, p value < 0.05). All data are presented as mean ± standard deviation.

Figure 4.11 shows quantification of platelet activation of LLDPE samples with distinct activation patterns. Similar to the data for TCPS in the activation study of ePTFE (Figure 4.10), platelet activation of TCPS in the LLDPE study has an increasing trend from round ($2.9 \pm 2.3\%$), dendritic ($11.9 \pm 7.4\%$), spreading dendritic ($5.2 \pm 2.9\%$), spreading ($9.2 \pm 4.0\%$), fully spreading ($19 \pm 11\%$), to aggregation ($46 \pm 3.8\%$). Most platelets on HA-LLDPE were either in the dendritic (36

$\pm 13\%$) or fully spreading stages ($25 \pm 7.2\%$). Almost no cells were aggregating on HA-LLDPE surfaces. Other morphologies appear to be evenly distributed are round ($8.0 \pm 7.9\%$), spreading dendritic ($11 \pm 8.9\%$), spreading ($5.6 \pm 4.3\%$). For virgin LLDPE, the dominant activation stage is dendritic ($50 \pm 8.1\%$). The following are percentages of platelets in other stages: round (8.1 ± 2.1), spreading dendritic ($13 \pm 7.0\%$), spreading ($4.4 \pm 6.2\%$), fully spreading ($2.3 \pm 3.2\%$), and aggregation ($6.2 \pm 8.7\%$).

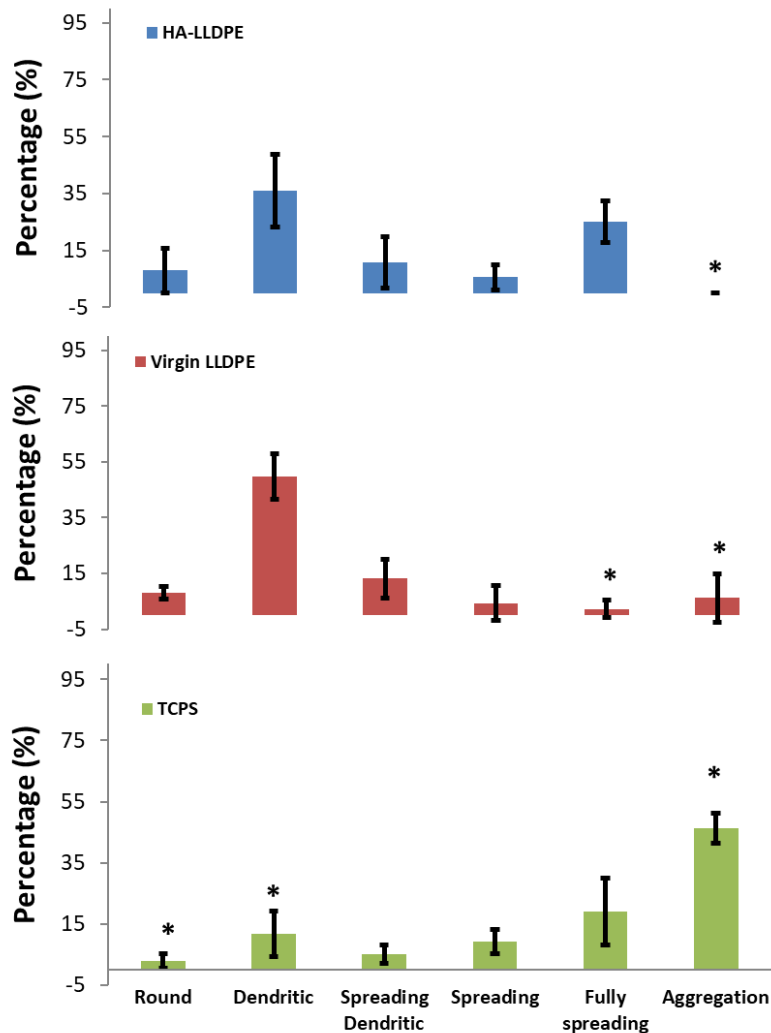


Figure 4.11: Quantitative analysis of the platelet activation study for HA-LLDPE, virgin LLDPE, and TCPS. Asterisk (*) means significant difference from other groups within the same activation step. ($n=3$, p value < 0.05). All data are presented as mean \pm standard deviation.

Representative images of platelets adhesion are shown on Figure 4.12. TCPS has the most platelets as seen by the two left most calcein stained images. There were platelets adhering on virgin LLDPE, but to a lesser extent than TCPS. The HA-LLDPE samples seem to have the least platelet adhesion. The quantitative analysis in Figure 4.13 reveals significant decrease in platelet adhesion when comparing HA treated ($0.27 \pm 0.11\%$) to virgin LLDPE ($0.81 \pm 0.46\%$). TCPS has the highest percentage of platelet coverage as expected ($1.88 \pm 1.32\%$). The results demonstrate that the HA treated LLDPE surface does reduce platelet adhesion. Although the standard deviation for TCPS appears large, there was a significant difference comparing to the HA-LLDPE. Calcein stained images of ePTFE samples could not be processed for platelet adhesion quantification, because the ePTFE samples auto fluoresced (excitation/emission: 493/514 nm).

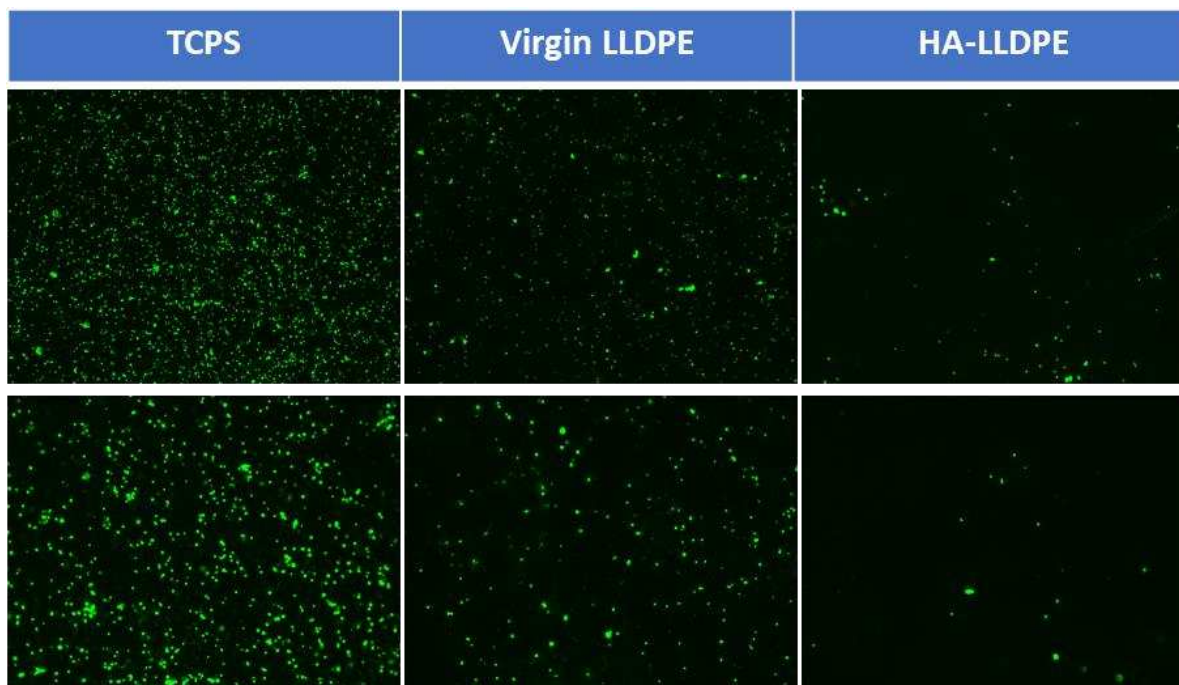


Figure 4.12: Fluorescent images of platelets from the calcein study. TCPS (positive control) seems to have the most coverage of platelets, then virgin LLDPE and HA-LLDPE. Images of ePTFE and HA-ePTFE were not collected due to autofluorescence from ePTFE.

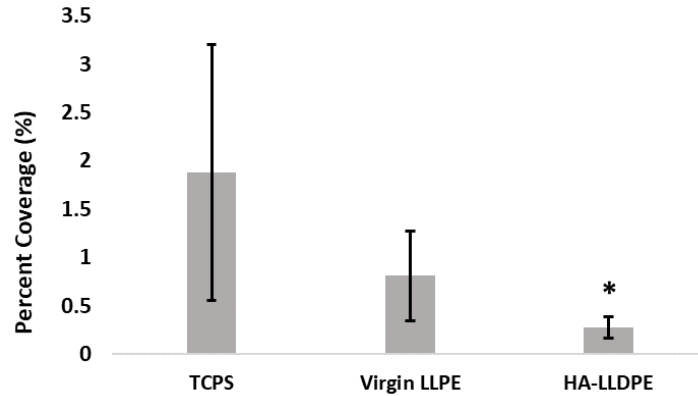


Figure 4.13: Percent coverage of platelets from the calcein staining experiment. There was significantly less platelets adhering to HA-LLDPE than TCPS and virgin LLDPE (p value = 0.1, $n=3$). Platelet coverage for ePTFE and HA-ePTFE were not calculated because ePTFE autofluoresces (excitation/emission: 493/514 nm). All data are presented as mean \pm standard deviation.

The study reveals that there is less platelet activation on HA-ePTFE than ePTFE. Platelets seem to aggregate readily on ePTFE, and this phenomenon could be explained by a combination of surface chemistry and topography. As described in chapter 1 and 2, ePTFE has a rough surface that is characterized by a series of nodal and internodal regions, with the latter consists of microfibril layers. SEM images of ePTFE in Figure 4.9 show the platelets preferably adhere to the microfibrils within the internodes. The exceptionally high percentage of platelet aggregation could be further explained by the hydrophobic surface of ePTFE, which could attract fibrinogen [19]. Thus, the rough internodal fibrils and the hydrophobic surface could be the main factors in platelet activation and aggregation [22].

The percentage of platelets in each activation stage of HA-LLDPE is comparable to that of virgin LLDPE. The exceptions are the last two stages. There were more platelets fully spreading on HA-LLDPE than virgin LLDPE, but HA-LLDPE has almost no platelet aggregation compared to the 6.2 ± 8.7 % on virgin LLDPE. The decreasing aggregation demonstrates that HA enhancement is

effective at reducing platelet activation, and this is further supported by the data from the calcein stained images (Figure 4.13) where significantly less platelets adhered to HA-LLDPE than LLDPE. It is interesting that, within the few platelets adhering to HA-LLDPE, $25 \pm 7.2\%$ were fully spreading while none were aggregating. In contrast, virgin LLDPE had $2.3 \pm 3.2\%$ aggregation. Similar observation is noted in previous work involving platelet activation study of HA-LLDPE [23]. Perhaps the relationship between platelet morphology and activation is complex, and further understanding of the mechanisms behind platelet adhesion could explain platelet spreading on HA-LLDPE.

The data concur with findings in literature, describing the decreasing platelet activation after HA enhancement of polymeric surfaces [15,25,26]. For example, Simon-Walker et al. demonstrated that isocyanate crosslinked HA on LLDPE can lower platelet adhesion and activation [15]. It is interesting that, although both HA-ePTFE and HA-LLDPE had HA rich surfaces, the activation of platelets was different on both materials. A larger percentage of platelets aggregated on HA-ePTFE than HA-LLDPE, but less platelets appeared at later activation stage (> stage 6) on HA-ePTFE than HA-LLDPE. This observation supports the results reported in the whole blood clotting study, where there was less clotting on HA-ePTFE and HA-LLDPE. Overall, the platelet activation results indicate that HA-ePTFE and HA-LLDPE could reduce platelet activation, an important process in thrombosis [24].

The decrease in platelet activation could be due to the surface charge of HA. The negatively charged carboxyl group of the crosslinked HA could repulse negatively charged proteins responsible for platelet adhesion, such as adenosine diphosphate and fibrinogen, from binding [27]. Moreover, HA is ubiquitous in the endothelial glycocalyx layer above the endothelium of blood vessels that has antiatherogenic properties [28,29], and the presence of HA may prevent platelet

adhesion. GAG chains, such as hyaluronan, have also been shown to sterically prevent binding of leukocytes and platelets under physiological conditions [28].

4.4 Limitations and Future Work

The cytocompatibility results show no cell death when HDF were incubated with HA-LLDPE and HA-ePTFE. This was an acute cytotoxicity study in an artificial environment that may represent a typical cardiovascular system. In addition, a longer duration study would reveal whether there is any long-term adverse effect from the biomaterials. Although the leaching study demonstrates that eluates of HA-LLDPE, similar study may need to be performed on HA-ePTFE. Future work should also consider testing in an *in vivo* environment that is closer to mimicking the human body. It is possible that the rigid TCPS used in the study partially influenced platelet activation. Platelets suspended in the plasma during incubation could have adhered to the polystyrene, become activated, and released substances that might have promoted adhesion of additional platelets from the surrounding plasma [7]. This could affect the results by overestimating the total platelet activation caused by the biomaterials. Therefore, the herein platelet activation results should only be used for comparison in relation to the HA enhancement. Future studies should consider a negative control, where no platelet binding and activation is expected, to verify whether any external factors could influence platelet activation. More research is required to understand how platelets and other clotting factors interact with HA-ePTFE and HA-LLDPE. Previous work has shown a HA enhancement of LLDPE leads to a general decrease in platelet factor 4 expression, thrombin activation, and fibrinogen [23]. Nevertheless, these results did not show statistical difference between the virgin LLDPE and the HA treated LLDPE. Future work may require more physiologically relevant studies involving animal and perhaps blood from a larger pool of sample

[30,31]. The herein studies used blood from only one donor, which is another limitation in the experimental design.

Although the whole blood clotting study shows that HA treated surfaces could lead to minor clotting, the environment of the experiment is not physiologically representative and should only be used for relative comparison with the control (TCPS) and the untreated samples. Blood sitting idly in dry air at ambient temperature will clot over time. Future studies should consider more physiologically relevant methods to simulate blood interactions with HA-ePTFE and HA-LLDPE [32,33]. Such designs could also be used to model pathological effects from synthetic vascular grafts such as compliance mismatch [4]. Perhaps testing in a dynamic environment mimicking physiological blood flows would provide more information on the clotting potential of HA-LLDPE and HA-ePTFE devices. More physiologically relevant experiments may involve animal studies as described in literature [30]. In general, the ISO 10993 standards should be used for guidance in designing the proper experiment model.

References

- [1] B.D. Ratner, S.J. Bryant, Biomaterials: where we have been and where we are going, *Annu. Rev. Biomed. Eng.* 6 (2004) 41–75.
- [2] U.T. Seyfert, V. Biehl, J. Schenk, In vitro hemocompatibility testing of biomaterials according to the ISO 10993-4, *Biomolecular Engineering*. 19 (2002) 91–96. doi:10.1016/s1389-0344(02)00015-1.
- [3] ISO 10993-5, Biological evaluation of medical devices–Part 5: Tests for in vitro cytotoxicity, International Organization for Standardization Geneva, Switzerland, 2009.
- [4] M.F.A. Cutiongco, D.E.J. Anderson, M.T. Hinds, E.K.F. Yim, In vitro and ex vivo hemocompatibility of off-the-shelf modified poly(vinyl alcohol) vascular grafts, *Acta Biomaterialia*. 25 (2015) 97–108. doi:10.1016/j.actbio.2015.07.039.
- [5] K.C. Popat, B.S. Smith, Titania Nanotube Arrays as Interfaces for Blood-Contacting Implantable Devices: A Study Evaluating the Nanotopography-Associated Activation and Expression of Blood Plasma Components, *Journal of Biomedical Nanotechnology*. Accepted-In Press (2012).
- [6] M. Fischer, C.P. Baptista, I.C. Gonçalves, B.D. Ratner, C. Sperling, C. Werner, C.L. Martins, M.A. Barbosa, The effect of octadecyl chain immobilization on the hemocompatibility of poly (2-hydroxyethyl methacrylate), *Biomaterials*. 33 (2012) 7677–7685. doi:10.1016/j.biomaterials.2012.07.007.
- [7] F. Jung, S. Braune, A. Lendlein, Haemocompatibility testing of biomaterials using human platelets, *Clinical Hemorheology and Microcirculation*. 53 (2013) 97–115.
- [8] B.S. Smith, S. Yoriya, L. Grissom, C.A. Grimes, K.C. Popat, Hemocompatibility of titania nanotube arrays, *Journal of Biomedical Materials Research Part A*. 95A (2010) 350–360. doi:10.1002/jbm.a.32853.
- [9] D.G. Barrett, M.N. Yousaf, Design and applications of biodegradable polyester tissue scaffolds based on endogenous monomers found in human metabolism, *Molecules*. 14 (2009) 4022–4050.
- [10] V. Forest, A. Figarol, D. Boudard, M. Cottier, P. Grosseau, J. Pourchez, Adsorption of Lactate Dehydrogenase Enzyme on Carbon Nanotubes: How to Get Accurate Results for the Cytotoxicity of These Nanomaterials, *Langmuir*. 31 (2015) 3635–3643. doi:10.1021/acs.langmuir.5b00631.
- [11] V.B. Damodaran, V. Leszczak, K.A. Wold, S.M. Lantvit, K.C. Popat, M.M. Reynolds, Anti-thrombogenic properties of a nitric oxide-releasing dextran derivative: evaluation of platelet activation and whole blood clotting kinetics, *RSC Advances*. 3 (2013) 10.1039/C3RA45521A. doi:10.1039/C3RA45521A.
- [12] S. Braune, A. Hnow, C. Mrowietz, J. Cui, K. Kratz, J. Hellwig, C. zm, R.V. Klitzing, A. Lendlein, F. Jung, Hemocompatibility of soft hydrophobic poly (n-butyl acrylate) networks

- with elastic moduli adapted to the elasticity of human arteries, *Clinical Hemorheology and Microcirculation*. 49 (2011) 375--390.
- [13] S.L. Goodman, Sheep, pig, and human platelet-material interactions with model cardiovascular biomaterials, *Journal of Biomedical Materials Research*. 45 (1999) 240–250. doi:10.1002/(sici)1097-4636(19990605)45:3<240::aid-jbm12>3.0.co;2-c.
- [14] H.T. Bui, A.R. Friederich, E. Li, D.A. Prawel, S.P. James, Hyaluronan enhancement of expanded polytetrafluoroethylene cardiovascular grafts, *Journal of Biomaterials Applications*. 33 (2018) 52–63.
- [15] R. Simon-Walker, J. Cavicchia, D.A. Prawel, L.P. Dasi, S.P. James, K.C. Popat, Hemocompatibility of hyaluronan enhanced linear low density polyethylene for blood contacting applications, *Journal of Biomedical Materials Research Part B: Applied Biomaterials*. 106 (2017) 1964–1975.
- [16] D.A. Prawel, H. Dean, M. Forleo, N. Lewis, J. Gangwish, K.C. Popat, L.P. Dasi, S.P. James, Hemocompatibility and hemodynamics of novel hyaluronan–polyethylene materials for flexible heart valve leaflets, *Cardiovascular Engineering and Technology*. 5 (2014) 70–81.
- [17] P. Król, Generalization of kinetics in the reaction of isocyanates and polyols for modeling a process-yielding linear polyurethane, 1, *Journal of Applied Polymer Science*. 57 (1995) 739–749.
- [18] F.M. Benoit, Degradation of polyurethane foams used in the mêmce breast implant, *Journal of Biomedical Materials Research*. 27 (1993) 1341–1348.
- [19] L.-C. Xu, C.A. Siedlecki, Effects of surface wettability and contact time on protein adhesion to biomaterial surfaces, *Biomaterials*. 28 (2007) 3273–3283. doi:10.1016/j.biomaterials.2007.03.032.
- [20] Y. Yan, L.-C. Xu, E.A. Vogler, C.A. Siedlecki, Contact activation by the intrinsic pathway of blood plasma coagulation, in: *Hemocompatibility of Biomaterials for Clinical Applications*, Elsevier, 2018: pp. 3–28. doi:10.1016/B978-0-08-100497-5.00001-X.
- [21] V. Leszczak, B.S. Smith, K.C. Popat, Hemocompatibility of Polymeric Nanostructured Surfaces, *Journal of Biomaterials Science. Polymer Edition*. 24 (2013) 1529--1548. doi:10.1080/09205063.2013.777228.
- [22] P. Parhi, A. Golas, E.A. Vogler, Role of proteins and water in the initial attachment of mammalian cells to biomedical surfaces: a review, *Journal of Adhesion Science and Technology*. 24 (2010) 853–888.
- [23] R. Simon-Walker, Hemocompatibility of hyaluronan enhanced linear low-density polyethylene for heart valve leaflet applications, Thesis, Colorado State University. Libraries, 2018. <https://mountainscholar.org/handle/10217/193185> (accessed March 19, 2019).
- [24] I. Reviakine, F. Jung, S. Braune, J.L. Brash, R. Latour, M. Gorbet, W. van Oeveren, Stirred, shaken, or stagnant: What goes on at the blood–biomaterial interface, *Blood Reviews*. 31 (2017) 11–21. doi:10.1016/j.blre.2016.07.003.

- [25] F. Wu, J. Li, K. Zhang, Z. He, P. Yang, D. Zou, N. Huang, Multifunctional Coating Based on Hyaluronic Acid and Dopamine Conjugate for Potential Application on Surface Modification of Cardiovascular Implanted Devices, *ACS Applied Materials & Interfaces*. 8 (2016) 109–121. doi:10.1021/acsami.5b07427.
- [26] H.P. Felgueiras, L.M. Wang, K.F. Ren, M.M. Querido, Q. Jin, M.A. Barbosa, J. Ji, M.C.L. Martins, Octadecyl Chains Immobilized onto Hyaluronic Acid Coatings by Thiol–ene “Click Chemistry” Increase the Surface Antimicrobial Properties and Prevent Platelet Adhesion and Activation to Polyurethane, *ACS Applied Materials & Interfaces*. 9 (2017) 7979–7989. doi:10.1021/acsami.6b16415.
- [27] M. Modic, I. Junkar, K. Stana-Kleinschek, R. Kostanjšek, M. Mozetič, Morphology Transformations of Platelets on Plasma Activated Surfaces, *Plasma Processes and Polymers*. 11 (2014) 596–605. doi:10.1002/ppap.201400001.
- [28] S. Dogné, B. Flamion, N. Caron, Endothelial Glycocalyx as a Shield Against Diabetic Vascular Complications: Involvement of Hyaluronan and Hyaluronidases, *Arteriosclerosis, Thrombosis, and Vascular Biology*. 38 (2018) 1427–1439. doi:10.1161/ATVBAHA.118.310839.
- [29] L.N. Broekhuizen, H.L. Mooij, J.J. Kastelein, E.S. Stroes, H. Vink, M. Nieuwdorp, Endothelial glycocalyx as potential diagnostic and therapeutic target in cardiovascular disease:, *Current Opinion in Lipidology*. 20 (2009) 57–62. doi:10.1097/MOL.0b013e328321b587.
- [30] M.J. Byrom, P.G. Bannon, G.H. White, M.K.C. Ng, Animal models for the assessment of novel vascular conduits, *Journal of Vascular Surgery*. 52 (2010) 176–195. doi:10.1016/j.jvs.2009.10.080.
- [31] D. Bezuidenhout, D.F. Williams, P. Zilla, Polymeric heart valves for surgical implantation, catheter-based technologies and heart assist devices, *Biomaterials*. 36 (2015) 6–25.
- [32] P. Zilla, D. Bezuidenhout, P. Human, Prosthetic vascular grafts: wrong models, wrong questions and no healing, *Biomaterials*. 28 (2007) 5009–5027.
- [33] P. Zilla, J. Brink, P. Human, D. Bezuidenhout, Prosthetic heart valves: Catering for the few, *Biomaterials*. 29 (2008) 385–406. doi:10.1016/j.biomaterials.2007.09.033.

Appendix

HA-CTA Complexation

Silylation of HA-CTA

Acetone Distillation

Xylene Distillation

HA-ePTFE Enhancement

HA-LLDPE Enhancement

Water Contact Angle Goniometry

Lactate Dehydrogenase Assay Protocol

Whole Blood Clotting

Platelet Activation

A.1 HA-CTA Complexation

Objective: Hydrophobic modification of hyaluronan for reaction in anhydrous solvents

Materials and Equipment

- Sodium hyaluronan (NaHA)
- Cetyltrimethylammonium bromide (CTAB)
- Fresh Deionized water (DI H₂O)
- 1000 ml beaker or flask
- 500 ml beaker or flask
- Magnetic stir bars
- Stir plates
- Freezer mill/Cryogrinder
- Liquid nitrogen
- Hyaluronan-cetyl trimethylammonium complex (HA-CTA)
- Vacuum oven
- Vapor trap
- Vacuum pump
- Thermal gloves
- Safety glasses
- Buckner funnel
- Filter paper
- Erlenmeyer flasks

Procedure

1. Prepare a 0.30% w/v solution of sodium hyaluronan in DI H₂O. Minimize large clumps when adding NaHA.
 - a. Example: 1.5g NaHA in 500 ml DI H₂O
 - b. Stir the reaction at room temperature until the NaHA is completely dissolved. This can take several hours depending on the molecular weight of the NaHA. Stir for 15 hours to 3 days. Parafilm the beaker.
 - c. When fully dissolved, the solution is clear.
 - d. To get the NaHA into solution, turn the stir bar RPMs high enough to get a vortex on the top part of the stir bar for at least 5 mins. Then, turn the RPMs down to a low setting to form a little vortex.
 - e. Record the following in lab notebook:
 - Date, Time, Mass of NaHA (g) used, Volume of DI H₂O (mL) used, Dissolve Time (from start of mixing to when CTAB is added), Manufacturer, Lot Number, Part Number, and when the bottle of NaHA was opened.
2. Prepare a 1.00% w/v solution of CTAB in DI H₂O.
 - a. Example: 1.69 g CTAB in 169 ml DI H₂O
 - b. Stir the reaction at 40°C until the CTAB is completely dissolved. When dissolved, the solution will be clear. This takes 10-15 mins.
 - c. Record the following in lab notebook:
 - Date, Time, Mass CTAB (g) used, Volume DI H₂O (mL) used, Dissolve time, Manufacturer, Lot Number, Part Number, and when bottle of CTAB was opened.

3. Slowly add the CTAB solution to the NaHA solution while under magnetic stirring. Parafilm the beaker. The mixture will become increasingly opaque as the CTAB solution is added. When the reaction is complete, a white precipitate forms and the supernatant is clear. Varying the addition rate affects the size of the precipitate (a slower addition rate produces a smaller precipitate). Stir for 15 hours – 36 hours.
 - a. Record the following in lab notebook:
 - Date, and Time of addition.
4. The precipitate is HA-CTA. Collect and wash the HA-CTA to remove excess CTAB using a Buckner funnel. Use a vapor trap on the oven.
 - a. Set up a Buckner funnel to two Erlenmeyer flasks. (pic)
 - b. Place filter paper on the funnel and wet it using DI H₂O.
 - c. Pour the HA-CTA/DI H₂O solution into the Buckner funnel slowly to prevent HA-CTA from getting under the filter paper.
 - d. Rinse the HA-CTA with 500 ml DI H₂O.
 - e. Use a spatula to scrape the HA-CTA into an Erlenmeyer flask with 300 ml DI H₂O.
 - f. Cover the Erlenmeyer flask with a serum stopper and shake it for 30 seconds.
 - g. Pour the contents of the Erlenmeyer flask in the Buckner funnel and vacuum off the water.
 - h. A second time, rinse the HA-CTA with 500 ml DI H₂O.
 - i. A second time, use a spatula to scrape the HA-CTA into an Erlenmeyer flask with 300 ml DI H₂O.
 - j. Cover the Erlenmeyer flask with a serum stopper and shake it for 30 seconds.
 - k. Pour the contents of the Erlenmeyer flask in the Buckner funnel and vacuum off the water.
 - l. A third time, rinse the HA-CTA with 500 ml DI H₂O.

- m. A third time, use a spatula to scrape the HA-CTA into an Erlenmeyer flask with 300 ml DI H₂O.
 - n. Cover the Erlenmeyer flask with a serum stopper and shake it for 30 seconds.
 - o. Pour the contents of the Erlenmeyer flask in the Buckner funnel and vacuum off the water.
 - p. A fourth time, rinse the HA-CTA with 500 ml DI H₂O.
 - q. A fifth time, rinse the HA-CTA with 500 ml DI H₂O.
 - r. Move the HA-CTA to the center of the filter paper, and carefully place the filter paper inside a petri dish. Spread the HA-CTA out.
 - s. Place the petri dish and filter paper in a vacuum oven to dry at 50°C for 3 days. Occasionally wipe the water off the inside of the oven door. Be sure to watch vapor traps to make sure they don't fill and are functioning correctly. <<note: combine with 5 below>>
 - t. Record the following in lab notebook:
 - Date, Process Start Time, Process End Time, and Oven in Time.
5. Dry HA-CTA in a vacuum oven (-25 in Hg, 50°C) for 3 days or until no change in weight is observed. A yield of about 2.5 g HA-CTA is expected for a starting NaHA weight of 1.5 g.
 6. Grind the dried HA-CTA to a powder using a freezer mill/cryogrinder.
 - a. Wear thermal gloves and safety glasses.
 - b. Slowly fill the cryogrinder with liquid nitrogen to the fill line. This typically requires about 5L of liquid nitrogen and will cool the cryogrinder down. Close the top cover and let the cryogrinder sit until vapor stops coming out of the rear vent.
 - c. Weigh the HA-CTA and record the weight.
 - d. Place the bottom cap on a cryogrinder tube, and place half of the HA-CTA into the tube with a magnet.

- e. Place the top on the cryogrinder tube, with the slotted end towards the outside so that it can be removed using the “tool”.
- f. Insert the cryogrinder tube into the cryogrinder so that the cap slot is aligned with the end of the tube chamber.
- g. Use a low impact frequency for a total of 3 mins.
- h. Collect the HA-CTA powder in a 50 ml centrifuge tube.
- i. Repeat the previous steps to cryogrind the remaining half of the HA-CTA.
- j. Periodically check the liquid nitrogen level and add more if needed.
- k. Clean cryogrinder tubes with 2% Liquinox and DI H₂O. **Do not use solvents, including acetone.** Clean metal caps and magnet with 2% Liquinox, DI H₂O, and acetone.
- l. Record the following in lab notebook:
 - Date, Process Start Time, Grind Time, Process End Time, and Oven in Time
7. Dry the ground HA-CTA in a vacuum oven (-25 mm Hg, 50°C) for 24 hours or until no change in weight is observed.
8. When dry, HA-CTA should be stored in a dessicator. Save a sample for FTIR analysis.

Notes

- Rinse all stir bars and spatulas with acetone and let air dry prior to use.
- Log lot numbers, etc. in documentation

Revision by NL (09/19/2013) – ADD MORE HERE. Changed “HA” to “NaHA.” Changed sodium hyaluronate abbreviation in Materials and Equipment to match the procedure. Added abbreviation for DI H₂O to Materials and Equipment. Clarified wording. Changed bullets to numbers and changed formatting to match required thesis formatting guidelines.

Revision by CD (11/16/11) – Changed concentration of CTAB:DIH₂O and CTAB:NaHA to match SBM protocol.

References

Zhang, M. and James, S.P., (2005). *Silylation of hyaluronan to improve hydrophobicity and reactivity for improved processing and derivatization.* , **46**(11):3639-3648.

A.2 HA-CTA Silylation

Objective

Hydrophobic modification of hyaluronan for reaction in anhydrous solvents

Materials & Equipment

- Hyaluronan-cetyl trimethylammonium complex (HA-CTA)
- Dimethyl sulfoxide $\geq 99.9\%$ ReagentPlus (DMSO)
- Hexamethyldisilazane $\geq 99.9\%$ ReagentPlus (HMDS $\geq 99.9\%$ ReagentPlus)
- Hexamethyldisilazane $\geq 97.0\%$ (HMDS $\geq 97.0\%$)
- 500 ml Round Bottom Flask (RBF)
- Graduated cylinders
- Serum stoppers
- Copper wire
- Needle nose pliers
- Keck clips
- Condenser
- Dry Nitrogen (N_2) gas
- Magnetic stir bars
- Stir plates
- Vacuum oven
- Vapor trap
- Vacuum pump

Procedure

Glassware preparation

Wash glassware with 2% liquinox, then rinse with DI H₂O, and then rinse with acetone. Place glassware in oven (125°C) for 24 hours. Remove glassware from oven and let cool. When cool, silylate glassware with HMDS ≥ 97.0% for at least 5 mins. Swish the HMDS around, making sure to contact the surface that will contact the silyl HA-CTA, staying below the neck of a RBF or separatory funnel. Pour HMDS into hazardous waste, and rinse the glassware with acetone. Place the glassware back in the oven for 10 mins to dry the acetone. Remove the glassware from the oven and let it cool. The glassware is now ready to use.

Add DMSO

1. Silylate a 50 ml graduated cylinder and a 500 ml RBF.
2. Place a stir bar and the cryoground HA-CTA powder into a 500 ml single neck RBF.
 - Be sure a sample for FTIR was taken.
3. Cap the RBF and a graduated cylinder with rubber stoppers and copper wire. The copper wire should be tight and pinch into the rubber.
4. Turn on the dry nitrogen and adjust to a low flow rate.
5. Vent the RBF and graduated cylinder with dry N₂. Depending on the nitrogen flow, venting five times for five seconds each time is recommended.
6. Add 50 ml of DMSO for every 1.5g of starting NaHA to the RBF via a cannula and dry N₂. Maintain positive pressure in the graduated cylinder and RBF. Mark the number of punctures in tally form on the bottle.
7. Swell the HA-CTA in the DMSO at room temperature until it is gel-like (about 4-12 hours).
8. Lower the RBF into a 50°C oil bath and continue to stir until the starting material is fully dissolved (4-24 hrs).
 - **Make sure the thermocouple light on the hot plate is turned on.**
9. Record the following in lab notebook:

- Date, Time, Manufacturer, Lot number, Part number, date the bottle of DMSO was opened, and time the heat was turned on.

Add HMDS

10. Silylate a 25 ml graduated cylinder.
11. Cap a graduated cylinder with a rubber stopper and copper wire. The copper wire should be tight and pinch into the rubber.
12. Vent the graduated cylinder with dry N₂ before adding HMDS. Depending on the nitrogen flow, venting five times for five seconds each time is recommended.
13. Add 25 ml of HMDS \geq dd 25 mReagentPlus for every 1.5g of starting NaHA to the RBF via a cannula and dry N₂ while maintaining positive pressure in the graduated cylinder and RBF. Increase the temperature of the oil bath to 75°C for 48 hours. Vigorous stirring is important to mix the HMDS and DMSO layers. Mark the number of punctures in tally form on the bottle.
 - **Make sure the thermocouple light on the hot plate is turned on.**
14. Periodically check stirring and hot plate temperature. Stirring is important for mixing the DMSO and HMDS to increase the degree of silylation.
15. Record the following in lab notebook:
 - Date, Time, Manufacturer, Lot Number, Part Number, and when the bottle of HMDS was opened.

Separating and washing silyl HA-CTA

16. Cool the reaction to room temperature.
17. Silylate a separatory funnel and a crystallizing dish.

18. Pour the reaction mixture into a 250 ml separatory funnel, and let the two phases separate for 5 mins.
 - a. The upper layer contains HMDS and silylated HA-CTA.
 - b. The bottom layer is DMSO.
19. Let the DMSO drain into a beaker and dispose of the DMSO into a hazardous waste bottle.
20. Let the upper layer drain into the RBF that was used for silylation. This RBF now contains the silyl HA-CTA.
21. Close the separatory funnel stopper and add 10 ml of xylenes. Cap the funnel and swirl the xylenes to rinse the funnel. Collect the xylenes into the RBF containing the silyl HA-CTA.

The purpose of this rinse step is to increase the yield of silyl HA-CTA.
22. Wash the silyl HA-CTA using a rotavap.
 - a. Fill the bowl of the rotavap with DI H₂O.
 - b. Heat the DI H₂O to 60-70°C. If the water heats to 75°C, cool it down to prevent degradation of the silyl HA-CTA.
 - c. Apply vacuum grease to the two stopcocks, to the top surface of the cold finger, and to the inside surface of the RBF condenser as needed (see how to grease a stopcock by Mike).
 - d. Place the cold finger inside the outer condensing column.
 - e. Place the rubber gasket flat against the rotavap arm as seen in Figure XX.
 - f. Screw the grey clamp partially on as seen in Figure XX.
 - g. Hold the edge of the coldfinger flat against the gasket and screw the grey piece until snug.
 - h. Attach the RBF condenser using a keck clip.
 - i. Fill the inner cold finger with ice.
 - j. Check vacuum tubing connection between the coldfinger and pump.
 - i. Follow pump protocols taped to front of fume hood along with below.

1. Make sure the exhaust port of the pump is not blocked by the back wall of the fume hood (or anything else).
 2. Run the pump for a few (2-3) minutes before connecting it to the rotovap until it has warmed up.
 3. Once finished rotovapping, let the pump run for three minutes disconnected from the system to make sure no vapors remain in the pump.
- k. Lower the rotavap arm using the lever so that the RBF containing silyl HA-CTA is partially submerged in water but still able to rotate.
 - l. Turn the vacuum pump strength to low, and turn the pump on. Wait for the vacuum to pull through the system.
 - m. Set the rotation speed to 60RPM.
 - n. Slowly increase the strength of the vacuum until vapor is pulled into the cold finger. Be careful to avoid boiling the solution because this could decrease the yield of silyl HA-CTA by pulling it into the cold finger.
 - o. When the silyl HA-CTA is mostly dry, turn the rotation off, turn the vacuum pump strength down, and turn the vacuum pump off.
 - p. Raise the rotavap arm using the lever.
 - q. Release the vacuum from the system using the upper stopcock, and let air back into the tubing by opening and closing the stopcock a few times.
 - r. Gently twist and pull the RBF containing silyl HA-CTA off of the rotavap.
 - s. Add 40 ml of xylenes to the RBF, cover with a serum stopper, and dissolve the silyl HA-CTA by swirling the flask.
 - t. When dissolved, uncap the RBF and attach it to the rotavap using a keck clip.
 - u. Wash the xylenes as in the previous steps.

- v. Add xylenes 4 more times and wash as described, for a total of 5 washes with xylenes (in addition to the first wash in HMDS).
 - i. The sample should be allowed to crystallize on washes 2 and 4 and the time recorded for the sample to dissolve back into xylenes recorded.
 - w. On the last wash, leave a few milliliters (~5 ml) of xylenes in the flask.
 - x. Pour the silyl HA-CTA/xylenes into a silylated crystallizing dish.
 - y. Add 5 ml more xylenes to the RBF to dissolve any remaining silyl HA-CTA, and pour it into the same crystallizing dish.
23. Dry the silyl HA-CTA at 50°C using a vapor trap until no weight change is observed. Save a sample for FTIR analysis. A yield of 2.0-2.5 g of silyl HA-CTA is expected when starting with 1.5 g NaHA.
24. Record the following in lab notebook:
- Date, Time, Oven in Time, Oven out Time, and Final Weight.

Note

- Cannula transfers should be done with at least two people. Never try a cannula transfer alone.

Protocol History

Revision by NL (09/19/2013) – ADD MORE HERE. Updated Materials and Equipment. Added glassware preparation procedure. Added nitrogen venting for glassware. Updated separating and washing procedure. Changed HMDS stir time from 72-96 hours to 48 hours. Changed “HA” to “NaHA.” Changed sodium hyaluronate abbreviation in Materials and Equipment to match the procedure. Added abbreviation for DI H₂O to Materials and Equipment. Clarified wording. Changed bullets to numbers and changed formatting to match required thesis formatting guidelines.

Revision by JG (02/21/2013)

Originator: CD

References

Kurkowski, R. *The chemical crosslinking, compatibilization, and direct molding of ultra high molecular weight polyethylene and hyaluronic acid microcomposites*, M.S. thesis, Colorado State University Department of Mechanical Engineering, Fort Collins, CO (2007).

Zhang, M. and James, S.P., (2005). *Silylation of hyaluronan to improve hydrophobicity and reactivity for improved processing and derivatization.* , **46**(11):3639-3648

A.3 Acetone Distillation

Distillation of Acetone Using Boric Anhydride
Emily Li – Version 1.0

Revision Date	Name	Version #

Purpose:

Using boric anhydride as a desiccant, acetone can be distilled to further remove some water content.

Materials:

- Stock acetone
- Boric anhydride
- 2 silylated 500 mL round bottom flasks
- Two plastic tubing
- Vacuum tape
- Teflon tape
- Tube of desiccant

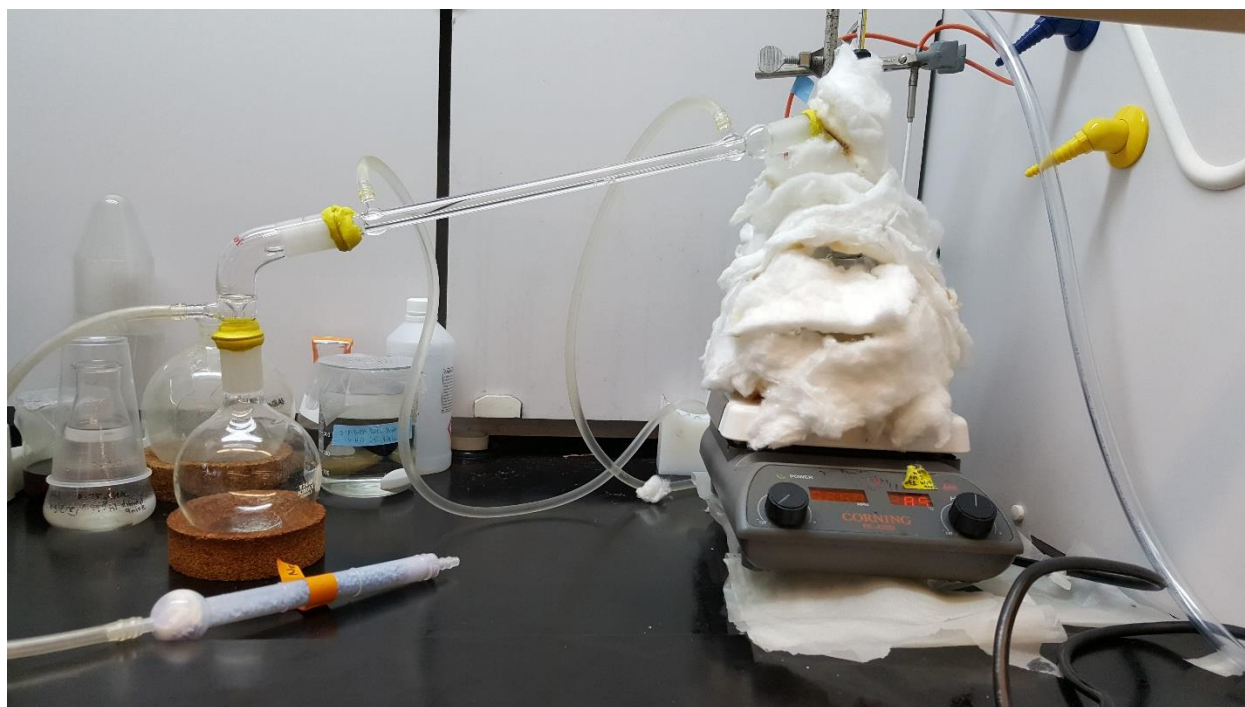
Procedure:

1. Use boric anhydride as a primary desiccant for 24 hours.
 - a. Use 15% (mass to volume) of boric anhydride. For example, use 67.5 g of boric anhydride for 500 mL of acetone.
 - b. Swirl the acetone and boric anhydride in a 500 mL Erlenmeyer flask to fully expose all of the boric anhydride to the acetone and let sit for at least 24 hours.
2. In a glove bag and using a funnel, slowly pour the acetone into a silylated 500 mL round bottom flask to avoid pouring in a large amount of the boric anhydride. Put a rubber stopper on the round bottom flask before removing from the glove bag. **Note: Allow the**

acetone and boric anhydride solution to sit for at least 2 hours before transferring into the Erlenmeyer so the boric anhydride can settle.

3. Set up the glassware as shown below in the following steps:
 - a. Clamp the round bottom flask with the acetone right above the oil bath.
 - b. Wrap teflon tape around the thread of the distillation thermometer adapter.
 - c. Attach the longer plastic tubing to the bottom end of the condenser and the short one to the top end.
 - d. Attach the desiccant to the distillation adapter.
 - e. Insert the distillation adapter into the empty silylated 500 mL round bottom flask. Make sure they are joint tightly and vacuum tape the joint twice. Use the white backs of the vacuum tape to press the tape in at the joint to get a tighter seal.
 - f. Repeat with the condenser into the distillation adapter and then with the distillation thermometer adapter into the condenser.
 - g. Insert the longer plastic tubing into the drain and attach the shorter one to the water supply
 - h. Very quickly, take the stopper off of the round bottom flask with acetone and insert the distillation thermometer adapter and purge the system with nitrogen immediately. Purge for about a minute.
 - i. Quickly, remove the nitrogen line, insert the thermometer and tighten the cap around the thread of the distillation thermometer adapter.
 - j. Vacuum tape the joint between the distillation thermometer adapter and the round bottom flask.

- k.** Lower the round bottom flask as low as possible into the oil bath without touching the bottom.
- l.** Make sure a thermal probe is plugged into the hot plate and is in the oil bath.
- m.** Wrap wool around the oil bath, round bottom flask, and distillation thermometer adapter.
- n.**



- 4.** Turn the water supply on until there is a constant stream of water through the tubing and condenser. Make sure there are no leaks.
- 5.** Turn the hot plate to 90°C.
- 6.** When the reading on the thermometer reaches 50°C, turn the hot plate down to 80°C.
- 7.** Distill for 2-3 hours, make sure the reading on the thermometer never exceeds 80°C.
- 8.** Once distillation is complete, turn the hot plate and water off.

9. Cut the vacuum tape off of the between the now-full round bottom flask and the distillation adapter.
10. With the nitrogen line going, quickly remove the adapter and insert a teflon stopper into the full round bottom flask. Label the flask.
11. Carefully disassemble the distillation apparatus, taking care not to spill the water in the plastic tubing or the mineral oil.
12. Raise the now-empty round bottom flask out of the oil and allow any leftover acetone to evaporate.
13. Clean the joints of the distillation glassware of any leftover vacuum tape.

Process Considerations:

- Only work with cool glassware. Inserting hot glassware into cool glassware can cause glass to break.
- When discarding of leftover boric anhydride, be mindful that it reacts very exothermically with water. Avoid putting the boric anhydride into a waste container with water in it.

A.4 Xylene Distillation

Objective

Xylenes distillation is performed to first remove excess H₂O and then to purify Xylenes solution.

Materials & Equipment

- Xylenes
- Molecular sieves
- Condensing column
- Elbow joint with vacuum port
- Elbow joint with thermometer port
- Thermometer with cap and washer
- Two silylated 1000 mL round bottom flasks (RBFs)
- Teflon stopper
- Boiling chips
- Large crystallization dish
- Ice
- Hot plate with mineral oil bath and temperature probe
- Wool
- Vacuum Rings
- Teflon tape
- Vacuum pump and vacuum hose (with pressure gauge)
- Two rubber water inlet and outlet hoses

Procedure

Drying Xylenes over Sieves/ Prepping Glassware (at least 24-36 hours in advance)

1. Weigh out 10% weight by volume sieves
 - a. i.e. 2L Xylenes = 200g sieves
2. Add sieves to Xylenes, place cap back on and swirl*
3. Silylate two 1000mL RBFs and clean other glassware with acetone- leave in drying oven until use

*do not add sieves if very hot

Transferring Xylenes to RBF (day of distillation)

1. Place Xylenes bottle with sieves, one silylated 1000mL RBF with a few boiling chips (no more than seven chips- too many chips can lead to flashing), clean glass funnel, Teflon stopper, and large kimtech wipe (for spills) in glove bag
2. Purge glove bag three times by alternating vacuuming and filling with N₂
3. Remove vacuum line and seal bag, leave N₂ flowing into bag at low rate
4. Carefully pour Xylenes into RBF (fill to just below neck)
5. Plug RBF with Teflon stopper, close Xylenes bottle

**When finished, replace N₂ line with vacuum line (to remove some Xylenes vapor from bag).

Open bag away from you, remove materials, turn off vacuum line, and fold up bag.

Setting up Distillation Apparatus

1. Attach elbow joint with vacuum port to collection flask
 - a. Seal joint with vacuum ring*
2. Attach distillation column (water valves up)
 - a. Seal joint with vacuum ring*

3. Attach elbow joint with thermometer port to distillation column
 - a. Seal joint with vacuum ring*
4. Set up Xylenes RBF in oil bath. Do not let it touch bottom of oil bath.
5. Fill large crystallization dish with ice
6. Set receiving flask apparatus in ice and line up elbow joint opening with boiling flask
7. Insert N₂ line into top of elbow joint (in thermometer port - light flow to continually purge system)
8. **Do this step as quickly as possible.** Remove Teflon stopper and insert elbow joint into boiling RBF
 - a. Seal joint with vacuum ring*
9. Begin heating at low temperature (~75°C)
10. Attach water inlet tube (higher valve point connected to green CW port) and water outlet tube (lower valve point draining into drain)
11. Attach vacuum pump
 - a. Connect with orange tube w/ gauge to vacuum valve by receiving flask
 - b. Point pump exhaust toward fume hood
12. **Do this step as quickly as possible.** Remove N₂ line/Replace with thermometer
 - a. Using Teflon tape, twist tape in same direction as cap
 - b. Keep N₂ line close to opening to continually purge system
 - c. Lower thermometer down to junction point of condensing column and boiling flask
13. Turn on vacuum pump, vacuum down to -21 inHg
14. Turn on H₂O slowly to get steady flow, no spills

15. Cover boiling flask and elbow joint (up to condensing column) with wool
16. Turn heat up to 115°C. Lower the temperature to 105°C if Xylenes drips more than 3 drops/sec
17. Watch for flashing – look for ~3 drops/sec

*follow directions in vacuum ring package → place rings ~2/3 up connection → twist until ring becomes clear. A good seal will allow system to vacuum down to -21 inHg

***Notes:**

- Periodically check boiling (no flashing)
- Periodically check pressure gauge (-21 inHg)
- Temperature on thermometer should be ~70°C

Completing Distillation

1. Turn off heat and water
2. **Do this step as quickly as possible.** Turn off vacuum and replace thermometer with N₂ line as soon as vacuum gauge reads zero
3. **Do this step as quickly as possible.** Remove elbow joint from receiving flask and replace with Teflon stopper (cleaned with acetone)
4. Dismantle and clean the rest of the apparatus

**Place excess Xylenes back in bottle with sieves

A.5 HA-ePTFE Enhancement

HA Enhancement of ePTFE - Protocol
Emily Li – Version 1.0

Revision Date	Name	Version #
9/17/16	Hieu Bui	2

Purpose:

The use of expanded polytetrafluoroethylene (ePTFE) vascular grafts in biomedical applications requires modifications to the sample to improve its hemocompatibility. Treating the ePTFE samples with an HACTA solution provides a layer of HA inside of the ePTFE graft to increase its hemocompatibility.

Part I. Spray Coating

Materials:

- ePTFE cardiovascular graft
- Airbrush gun and accessories
- Air compressor or nitrogen line.
- Micropipettes
- Respirator Mask
- 50 ml color coded glass jars (one per sample)

Procedure:

14. Prepare the 0.4% HACTA solution.

- a. For every 100 mL, use 0.4 g of HACTA. For example, use 60 mg of HACTA for 15 mL of solution. Measure out the HACTA into a clean scintillation vial.

- b. Measure the desired volume of ethanol (15 mL for coating two samples) into the scintillation vial as well.
- c. Stir at 50°C for a minimum of 3 hours.

15. Spray coat the ePTFE graft with the HACTA solution via airbrush.

- a. Cut out 2 cm for each sample of the ePTFE graft and put each into a 50 mL color coded glass jar.
- b. Rinse samples with ethanol by pouring ethanol directly into jar, swirling, and dumping ethanol out. Put samples into solvent oven to dry.
- c. Check the HACTA solution for particulates. Make sure the HACTA is fully dissolved and that the solution is clear.
- d. Using a micropipette, transfer 5 mL of the HACTA solution into a 5 mL scintillation vial. Repeat for each sample and color code the vials.
- e. Set up a cardboard box with a vent in its side with the vent facing up into the fume hood. Keep a 50 mL glass jar in the box for stabilization of the airbrush.
- f. Connect the clear tubing to the air line and clamp the clear tubing to the valve of the airbrush using a tubing clamp and tightening with a flat head screwdriver.
- g. Hook the valve to the pressure gauge and then the actual airbrush to the pressure gauge.
- h. Open the valve (arrow pointing up) and turn the air on slowly. Then turn the gauge on, press down the button on the airbrush, and close the valve.
- i. Adjust the air to get the pressure on the gauge to read between 23 and 26 psi.

Note: Always keep either the gun or valve open to prevent pressure from building up. Keep an eye on the pressure gauge throughout.

- j. Pour ethanol into a 50 mL glass jar and connect the airbrush to the jar. Spray the airbrush to clean it, detach it from the jar, and cover the jar with a watch glass.
- k. Remove samples from the oven, weigh and record weights.
- l. Move samples into the cardboard box with airbrush. Spray the airbrush with just air then close the nozzle. Attach airbrush to 5 mL vial of HACTA solution.

Respirator must be worn during spraying to prevent inhaling any HACTA.

- m. Slowly open nozzle to get a strong mist from airbrush. Spray coat the inside of the graft by putting the nozzle right up to the sample and slowly turning it and flipping it after each full turn. Periodically check by spraying on gloves that mist is still strong and there are no clogs. Spray fast to avoid shrinking sample a great amount, but not too fast as to where solution is dripping off of sample.
- n. Once 5 mL of HACTA solution is used up, clean airbrush by spraying the cardboard box with only ethanol. Spray coat the other samples as described above.
- o. Dry samples for at least 1 hour in the vacuum oven at 50 C and -25 inches Hg.
- p. Weight samples after drying, and they can be stored in a dry environment.

Part II. Crosslinking

Materials:

- ePTFE cardiovascular graft
- Distilled acetone
- Two silylated 50 mL Erlenmeyer flasks
- One silylated 5 mL glass vial
- One silylated graduated cylinder that's at least 40 mL
- Silylated scintillation vials (one per sample)
- Poly(hexamethylene diisocyanate) (HMDI)
- 50 ml color coded glass jars (one per sample)

Procedure:

1. Make the 2.5% crosslinker solution while the sample is drying.
 - a. Clean a small rubber stopper for the 50 mL Erlenmeyer flask with acetone.
 - b. Set up and purge the glove bag containing an electronic balance, HMDI crosslinker, one silylated graduated cylinder, 2 silylated Erlenmeyer flasks (one is insurance in the case of a spill), a stir bar, one silylated 5 mL glass vial, distilled acetone, the rubber stopper, and a few kimwipes.
 - c. Put the Erlenmeyer flask on the balance, and tare the weight.
 - d. Weigh out and directly add the crosslinker (density of 1.12 g/ml) into the Erlenmeyer flask. Prepare a roughly 2.5% crosslinker solution. For example, weigh out 1.12 g of HMDI for 40 mL of acetone, which yields a 2.43% solution; this is acceptable. Pour the crosslinker into the 5 mL silylated glass vial to measure into the 50 mL Erlenmeyer.
 - e. Wipe the lip of the Erlenmeyer to get rid of any excess HMDI. Using a kimwipe wetted with the distilled acetone is helpful.
 - f. Measure the desired volume of distilled acetone with the silylated graduated cylinder and pour into the Erlenmeyer.
 - g. Add stir bar to Erlenmeyer and stopper the flask.
 - h. Remove Erlenmeyer flask from the glove bag and make sure there are no particulates.
 - i. Stir the crosslinker solution for at least 20 minutes but no more than a day.
2. Crosslinking HACTA-ePTFE Samples

- a. Warm up a metal aluminum block with holes in it with a hot plate to 50°C. Put a vial of mineral oil containing a thermometer and thermal probe into one of central holes of the block. Insulate with wool. Temperature stabilized when the digital readout is not blinking.
 - b. Weigh the samples after drying and put into the glove bag.
 - c. In the glove bag, transfer 10-15 mL of the crosslinker solution into color-coded silylated scintillation vials.
 - d. Add samples to the scintillation vials and cap vials.
 - e. Place vials near vial of mineral oil and soak the samples for exactly 1 hour.
3. Cure crosslinked HACTA-ePTFE samples
- a. Remove samples from crosslinker solution and put them into clean color-coded glass jars and cure for exactly 1 hour in the vacuum oven at 50 C and -25 inches Hg. Weight the cured samples afterward.
4. Remove excess crosslinker from the samples.
- a. Soak the cured ePTFE samples in acetone for at least 5 minutes. Gently agitate the samples for at 30 s while soaking.
 - b. Dry for approximately 5 minutes in the vacuum oven at 50 C and -25 inches Hg for fully remove acetone.
 - c. Weigh the dry samples afterward to ensure excess HMDI was rinsed away.
 - d. Samples can be stored afterward in a dried environment.

Part III. CTA Removal

Materials:

- HACTA crosslinked ePTFE cardiovascular graft
- Di Water

- Ethanol
- Sodium Chloride (NaCl)
- Sonicator
- 500 ml Erlenmeyer flasks
- 50 ml color coded glass jars (one per sample)

Procedure:

1. Prepare the 0.2 M NaCl solution for ionic exchange.
 - a. For 400 mL of solution, weigh out 4.675 g of NaCl.
 - b. Add 200 mL of DI water and 200 mL of ethanol to a 500 mL Erlenmeyer flask.
 - c. Add a stir bar to the Erlenmeyer.
 - d. While solution is stirring, add in the NaCl.
 - e. Cover Erlenmeyer with parafilm and stir until NaCl is dissolved.

2. Reverting HACTA back to HA.
 - a. Place samples in the 50 ml color coded glass jars.
 - b. Fill each jar about $\frac{3}{4}$ of the way with the NaCl solution.
 - c. Sonicate samples for 60 minutes. Keep the lid on for the first cycle.
 - d. Sonicate for 4 cycles total, changing out the solution every cycle. Ensure the temperature does not exceed 50°C but eventually does get above 37 C. Heat helps catalyze ionic exchange.

3. Removing uncrosslinked HACTA and HA.
 - a. Rinse samples with DI water and place in clean color coded jars.
 - b. Prepare a 3:2 solution of DI water to ethanol. For example, for 100 mL of solution, use 60 mL of DI water and 40 mL of ethanol.
 - c. Mix solution in graduated cylinder and divide into each jar.
 - d. Cover jars with watch glasses and leave samples to soak overnight.

A.6 HA-LLDPE Enhancement

Objective

Linear low-density polyethylene (LLDPE) will be integrated with silylated hyaluronan-cetyltrimethylammonium complex (SHACTA) by swelling the LLDPE in a solution of SHACTA and xylenes followed by vapor cross-linking. The volumes and masses given in this procedure are specific for 2 cm x 3 cm LLDPE samples.

Materials & Equipment

- Dowlex 2056 LLDPE films
- Fiskars Rotary Fabric Cutter
- Distilled Xylenes
- Large crystallizing dish
- Solvent vacuum oven
- One 250 mL round-bottom flask
- Teflon stoppers
- Teflon stir bars
- Two 100 mL graduated cylinders
- 100 mL glass jars with caps
- SHACTA
- Polyethylene glove bag
- Hot plate with thermal probe
- Heating block
- Infrared thermometer

- Small crystallizing dishes
- Metal binder clips
- Teflon scaffolds
- 250 mL Erlenmeyer flasks
- Needle-nosed tweezers
- Toluene 2,4-diisocyanate (TDI)
- P1000 Micropipette and tip
- Half-moon Teflon blocks
- NaCl
- Ethanol
- Small jars

Notes before starting

Untreated LLDPE films can be cleaned in bulk and stored

TDI is extremely toxic; handle with extreme care.

Procedure

Preparing LLDPE Films

1. Use Fiskars rotary fabric cutter to cut out LLDPE films approximately the size of the Teflon scaffolds.
2. Put LLDPE films in a jar, pour in enough acetone to submerge the films, and rinse.
3. Soak the films in xylenes for 12 hours at room temperature. Xylenes do not have to be distilled.

4. If treatment is planned for the next day, prepare the following glassware (wash and silylate):
 - a. A slow-draining fritted funnel for every 2 samples
 - b. Round-bottom flask (RBF) large enough for 40 mL of solution per 2 samples. E.g.
For 4 samples, the RBF needs to hold at least 80 mL of solution.
 - c. 100 mL graduated cylinder
 - d. One medium glass jar (that can be capped) for every 2 samples.
5. Pull films from xylenes, rinse with acetone.
6. Line a large crystallizing dish with a large kimwipe.
7. Place clean films into lined crystallizing dish. Ensure they do not touch the glass.
8. Dry films in solvent vacuum oven for at least 3 hours. Store in a labelled jar.

Swelling in SHACTA and Xylenes Solution

1. Prepare a 1% (w/v) solution of SHACTA and xylenes, 40 mL for every 2 samples.
 - a. Measure out the SHACTA into the silylated RBF.
 - b. Place a Teflon stir bar, Teflon stopper, RBF with SHACTA, silylated graduated cylinder, and distilled xylenes into the glove bag.
 - c. Purge the glove bag with nitrogen 3 times.
 - d. Add the appropriate volume of xylenes for a 1% (w/v) SHACTA xylenes solution.
 - e. Stir at 50°C until all the SHACTA is dissolved.
2. Warm heating block in glove bag to 50°C. Place medium glass jars in the block.
3. Sandwich 3 Teflon scaffolds together and use a binder clip to secure a clean LLDPE film to each side. (i.e. clipped together would be LLDPE, scaffold, scaffold, scaffold, LLDPE). The

multiple scaffolds prevent the films from touching each other. Check to confirm this construct will fit in the fritted funnel.

4. Gently blow samples with nitrogen to get rid of any dust.
5. Use infrared thermometer to confirm the heating block has reached 50°C.
6. Place lids to glass jars, kimwipes, LLDPE samples, silylated graduated cylinder from step 1 (rinsed with acetone), and SHACTA solution (wipe up any condensation on the bottom) in the glove bag.
7. Purge the glove bag with nitrogen 3 times.
8. Place the samples into the glass jars, one construct per jar.
9. Measure out 40 mL of SHACTA solution into each jar.
10. Cap jars and swell for one hour. Meanwhile, place the silylated fritted funnel on top of a 250 mL Erlenmeyer flask with the long stem extending into the flask. Warm the flask and funnel up in the solvent oven.
11. Disconnect the solvent vacuum from the pump and connect it to the house vacuum.
12. *Quickly*, use needle-nosed tweezers to extract the samples from the jars and place each construct vertically into a fritted funnel.
13. Pour the SHACTA solution into the funnel. Make sure the films do not touch the sides of the funnel. Return the funnel and Erlenmeyer back to the solvent vacuum oven.
14. Keep air flowing out of the oven while the house vacuum continually pumps it down to maintain a pressure between -13 to -15 in. Hg while the SHACTA solution drains into the Erlenmeyer.

15. When draining is complete, transfer the funnel with the samples into a clean 250 mL Erlenmeyer flask and dry in the solvent oven, vacuumed all the way down, for at least 3 hours.
16. Prepare (wash and silylate) glassware for cross-linking.
 - a. One medium glass jar per sample.
 - b. 125 mL Erlenmeyer flask with a 24/40 neck.
 - c. 100 mL graduated cylinder.

Vapor Cross-Linking:

1. Prepare a 2% (v/v) toluene diisocyanate (TDI) solution in xylenes, 10 mL per sample. Note: TDI is extremely volatile and toxic, use with great care.
 - a. Place a P1000 micropipette (set at the correct volume for TDI), its tip, a kimwipe, distilled xylenes, silylated graduated cylinder, 125 mL Erlenmeyer flask with a stir bar, and a Teflon stopper in the glove bag.
 - b. Purge with nitrogen 3 times.
 - c. Measure out the correct volume of TDI with the micropipette into the Erlenmeyer.
 - d. Measure out the correct volume of xylenes into the Erlenmeyer.
 - e. Place stopper in the Erlenmeyer and stir for 15 minutes.
2. Connect the house vacuum to the glove bag and make sure everything is capped before opening the glove bag.
3. Keep the pipette tip that contacted TDI in the fume hood.
4. Warm the heating block up to 60°C.

5. Place a half-moon shaped Teflon block in each glass jar (1 per sample) with the flat side up and warm them in the heating block.
6. Secure both ends of each LLDPE sample to its own Teflon scaffold.
7. Use the infrared thermometer to confirm that the heating block has reached 60°C.
8. Place the TDI solution, graduated cylinder from step 1 (rinsed with acetone), caps for each jar, and LLDPE samples in the glove bag. Purge with nitrogen 3 times.
9. Pour 10 mL of the TDI solution into each jar. Do not pour directly onto the Teflon block. Warm the solutions up in the heating block for 2-3 minutes.
10. Place the samples on top of the Teflon blocks. Make sure the samples do not touch the Teflon block. (i.e. the order from bottom up goes half-moon Teflon block, Teflon scaffold, sample).
11. Cap tightly, cross link for one hour.
12. Remove samples from Teflon scaffolds and dry in the solvent vacuum oven on a kimwipe-lined crystallizing dish.

Hydrolysis

1. Prepare a 1:1 solution of 0.2M NaOH to ethanol, about 150 mL per sample.
2. Run sonicator for 5 minutes to de-gas.
3. Place each sample into a small glass jar. Fill each jar with roughly 50 mL of hydrolyzing solution and sonicate for 60 minutes. Keep the temperature between 30°C and 40°C.
4. Repeat for 3 total cycles, 60 minutes each. Switch the solution out each time.
5. Prepare a 0.2 M NaOH solution, about 50 mL per sample.
6. Use tweezers to pull the samples out of the NaOH ethanol solution and rinse with DI water.
7. Place samples in new small jars.

8. Fill the jars with roughly 50 mL of the 0.2M NaOH solution.
9. Sonicate for 60 minutes. Keep the temperature under 40°C.
10. Prepare a 3:2 solution of water:ethanol, 50 mL per sample.
11. Use tweezers to pull the samples out of the 0.2M NaOH solution and rinse with DI water.
12. Place samples in new small jars.
13. Fill the jars with water:ethanol solution, cover with watch glasses, and let sit for at least 2 hours.
14. Rinse samples with DI water and put them in new small jars.
15. Sonicate for 30 minutes in DI water.
16. Dry in the water oven on a kimwipe-lined crystallizing dish.

A.7 Water Contact Angle Goniometry: Captive Bubble Technique

Materials

- Glass box
- 3-D printed slide holders
- Glass slide
- Carbon tape
- Scissors
- Hooked air-bubble needle
- Sample

Preparation:

Cut out a piece of carbon tape that is big enough to fit the sample. Put the carbon tape on the glass slide and stick the sample on the tape, either directly on it or on a puck.

Procedure

1. Take the cap off the goniometer's camera (refer to #1 on picture) and turn on the light by turning the dial - on the fiber optic illuminator behind the goniometer (#2) - to the right.
2. See if the syringe (#3) has water in it. If so, take the syringe out of its holder by loosening the black screw right next to it. Go over to the sink, carefully twist the middle cap off of the syringe, and drain out all of the water, replacing the cap when done. Attach the syringe back to its place and remove the straight needle.
3. Fill the glass box 2/3's of the way up with DI (deionized) water from the dispenser in the sink closest to the door. Set the water-filled box on the goniometer's stage (#4), careful not to hit or bend the needle.
4. Carefully place the glass slide with the sample in the slide holders, but so that the sample and the carbon tape face down. Slowly slide the samples into the water and slide the

holders onto the sides of the box. The slide should be perpendicular to the positioning of the camera (#1) and backlight (#5).

5. Now place the hooked needle on the syringe by attaching to where the straight needle had been before. The needle should go into the water, but shouldn't bend, touch the samples, or touch the bottom of the box.
6. Use the screw in the back of the pole that the needle is attached to, to lower the needle until it is neither touching the bottom of the box nor touching the sample. There are two black screws on the gray metal holder of the syringe: the one farthest back control up and down and the one in front of it controls right and left.
7. Open the computer program "DropImage" on the computer next to the goniometer (#6) and carefully raise the stage until the black bar can be seen. Move that up to the very top of the image.
8. Use the handle on the front of the goniometer (#7) to move the stage back and forth until the sample can be seen. Use the handle on the left side (#8) to focus in on the sample.
9. If there are lots of bubbles on or surrounding the sample, take the holders off of the box and shake off the water, and then slide the glass back into the water at an angle, as to eliminate possibility of bubbles.
10. Use the three screws that control the needle to bring it to the center of the image on the computer program. Once it is in the center, keep enough space between the sample and the tip to release the air bubble by having the needle 1/4 of the way up and the sample/slide covering 1/4 of the top of the image.

11. Go to the “Tools” bar on DropImage and click “Contact Angle”. A pop-up window should appear with numerous commands. Click “Start”. Three lines should come up on the image, two green and one yellow.
12. Slowly twist the top of the syringe until an air bubble is released. When it attaches to the sample, use the screws under the stage to align the baseline so that it is parallel to the horizontal green line on the computer program.
13. Position the vertical lines within the bubble, but do not place them where they cross over the white glare on the bubble.
14. Move up the baseline until it is positioned directly in line with the bottom of the bubble that is in contact with the surface.
15. Click “measure” on the pop-up window. Ideally, the left and right-angle measurements should be about equal. If they are not, try shifting the stage and making it align with the baseline until the measurements are accurate enough. To delete inaccurate measurements, click on the values and press “delete”.
16. To move on to the next sample, use the handle on the front of the goniometer.
17. Repeat processes 12 to 15 for the next measurements.
18. When finished, click “stop” and go to “File” and click “Generate Log”. Save the measurements to the computer and close all the windows.
19. Take the hooked needle off the syringe and replace it with the straight one. Take the holders with the slide and set them on texwipes to dry and go over to the sink and pour out all the DI water in the box. Use texwipes to dry off all of the equipment and then put them all in the glass box. Bring that back to the lab.

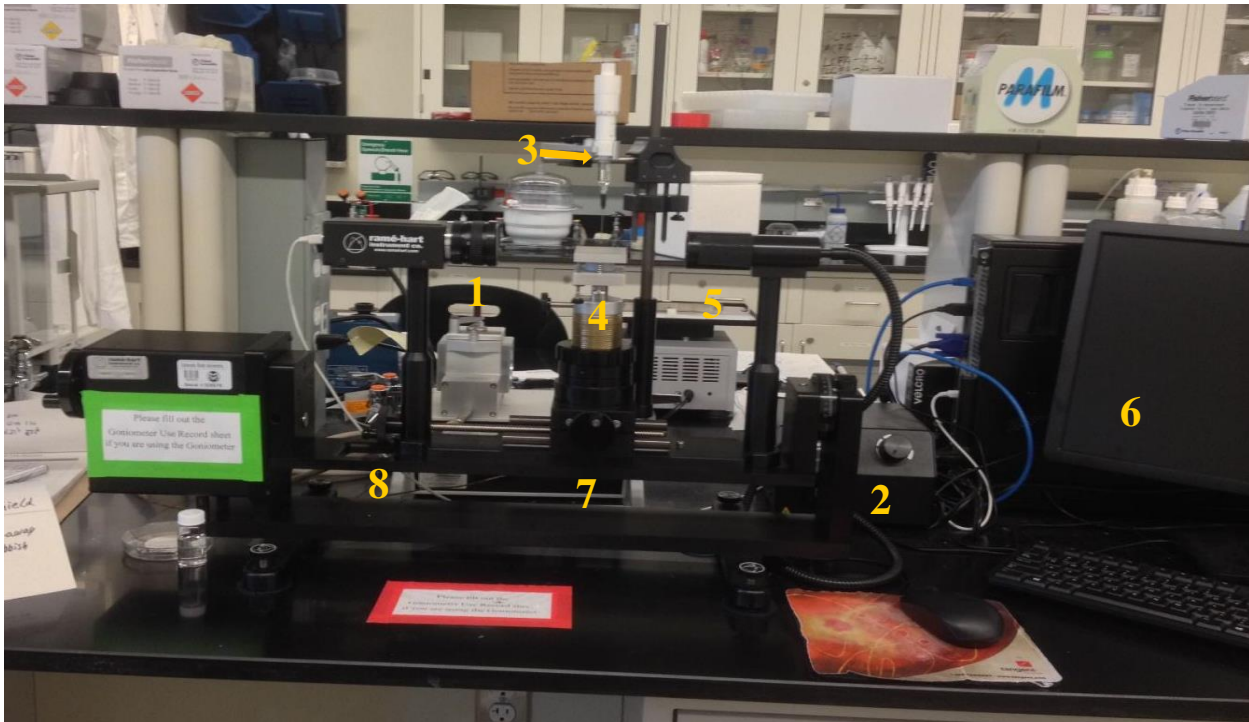


Image of the goniometer

A.8 Toluidine Blue O Staining Assay

Objective

TBO (toluidine blue O) assay is used to identify acidic tissue molecules. On HA-LLDPE treated samples, TBO binds to the carboxyl groups in HA staining them blue/purple, differentiating them from the cross-linker and the LLDPE film.

Materials & Equipment

- Scintillation vial & cap
- Small stir bar
- TBO
- Urea
- X-Acto knife
- Needle

Notes before starting

TBO stained items can be cleaned with ethanol or 2% Liquinox

Use stir bars that already appear to be stained blue if possible

TBO stain can be reused for ~1 week

Procedure

Prepping HA-LLDPE Samples

1. Hydrate samples in DI H₂O for at least 24 hours prior to staining
2. Dry samples with a Kim Tech wipe prior to placing in TBO assay to avoid diluting the solution

Making 10mL 0.1% TBO Stain in 8M Urea

4. Measure 10mL DI H₂O and add to cleaned scintillation vial with stir bar
5. Add 4.8g urea to scintillation vial
6. Stir at room temperature for 30 minutes
7. Add 0.01g TBO to aqueous urea solution allowing it to dissolve completely

Staining Samples

1. Place sample on needle by puncturing an edge*
2. Submerge sample in TBO solution for 20 minutes at room temperature
3. Rinse excess TBO using DI H₂O, leaving behind bound TBO
4. Dip stained sample in fresh DI H₂O and agitate until excess dye is leached out
5. Dry sample on Kim Tech wipe
6. Place sample in vial and allow to dry in drying oven
7. Take photos of samples from each treatment group

* Using needle keeps sample submerged in solution

Revision history

- v{version of revision} [{Name of reviser} {Date of revision}]
 - Brief details of what was revised

A.9 Toluidine Blue Elution

Objective

TBO stain on HA-LLDPE samples can be completely eluted in 50% Acetic Acid leaving behind a blue solution. The solution's absorbance can be measured in a plate reader at 630nm in order to approximate HA surface density on a sample.

Materials & Equipment

- TBO stained HA-LLDPE films
- Stock Glacial Acetic Acid (17.4M , pH = 1.25)
- DI H₂O
- Scintillation vials
- Micropipettes and tips
- Beaker
- Stir bar
- Macropipettes
- Kim Tech wipes
- Vortex machine
- Well plate

Notes before starting

See TBO Assay Protocol for staining procedure

Acetic acid waste should be placed in its own container

Take photos of samples before and after elution

Procedure

Making 50% Acetic Acid (50mL solution)

1. Place 100mL beaker with magnetic stir bar on stir plate and add 25mL of DI H₂O using a macropipette

2. Slowly add 25mL stock glacial acetic acid to DI H₂O while stirring using a macropipette
 - a. Be sure to use two different pipettes in order to avoid cross contamination
3. Stir for 10 minutes before using

Making Standards and Serial Dilution Ladder

Keep 50% Acetic Acid in DI H₂O constant. Test varying TBO concentrations.

See TBO Elution Calculations file to see example dilution and ladder calculation

4. Make 10mL of 1000 μ M TBO solution in 50% Acetic Acid*
 - d. Add 5mL stock glacial acetic acid to 5mL DI H₂O, mix well
 - e. Add 0.00305g TBO, vortex for ~30 seconds to mix well
5. Dilute down to 2mL of 100 μ M TBO solution in 50% Acetic Acid
 - f. 200 μ L of 1000 μ M TBO solution and 1800 μ L of 50% Acetic Acid in DI H₂O
6. Perform serial dilutions to create standards
 - g. Recommended TBO Concentration Range: 0-10.5 μ M TBO
 - h. Measure absorbance of 100 μ L of each dilution in triplicate in plate reader at 630nm
 - i. Plot Absorbance vs. TBO concentration to create ladder

*1000 μ M TBO solution made due to accuracy restrictions of measuring small amounts of TBO

Prepping Samples

7. Cut samples into relatively equal rectangles*(or 8mm punch), and measure surface area.
 - a. Be sure to double the area when doing calculations in order to account for both sides of the sample
 - b. Attempt to cut representative sample (not a completely dark region, not completely light region, do not include grooved edge); see *figure 1*
 - i. If using 8mm punch, use entire sample
8. Hydrate TBO stained samples for at least one hour prior to elution

9. Dry samples with Kim Tech wipe before placing in elution solution to avoid dilution

*rectangles allow for more accurate area calculations

Eluting TBO from Samples

10. Submerge sample in 10mL of 50% Acetic Acid solution for 30 minutes

a. If using 8mm punch, use 3mL of 50% Acetic Acid solution for elution

b. Agitate solution occasionally

11. After 30 minutes, remove samples from solution

12. Rinse samples well with DI H₂O

13. Dry samples with Kim Wipe

14. Place samples in second solution of 3mL of 50% Acetic Acid solution for 30 minutes

c. Agitate solution occasionally

15. After 30 minutes, remove samples from solution

16. Take 3, 100μL samples from each solution and place in well plate

17. Measure absorbance at 630nm

18. Save excel file and calculate HA surface density

d. See TBO Elution Calculations file

Figures

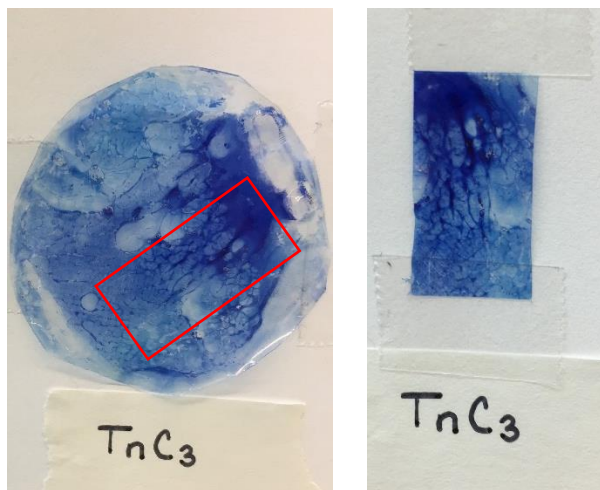


Figure 1

References (if any)

Based on procedure briefly outlined in: “A simple one-step modification of various materials for introducing effective multi-functional groups” by Si Chen, et. al.

A.10 TBO Elution Calculations

** must open with word to see equations

Overview

Example calculations to supplement TBO Elution Protocol

Procedures and Figures

1. Example Dilution

ACETIC ACID + TBO STANDARDS			
Solvent: 50% Acetic Acid			
Starting TBO Solution: 100microM			
M1V1 = M2V2			
Solvent Needed (mL):			
	15.8		
Dilutions			
Making (microL)	Concentration (nM)	Amnt of Prev. Soln. (microL)	Amount of Solvent (microL)
8000	10.5	840.0	7160.0
7500	9.75	6964.3	535.7
7000	9	6461.5	538.5
6500	8.25	5958.3	541.7
6000	7.5	5454.5	545.5
5500	6.75	4950.0	550.0
5000	6	4444.4	555.6
4500	5.25	3937.5	562.5
4000	4.5	3428.6	571.4
3500	3.75	2916.7	583.3
3000	3	2400.0	600.0
2500	2.25	1875.0	625.0
2000	1.5	1333.3	666.7
1500	0.75	750.0	750.0
1000	0	0.0	1000.0

Figure 1

2. Example Ladder

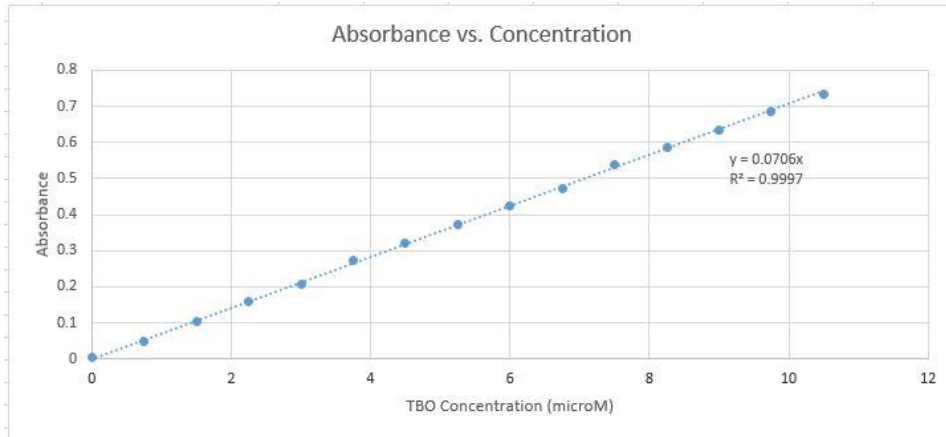


Figure 2

3. HA Surface Density Calculations

- **Concentration TBO → Molecules TBO**

$$TBO \text{ Concentration } \left(\frac{\mu\text{mol}}{L} \right) \times \text{Volume of Elution Solution} = \text{moles TBO}$$

Can use equation from ladder to calculate molecules of TBO from unknown solutions

Ex: $y = 0.0706x$

y: absorbance

x: TBO concentration

plug in known absorbance to get concentration → molecules TBO

- **Number of repeating units in HA molecule**

Check batch lot number to see exact HA MW used (eg. B007 = 738,000Da)

$$\frac{\text{Molecular Weight of HA used}}{379.32\text{Da/unit}} = \text{number of repeating units}$$

- **Relating molecules of TBO to molecules of HA**

Ratio is 1:1 (TBO : Repeating Unit of HA)

$$\frac{\text{molecules TBO from absorbance}}{\frac{\text{number of repeating units}}{1 \text{ molecule HA}}} = \text{molecules HA per sample}$$

- **Surface Density**

Can be in moles or molecules per cm^2

$$\frac{\text{molecules HA per sample} \times \frac{1 \text{ mol HA}}{6.02 \times 10^{23} \text{ molecules HA}} \times \frac{1 * 10^6 \mu\text{mol}}{1 \text{ mol}}}{\text{surface area of sample}} = \text{surface density} \left(\frac{\mu\text{mol}}{\text{cm}^2} \right)$$

References (if any)

“CHEMICAL SURFACE MODIFICATION OF POLYIMIDE FILM FOR ENHANCED COLLAGEN IMMOBILIZATION AND CELLULAR INTERACTIONS” by SHOKOUFEH TEYMOURI: Master of Science Thesis (page 40-42)

A.11 Pierce LDH Cytotoxicity Assay Protocol

Biomaterials Research and Engineering Laboratory

For use with the Thermo Scientific LDH kit

Warning: Some cell line dies without serum such as 3T3, therefore the media used must contain serum and control group with serum should be included. Never include calf serum in the study, this could greatly affect absorbance reading.

Materials Needed

- Cultured Cell Line
- 24-well plate
- 96-well plate compatible with spectrophotometry
- Spectrophotometry plate reader for wavelengths of 490nm and 680nm
- Thermo Scientific Pierce LDH Cytotoxicity Assay Kit (Numbers 88953, 88954)
- Compound to test

Reagent Preparation- Reaction Mixture

1. Dissolve one vial of the Substrate Mix (lyophilizate) with 11.4mL of ultrapure water in a 15mL conical tube. Mix gently to fully dissolve lyophilizate.
2. Thaw one vial of the Assay Buffer (0.6mL) to room temperature. (Protect Assay Buffer from light and do not leave at room temp longer then necessary)
3. Combine 0.6mL of Assay Buffer with 11.4mL of Substrate mix in 15mL conical tube. Mix well by inverting gently. (Protect from light, can be stored for 3-4 weeks at -20°C)

Chemical Compound-Mediated Cytotoxicity Assay

- 1) Prepare samples in the following order
 - a) Spontaneous LDH Activity Controls
 - b) Maximum LDH Activity Controls: Add nothing to one set of triplicate wells of cells.
 - c) Samples: Add the samples to one set of the triplicate wells.

- 2) Seed 20,000 cells in a 24-well plate with 1 ml of media in triplicate wells. (3 wells per test sample)
 - a) Include 3 wells of a complete media control without any cells if serum is used.
 - b) Include 3 wells for Spontaneous LDH Activity Controls with cells
 - c) Include 3 wells for Maximum LDH Activity Controls with cells

3) Incubate at 37°C, 5% CO₂ as needed

4) Add 100µL of Lysis Buffer (10X) for every 1 ml of cell media to the Maximum LDH Activity Controls, and mix by gentle tapping.

- a) Avoid creating any bubbles (may inhibit absorbance readings)

5) Incubate at 37°C, 5% CO₂ for 45 minutes.

6) Transfer 50µL of each sample medium (e.g., complete medium, serum-free medium, Spontaneous LDH Activity Controls, compound-treated and Maximum LDH Activity Controls) to a 96-well plate for the spectrophotometry.

NOTE: Perform the next 3 steps in the dark hood and wrap the well plate in aluminum foil when moving to the plate reader.

7) Transfer 50µL of Reaction Mixture to each sample well and mix using a multichannel pipette.

8) Incubate the plate at room temperature for 30 minutes protected from light.

9) Add 50µL of Stop Solution to each sample well and mix by gentle tapping.

10) Measure the absorbance at 490nm and 680nm. To determine LDH activity, subtract the 680nm absorbance value (background) from the 490nm absorbance before calculation of % Cytotoxicity [(LDH at 490nm) - (LDH at 680nm)]

- a) LDH Activity = (LDH at 490nm) – (LDH at 680nm)

11) To calculate % Cytotoxicity use the following formula.

$$\text{a) \% Cytotoxicity} = \frac{(\text{Compound treated LDH activity} - \text{Spontaneous LDH activity})}{(\text{Maximum LDH activity} - \text{Spontaneous LDH activity})} * 100$$

A.12 Whole Blood Clotting/Free Hemoglobin Protocol

Materials

- Petri dishes (for pipetting blood onto the samples, one for each treatment group)
- 24 well plates (for freeing hemoglobin)
- 96 well plate (for plate reading)
- DI water
- Timer
- 20 μ l, 200 μ l, and 1000 μ l pipettes and pipette tips
- Vacuum tubes not coated with anticoagulant
- Plate Reader (Popat Lab)

Note: Blood must be drawn on site so that it can be immediately transferred onto samples/well plates!!! You must make an appointment to have the phlebotomist come to the lab. May need to lower concentration of blood due to high susceptibility for clotting (ePTFE).

Preparation

- Determine how much blood and how many samples needed prior to the study. Samples will be run in triplicate for three different time points (15 min, 30 min, and 60 min). Total samples needed per treatment group are 12. Each sample will have 10 μ l of whole blood pipetted onto the surface. A 5:1000 of Blood/DI water solution will be used for data analysis.
 - Determining Number of Samples and Total Volume of Blood for 2 treatment groups.

12 samples x 5 μ l of blood= 60 μ l of blood per treated group

60 μ l of blood x 2 groups= 120 μ l total blood for treatment

120 μ l+ 30 μ l of blood for t_0 (5 μ l for 6 wells) = 150 μ l total blood for the study

- One blood vacuum tube holds approximately 6 *ml* of blood.
- Make sure to label the 24-well plate according to the time points and treatment groups that will be used. Only one 96 well plate is needed for plate reading. At least 4 wells should be blanks.
- For 8 mm samples, be sure to use carbon tape to seal them on center of the 24 well plate and have them hydrated for at least 2 hours prior to the test.
- For LLDPE samples, carbon tape them onto PTFE pucks.
- Pipette 1000 μ l and 200 μ l of DI water into each T₀ and blank well, respectively
- Cover all well plates while waiting for the phlebotomist

Procedure

1. Have phlebotomist draw blood into vacuum tubes which have not been coated with anticoagulant. The first will be thrown away as it contains the skin plug and locally activated platelets. The second will be used for the study.
2. Pipette 5 μ l of blood into the each T₀ well already containing 1000 μ l DI water on a separate well plate. Gently agitate on the Titer plate shaker for 30 s at speed 1. Let wells sit for five minutes to allow blood to be fully dissolved in the DI water.
3. Transfer 5 μ l of whole blood onto each of the T₁₅ samples. Start the timer as the first drop is placed on the samples. Ensure the blood is in the center of the materials. Be sure to change pipette tip each time to avoid cross contamination. DO NOT reuse pipette tips.
4. Repeat step 3 for T₃₀ and T₆₀ samples.
5. When each time point reached, transfer 1000 μ l of DI water (in the same order in which blood was transferred) to the corresponding wells on the 24-well plate.

6. Gently agitate on the Titer plate shaker for 30 s at speed 1. Let sit for five minutes to allow the free hemoglobin that was not trapped in the blood clot to be released into the water.
7. After 5 minutes, pipette 200 μ l of the blood +DI solution into the 96-well plate. Be sure to change pipette tip to avoid cross contamination.
8. Analyze results using the plate reader at 540 nm wavelength. Open CLOTTING method on the plate reader in Popat's Lab.

A.13 Platelet Activation

Materials

- Plate Shaker
- 1000 μ l pipettor and tips
- 24 well plates
- Phosphate buffer saline (PBS)
- Sterile tweezers for transferring samples
- EDTA coated Vacutainer tube

Safety Considerations

- Work carefully and avoid contact with blood at all time.
- Remember to take the Blood-borne Pathogens (BBP) Precautions and Training offered by CSU.

Process Considerations

- If using polystyrene pucks to submerge samples, be sure to sand the puck well to remove rough edges that can activate platelets.
- Be gentle, work diligently and slowly to prevent activation of platelet.
- Avoid bubbles when pipetting blood and plasma.

General Procedure¹

1. Be sure to sterilize samples and keep them hydrated in sterile DI water.
2. Collect blood from the phlebotomist and store them in EDTA coated tubes to prevent coagulation. Each tube can hold approximately 2 ml of plasma.
3. Using a centrifuge, spin blood at 150 g for 15 minutes and let it rest for another 15 minutes.²
4. There should be two visible layers of solution in the centrifuged blood tube: platelet rich plasma (PRP) on top, and blood cells (bottom). The buffy coat is located in the middle, but this is not always noticeable with the naked eye.
5. Pool PRP into one tube.
 - a. Draw amount smaller than 1 ml each teach time can prevent liquid entering and sucking blood.

- b. Draw only 2/3 of plasma layer to prevent the risk of drawing blood and the buffy coat.
 - c. This step can be time consuming. One in a while, rock the plasma/blood tube back and forth gently to prevent platelet aggregation.
 - d. If accidentally mixed blood, centrifuge the tube for 5 minutes.
6. Aspirate DI water from the wells containing samples, and use tweezers to transfer the samples into the plasma containing wells. Ensure there is no water left on the sample (but hydrated) to avoid dilution of plasma.
 7. Pipet 1 ml of PRP into each well of the 24 well plate.
 - a. Avoid pipetting PRP onto the sample.
 8. Put well plate on a shaker storing in the cell culturing incubator (37 C, 5% CO₂), and shake at 100 RPM for 2 hours.
 9. Either aspirate the plasma. Avoid aspirating directly on the sample that could suck platelets.
 10. Rinse the samples twice with PBS. Avoid pipetting directly at the sample to prevent adhered platelets from washing away.
 11. Move on the SEM fixing (morphology analysis) or Calcein staining (cell quantification).

References

1. Hieu Bui's lab notebook pg. 45
2. Riedel, N. A., Smith, B. S., Williams, J. D., & Popat, K. C. (2012). Improved thrombogenicity on oxygen etched Ti6Al4V surfaces. *Materials Science and Engineering: C*, 32(5), 1196-1203.

Revision Date	Name	Version
5/29/2016	Hieu Bui	1
6/13/2016	Hieu Bui	2

A.14 SEM Fixing

Materials

- Petri dishes
- 10 ml pipettor and tips
- Sodium cacodylate
- Sucrose
- DI water
- Ethanol
- beaker (to make buffer/fixative solution)

Process Considerations

- Make fixing solution and buffer solution simultaneously to save time.
- 10 ml of each solution in step 1 of the procedure is usually enough.

Fixative and Buffer Preparation^{1,2}

- Fixative: 3% glutaraldehyde in 0.1 M sodium cacodylate and 0.1 M Sucrose
- To make 10 ml buffer and 10 ml of fixative:
 1. Obtain 19.4 ml of DI water
 2. Add 0.68 g of sucrose and 0.43 g of sodium cacodylate to DI water, and swish until everything is fully dissolved.
 3. Remove 10 ml the mixing solution. This is the buffer solution.
 4. Add 0.3 ml of glutaraldehyde to the remaining solution. Swish gently. This is the fixative solution.

Procedure^{1,2}

1. Prepare the following solutions and add them to a Petri dish of their own: fixative solution, buffer solution, 35% ethanol, 50% ethanol, 70% ethanol, 100% ethanol, and HMDS.
2. Transfer samples to the fixative solution and sit for 45 minutes. Be gentle when transferring to prevent platelet displacement.

3. Transfer samples to the buffer solution and let sit for 10 minutes. If crunched on time, the samples can be incubated in the buffer solution overnight.
4. After incubating in buffer solution, move the samples into the following solutions for the designated times:
 - a. 10 min- 35% ethanol
 - b. 10 min- 50% ethanol
 - c. 10 min- 70% ethanol
 - d. 10 min- 100% ethanol
5. Allow air dry of ethanol residue and store them in the desiccator prior to SEM imaging.

References

3. Hieu Bui's lab notebook pg. 46
4. Rachael Simon-Walker's lab notebook pg.11

Revision Date	Name	Version
5/29/2016	Hieu Bui	1
7/29/2017	Hieu Bui	2

A.15 Calcein Staining

Materials

- Calcein AM (stored in -20 freezer)
- 1000 μ l pipettor and tips
- Conical tubes for working calcein solution
- Phosphate buffer saline (PBS)
- Sterile tweezers for transferring samples

Process Considerations

- Use the dark hood for the entire process.
- Calcein is sensitive to white light, so use the red lamp for working.

General Procedure¹

12. Be sure to sterilize samples and keep them hydrated in sterile DI water.
13. Thaw calcein solution. If not premixed, reconstitute the crystal in 50 μ l of DMSO for each vial.
14. Vortex the stock solution.
15. Make 5 μ M of working Calcein solution
 - a. 5 μ l of stock solution for 1 ml of PBS. For example: 120 μ l of stock solution for every 24 ml of PBS.
16. Transfer samples from plasma solution to a clean 24 well plate and rinse twice with PBS. Avoid pipetting and aspirating directly at the sample to prevent adhered platelets from washing away.
17. Add 1 ml of Calcein working solution to each sample's well.
18. Incubate at room temperature for 20 minutes.
19. Aspirate the staining solution and rinse with 1ml of PBS.
20. Keep the samples hydrated in a new solution of PBS while take images.

References

5. Hieu Bui's lab notebook pg. 47
6. Blood Study protocol from the Popat lab

Revision Date	Name	Version
5/29/2016	Hieu Bui	1